

UNIVERSITA' DEGLI STUDI DI NAPOLI "FEDERICO II"

DIPARTIMENTO DI FARMACIA



DOTTORATO DI RICERCA IN

SCIENZA DEL FARMACO

XXVIII CICLO

**IDENTIFICATION OF NOVEL INHIBITORS OF CDC25
PHOSPHATASES AS NEW ANTI-MELANOMA AGENTS BY
LIGAND- AND STRUCTURE-BASED
VIRTUAL SCREENING STUDIES**

Tutor
Prof. Antonio Lavecchia

Candidate
Carmen Cerchia

Coordinator
Prof.ssa Maria Valeria D'Auria

To my family

Acknowledgements

First and foremost, I would like to express my deepest gratitude to my supervisor, Professor Antonio Lavecchia, for the continuous guidance, motivation and support throughout the course of my studies.

I also would like to thank the coordinator of the PhD program, Professor Maria Valeria D'Auria, for all her help and advice.

A special thank goes to Dr. Carmen Di Giovanni, who welcomed me with great enthusiasm. Your help and suggestions were essential during these years. Thank you especially for being a friend.

Many thanks also to former and current members of the Drug Discovery Lab, for being a part of my scientific growth.

I am grateful to all the people who collaborated to this project, especially for all the insightful discussions: Professors Emmanuele De Vendittis, Rosaria Ruocco, Stefania Villa, Dr. Alessandra Capasso.

Abstract

Cell division cycle 25 (CDC25) proteins are highly conserved dual specificity phosphatases that regulate the proper advancement of the cell cycle by activation of CDK/cyclin complexes. Overexpression of CDC25s, resulting in genomic instability and dysregulated cell growth, is frequently related to aggressiveness, high-grade tumors and poor prognosis. Thus, this family of enzymes represent an attractive target for drug discovery. Recently, compound **11**, 3-(4,5,6-trihydroxy-3-oxo-3H-xanthen-9-yl)propanoic acid, and compound **19**, 4-(2-carboxybenzoyl)phthalic acid, were identified as novel inhibitors of CDC25s with a different inhibition profile, by using a structure-based virtual screening approach. Both compounds arrested cells at the G₀/G₁ and G₂/M phases of the cell cycle, increased Cdk1 hyperphosphorylation in K562 leukemia cells, and significantly suppressed the growth of human MCF-7 breast, PC-3 prostate cancer lines as well as K562 leukemia cells, thus representing novel interesting leads. This thesis project focused on the computer-assisted lead optimization of the initial hits **11** and **19**. Firstly, in order to expand our understanding of structure-activity relationships within the 6-xanthone class of CDC25 inhibitors, we identified a series of structural analogs of compound **11** by ligand-based chemoinformatic approach. We examined their activity against melanoma cancer cell lines, as well as the mechanism of action involved. Nine compounds (**3**, **5–9**, **21**, **24**, and **25**) were identified with *K_i* values for CDC25A, -B and -C ranging from 0.01 to 4.4 μM. One of these analogs, **7**, showed a high antiproliferative effect on human melanoma cell lines, A2058 and SAN, associated with an arrest in G₂/M phase of the cell cycle. Furthermore, **7** induced apoptosis through intrinsic pathway. Interestingly, compound **7** decreased the protein levels of phosphorylated Akt and increased those of p53, thus contributing to the regulation of chemosensitivity through the control of downstream Akt pathways in melanoma cells. Secondly, a series of novel derivatives of compound **19** was rationally designed by using a structure-based approach, guided by preliminary docking studies, with the aim to improve its binding affinity, pharmacokinetic properties as well as to investigate its anti-melanoma effect. A focused library of 24 derivatives was synthesized: a preliminary screening of the inhibitory activities toward CDC25B showed that ten

molecules (compounds **2**, **3d**, **4**, **4a**, **4b**, **5f**, **6**, **6a**, **6b**, **7**) acted as powerful inhibitors with K_i values ranging between 2.8–20.1 μM . Among them, compounds **2** and **6a** showed good antiproliferative effects on melanoma cell line A2058. Taken together, our data emphasize that CDC25 could be considered as a possible oncotarget in melanoma cells and that the designed compounds represent small molecule CDC25 inhibitors that merit to be further evaluated as chemotherapeutic agents for melanoma, likely in combination with other therapeutic compounds.

TABLE OF CONTENTS

Abstract	i
1. Introduction	1
<i>1.1 Protein phosphatases</i>	<i>1</i>
<i>1.1.1 Structure and function of CDC25</i>	<i>2</i>
<i>1.1.2 CDC25 in cell cycle regulation</i>	<i>6</i>
<i>1.1.3 Control of CDC25 expression and activity</i>	<i>7</i>
<i>1.1.4 Cell cycle checkpoints</i>	<i>8</i>
<i>1.1.5 CDC25 phosphatases as therapeutic targets</i>	<i>9</i>
<i>1.1.6 CDC25 inhibitors</i>	<i>10</i>
<i>1.2 Melanoma</i>	<i>14</i>
<i>1.2.1 Mechanisms and pathophysiology</i>	<i>15</i>
<i>1.2.2 Cell cycle alterations in melanoma: the role of CDC25</i>	<i>18</i>
<i>1.2.3 Therapeutic treatment of melanoma</i>	<i>19</i>
<i>1.3 Aim of the work</i>	<i>24</i>
2. Results and discussion	25
<i>2.1 Ligand-based chemoinformatic selection of new analogs of compound 11</i>	<i>25</i>
<i>2.1.1 Similarity search using molecular fingerprints</i>	<i>25</i>
<i>2.1.2 Substructure search</i>	<i>27</i>
<i>2.1.3 Biological evaluation</i>	<i>30</i>
<i>2.2 Lead optimization of compound 19</i>	<i>40</i>
<i>2.2.1 Structure-based drug design strategy</i>	<i>40</i>
<i>2.2.2 Synthesis of rationally designed compounds</i>	<i>43</i>
<i>2.2.3 Inhibitory activities of rationally designed compounds toward CDC25B</i>	<i>48</i>

<i>2.2.4 Docking studies and SAR rationalization</i>	<i>51</i>
<i>2.2.5 Antiproliferative effects of compounds 2, 4, 4a, 4b, 6, 6a, 6b and 7</i>	<i>53</i>
<i>2.3 Conclusions</i>	<i>55</i>
3. Experimental section	57
3.1 Computational chemistry	57
<i>3.1.1 Chemoinformatic methods</i>	<i>57</i>
<i>3.1.2 Molecular modeling</i>	<i>58</i>
<i>3.2 Biology</i>	<i>59</i>
<i>3.3 Chemistry</i>	<i>64</i>
References	82

1. Introduction

1.1 Protein phosphatases

The reversible phosphorylation of proteins represents a fundamental mechanism in eukaryotic signaling, with up to 30% of all proteins being phosphorylated at any given time [1]. Many biological functions are regulated through this mechanism including DNA replication, cell cycle progression, energy metabolism, cell differentiation and development [2-3]. Levels of cellular protein phosphorylation are controlled by protein kinases, which catalyze the formation of phosphate ester bonds, and protein phosphatases, which catalyze phosphate ester hydrolysis. Because of this broad spectrum in activity, it is not surprising that malfunctions of PTPs are associated with various diseases, for example neurological disorders, diabetes, or cancer [4]. Protein phosphatases evolved from diverse ancestors, resulting in different domain architectures, reaction mechanisms and active site properties. In humans, protein phosphorylation predominantly occurs on tyrosine, serine and threonine residues with phosphoserine accounting for most of the phosphorylated sites (86.4%), followed by threonine (11.2%) and finally tyrosine being the least abundant (1.8%) [5]. Two distinct families of protein phosphatases are known: the serine/threonine phosphatases, which dephosphorylate substrates in a single-step reaction via a metal-activated water molecule and the protein tyrosine phosphatases (PTPs), which dephosphorylate phosphotyrosine in a two-step reaction [6-9]. PTPs also include a subfamily of dual-specificity protein tyrosine phosphatases (DSPs), which hydrolyze both tyrosine and serine/threonine phosphoesters [9], and thereby play important roles in regulating various intracellular activities and mechanisms associated with human diseases [10]. The cell division cycle 25 (CDC25) phosphatases are a subfamily of DSPs that are vital to cell cycle regulation via the activation of Cdk/cyclin complexes.

1.1.1 Structure and function of CDC25

CDC25 was first identified in the fission yeast *Saccharomyces pombe* as the twenty-fifth protein that regulated the cell-division cycle [11]. CDC25 phosphatases are found in all eukaryotic organisms except plants [12]. Three isoforms have been identified in humans: CDC25A, CDC25B and CDC25C [13-15]. CDC25A, -B and -C contain 524, 580 and 473 amino acids, respectively, resulting in molecular masses in the 53–65 kDa range [16]. The three human CDC25 isoforms, although sharing functional and sequence homology, are encoded by unique genes that localize to three different chromosomes: CDC25A is found on 3p21, CDC25B on 20p13 and CDC25C on 5q31 [17]. CDC25 proteins are structurally divided into two principal domains: an N-terminal regulatory domain and a C-terminal catalytic domain. The C-terminal catalytic domains are highly similar between all three proteins, with approximately 60% sequence identity between any of the family members. The regulatory domains vary widely between the three proteins, with multiple splice variants being reported: at least two for CDC25A, five for CDC25B and five for CDC25C [18-21]. The N-terminal domain of the CDC25 proteins contains a nuclear export signal (NES) and a nuclear localization signal (NLS), as well as many phosphorylation sites involved in the regulation of the activity, protein stability and the association with regulatory partners [22]. The carboxy-terminal domain contains the canonical PTPase active site motif HCX₅R: H is a highly conserved histidine residue, C is the catalytic cysteine, X₅ are five residues that form a loop in which all of the amide hydrogen molecules are bound to the phosphate of the substrate, and R is a highly conserved arginine required for binding to the phosphorylated amino acid of the substrate. The crystal structures of the catalytic domains of CDC25A and CDC25B have been reported at 2.3 Å and 1.9 Å resolution, respectively, but no crystal structure for the full-length protein is available. Examination of the structure of CDC25s has revealed that, in contrast to other protein phosphatases, their active site is surprisingly flat and extremely shallow, with a lack of auxiliary loops and no obvious features for mediating substrate recognition, which suggests a broad protein interface [23-24]. Indeed, substrate recognition has been proposed to rely on hotspot residues (R488, R492 and Y497 on CDC25B) located 20-30 Å from the active site [25-26]. Although the overall structures of the two CDC25 catalytic domains are similar, the

catalytic site of CDC25A failed to bind oxyanions, while that of CDC25B readily bound tungstate and sulphate in a mode similar to other PTP- and DSPases [24]. The CDC25A catalytic domain also lacks any flexible peptide loops proximal to the active site that might facilitate substrate binding [23-24]. One of the largest cavities on the surface of CDC25B is adjacent to the catalytic pocket and is known as the “swimming pool”, for the abundance of well-ordered water molecules contained within the pocket [27]. Key differences between the CDC25B and CDC25A catalytic domains are located in the C terminus (residues 531–547 in CDC25B numbering). The carboxy-terminal tail of CDC25B folds back on its active site, whereas the carboxy-terminal tail of CDC25A is directed away from the active site cleft, which results in a more open structure (Figure 1).

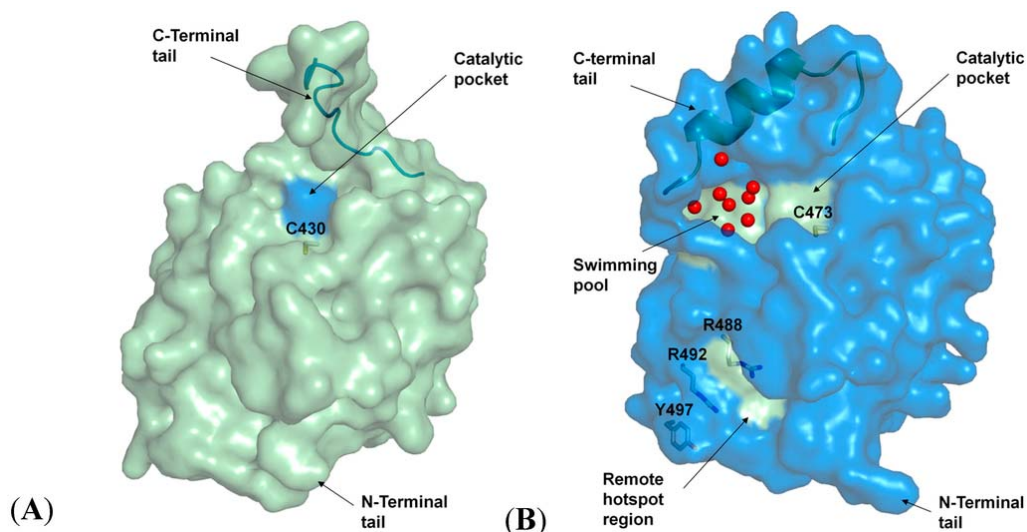


Figure 1. Structures and domains of CDC25A and CDC25B. A) Surface view of CDC25A (palegreen). The catalytic site is indicated in blue marine. The C-terminal tail (residues 484-495) is shown in palegreen cartoon. B) Surface view of CDC25B (blue marine). The catalytic site and the adjacent “swimming pool” pocket are indicated in palegreen. The water molecules are represented as red spheres. The hotspot residues (R488, R492 and Y497), which govern the association with the protein substrate, are shown in blue sticks. The remote hotspot region is highlighted in palegreen. The α -helical C-terminal tail (residues 531–550) is shown in palegreen cartoon [16].

CDC25s utilize a two-step reaction for phosphate monoester hydrolysis, as shown in Figure 2 [28]. The first step is the nucleophilic attack from a PTP cysteine side chain toward the phosphate ester substrate, with a possible H^+ transfer from a general acid to the leaving group. A thiophosphorylated-PTP intermediate is formed, and the dephosphorylated substrate dissociates from the active site cavity. In the second reaction step the PTP intermediate is hydrolyzed, whereby the phosphate group is released and free enzyme is regenerated [25,29].

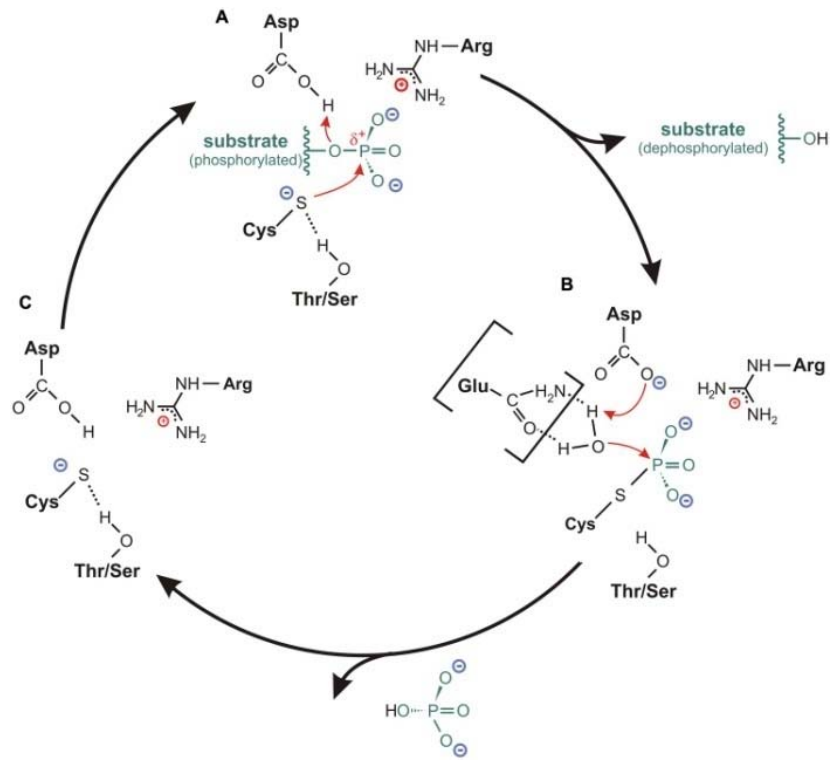


Figure 2. Catalytic cycle for cysteine-based PTPs. Adapted from [28].

Almost all PTPs use as a general acid, an Asp residue located in a mobile loop (the WPD loop) [29]. CDC25s lack an analogous catalytic acid residue near the active site or in a flexible loop that could donate a H^+ to the leaving group [23-24]. Hence, the identity of the general acid on CDC25s remains vague. It has been suggested that the catalytic acid is an E residue (E474 on CDC25B) located in the active site just after the catalytic cysteine (C473 on CDC25B) [23,30]. This E residue is conserved among all known CDC25 isoforms [29]. However, Chen et al. proposed that the putative catalytic acid residue may instead be located on the protein substrate rather than on CDC25B [31]. Another proposal suggested that the substrate could bind as a phosphate monoanion rather than dianion and transfer the proton itself to the leaving group [32]. This latter mechanism has been recently supported by Rudolph and co-workers through QM/MM minimum free energy path calculations [33].

1.1.2 CDC25 in cell cycle regulation

Progression through the cell cycle is regulated by the action of Cyclin/Cyclin dependent kinase (CDK) complexes. These latter are held inactive by the phosphorylation of two residues (Threonine 14 and Tyrosine 15 on CDK1) by the WEE1 and MYT1 kinases. When CDK activity becomes required for cell cycle progression, the CDC25s dephosphorylate these two residues, thereby activating the CDK-Cyclin complexes [34]. CDC25A is predominantly found in nucleus [35], whereas the other two isoforms shuttle in and out the nucleus throughout cell cycle progression [36-37]. It is believed that all three isoforms are essential for the proper execution of the cell cycle, although it has been shown that CDC25A alone is sufficient for initiation of each step in the cycle [37-38]. A simplified overview of the cell cycle regulation is shown in Figure 3.

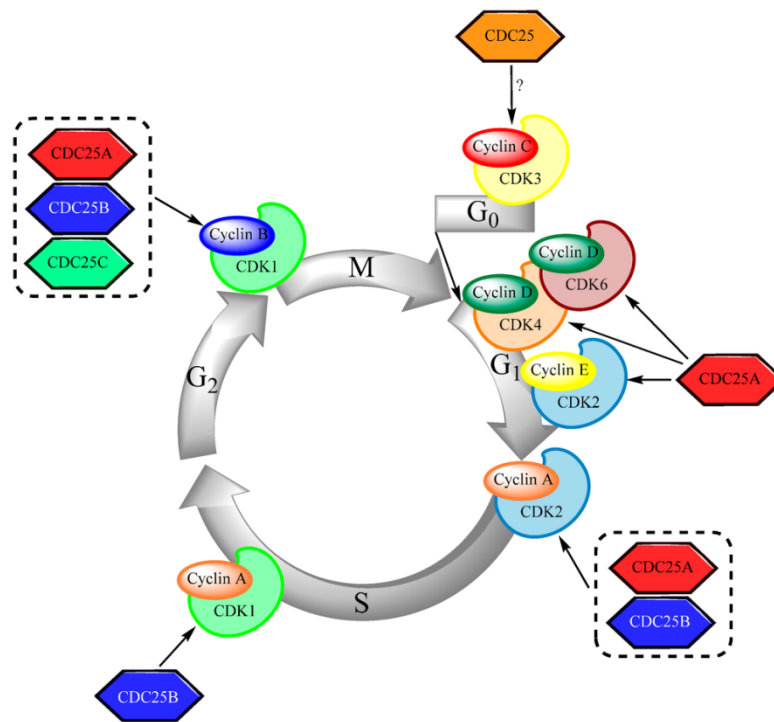


Figure 3. An overview of the regulatory function of CDC25s in cell cycle progression [16].

At G₀-phase, the CDK3/cyclin C complex initiates the re-entry of quiescent cells into the cell cycle. In middle G₁-phase, CDC25A activates CDK4 and CDK6 that are in

complex with cyclin D [39]. CDC25A reaches its highest expression level at late G1-phase during which, in combination with CDC25B, it facilitates the transition into S-phase by dephosphorylation of CDK2/cyclin A [40]. CDC25C controls the initiation of the S-phase [41]. At late S-phase, CDC25B dephosphorylates CDK1/cyclin A, a less active complex compared to CDK2/cyclin A, which persists throughout G2-phase [40]. All three CDC25 isoforms are involved in the G2/M-transition but CDC25B appears to take the key role in this process [42]. Infact, CDC25B is most abundant and active at late G2-phase and during mitosis, and is localized to the centrosome where it dephosphorylates CDK1/cyclin B [42-43]. This latter is subsequently translocated to the nucleus, where it is completely activated by CDC25C leading to mitotic onset [40]. At the end of mitosis, both CDK1/cyclin B and the CDC25s are degraded resulting in transition into interphase. The proteins are subjected to anaphase promoting complex/cyclosome (APC/C)-dependent ubiquitination leading to proteasome-mediated degradation [44].

1.1.3 Control of CDC25 expression and activity

CDC25 phosphatase activities are highly regulated by multiple mechanisms, including inhibitory and activating phosphorylations, changes in intracellular localization and interactions with partner proteins. Phosphorylation of the N-terminal regulatory domains by several kinases, including the CDK/cyclin complexes themselves, has been reported to regulate the activities of the CDC25 phosphatases [22,45]. Two other important kinases positively regulate CDC25s and promote mitosis: the polo-like kinase 1 (PLK1) and Aurora kinases. The former activates CDC25C both directly and indirectly by CDK1/cyclin B phosphorylation and inhibition of the Wee1-like kinase Myt1 [46], in addition to favoring the nuclear import of CDC25C [47], whereas the latter activates both PLK1 and CDC25s [48-49]. PLK1 also plays a role in mitotic exit, as it is a positive regulator of the APC/C activity [50]. Phosphorylation has also been reported to influence the ability of the CDC25s to interact with 14-3-3 proteins, which function to retain proteins in various subcellular compartments [17]. At the transcription level, CDC25s are activated by the transcription factors E2F1, E2F2 and E2F3, the antagonists of Rb. Signal transducer and activator of transcription 3

(STAT3) usually activates CDC25 gene transcription, but through Rb recruitment it can also exhibit an inhibitory effect [51]. The transcription factor p53, which regulates the expression of genes impinging on cell cycle arrest, was reported to be responsible of the transcriptional repression of the three CDC25 phosphatases [52-53].

1.1.4 Cell cycle checkpoints

Multiple checkpoint pathways are activated in response to DNA damage or environmental insults in order to block the cell cycle progression. At the G1/S checkpoint, DNA synthesis is inhibited, whereas intra-S phase arrest blocks mitotic entry until the S-phase is completed [40]. Finally, at the G2/M checkpoint, damaged cells are arrested in order to allow for cell repair or apoptosis [54]. CDC25s are inactivated by checkpoint kinases (CHK1 and CHK2) in an ataxia-telangiectasia mutated (ATM) and AT and Rad3-related (ATR) kinases-dependent manner. Upon DNA single-strand damage, ATR activates CHK1, whereas ATM activates CHK2 and the tumor suppressor protein p53 mainly as a result of double-strand breaks [47,55]. Activated CHK1/CHK2 target CDC25 leading to its inhibition or degradation. The checkpoint kinases also increase the amount of Wee1 resulting in inactivation of CDKs [55], and the CDC25 activator PLK1 appears to be inhibited in an ATM/ATR-CHK1/CHK2-dependent manner. In detail, CHK2 inhibits CDC25A through p53 [56] resulting in inactivation of CDK4/cyclin D and CDK2/cyclin E, thus blocking S-phase entry [56-57]. On the other hand, all three isoforms of CDC25 are phosphorylated by CHK1 in order to prevent mitotic onset. Phosphorylated CDC25A/B can no longer activate CDK1/cyclin B [58-59], and inactivation of CDC25B/C sequesters the proteins in the cytoplasm [60-61]. Also, hyperphosphorylation of CDC25A leads to its degradation [58,62]. The checkpoints are silenced after repair or degradation of the damaged cells [54], and the re-entry into mitosis upon DNA-damage arrest is controlled by CDC25B upon activation by PLK1 [63]. PLK1 also inactivates CHK1 by mediated degradation of Claspin, the adaptor and activating partner of CHK1 [64]. In addition to the checkpoint kinases, several other proteins are involved in CDC25 inhibition, for example protein kinase B (PKB/Akt) and mitogen-activated protein kinases (MAPKs). The latter negatively regulate CDC25 upon DNA damage mediated by heat shock,

oxidative stress, irradiation, feed deprivation and chemotherapy [40,65]. The effects of the PI3K-Akt-mTOR pathway on cell cycle progression are not completely understood and conflicting results have been obtained. On one side, Akt sequesters CDC25s in the cytoplasm upon binding to protein 14-3-3, thus inhibiting mitosis [66]. Also, it seems as if CDC25B activity itself is required for the activation of Akt and the p38 MAPK kinase [67], thus indicating a mutual regulation of these proteins. On the contrary, several studies have shown that Akt acts as an initiator of mitosis [68-69] and inactivation of both CHK1 [70] and CHK2 [71] by Akt have been observed, thus circumventing the degradation of CDC25s. Following DNA damage for instance, Akt impairs the activation of CHK1 in an ATR-independent manner, thus circumventing the cell cycle checkpoint and inhibiting apoptosis [72]. In concordance with this, inhibition of Akt led to restored CHK1 activity [73].

1.1.5 CDC25 phosphatases as therapeutic targets

As detailed above, CDC25 phosphatases must be tightly regulated throughout the cell division cycle to maintain the precise spatial and temporal level of CDK–cyclin activities. In addition, CDC25 phosphatases must be inactivated in response to checkpoint activation to stop cell cycle progression and allow the cell to either repair the DNA or initiate apoptosis [47]. Misregulation of these processes can contribute to genomic instability. Dysregulation in the case of CDC25A, for example, accelerates the G1/S-phase transition [74], whereas an overexpression of CDC25B leads to premature mitotic entry [75]. Elevated levels of CDC25A and CDC25B have been noted in many human tumor types, such as breast, ovarian, prostate, lung, colorectal, oesophageal, thyroid, laryngeal, hepatocellular, gastric, pancreatic, endometrial, head and neck cancer, neuroblastoma, glioma and non-Hodgkin lymphoma [22], where there seems to be a remarkable association with high protein levels and either tumor aggressiveness or poor prognosis [17,76-77]. CDC25A and CDC25B have been reported to transform cells in cooperation with the RAS oncogene or in the absence of the retinoblastoma tumor suppressor protein [78]. CDC25A and B are also transcriptional targets of the c-MYC oncogene, and have oncogenic properties in cooperation with either Ha-RAS or Rb1 [79]. The involvement of CDC25A in the adhesion-dependent proliferation of acute

myeloid leukaemia (AML) cells has also been described [80]. CDC25A and CDC25B have also been observed to be highly expressed in the brains of patients with Alzheimer's disease and may contribute to the pathology of neurodegeneration [81-82]. With regard to CDC25C, only a few studies showed an overexpression of this form in cancers [83-84]. However, growing evidence suggests that the overexpression of CDC25C could be underrated because of the non-consideration of its alternative splicing [85-86]. Although the mechanism by which CDC25s become overexpressed is poorly understood, their expression may be elevated by increased gene expression, increased protein stability as a result of deficiencies in protein turnover, or both [17,62,87-88]. There is currently no evidence that CDC25 overexpression results from gene amplification or rearrangements or any other specific genetic mutations that may be responsible for deregulating CDC25 phosphatase activities in cancer [47]. In addition, the lack of significant correlation between transcript and protein levels suggests that the CDC25 phosphatases can become misregulated at any stage between transcription and translation, even at the post-translational level [47]. Given their critical role, CDC25s constitute attractive targets for drug discovery.

1.1.6 CDC25 inhibitors

Strategies to identify small molecule inhibitors of CDC25s generally followed the approaches used for other PTPs [89]. Either low or high throughput screens have been developed using recombinant protein with a variety of small molecule substrates including p-nitrophenyl phosphate, 6,8-difluoro-4-methylumbelliferyl phosphate, fluorescein diphosphate or O-methyl-fluorescein phosphate [89].

Until the mid-1990s, the only readily available inhibitor was the broad-spectrum PTP inhibitor sodium orthovanadate [17]. Natural products have been a rich source of inhibitors and a good starting point for the development of synthetic analogues. Representative members in this group include the natural products dnacin B1 [90], dysidiolide [91], menadione [92], sulfircin [93] and coscinosulfate [94], which inhibit the CDC25 family with IC₅₀ values in the 1–10 μ M range (Figure 4).

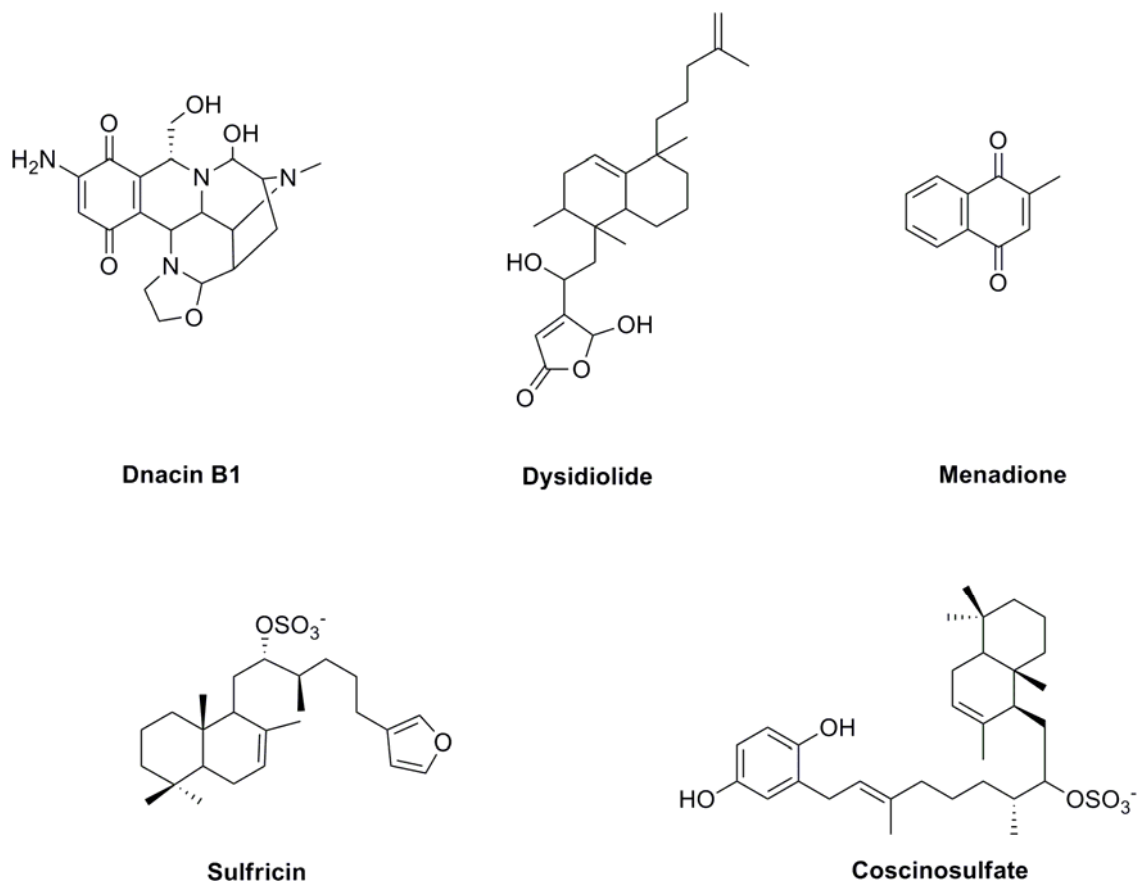
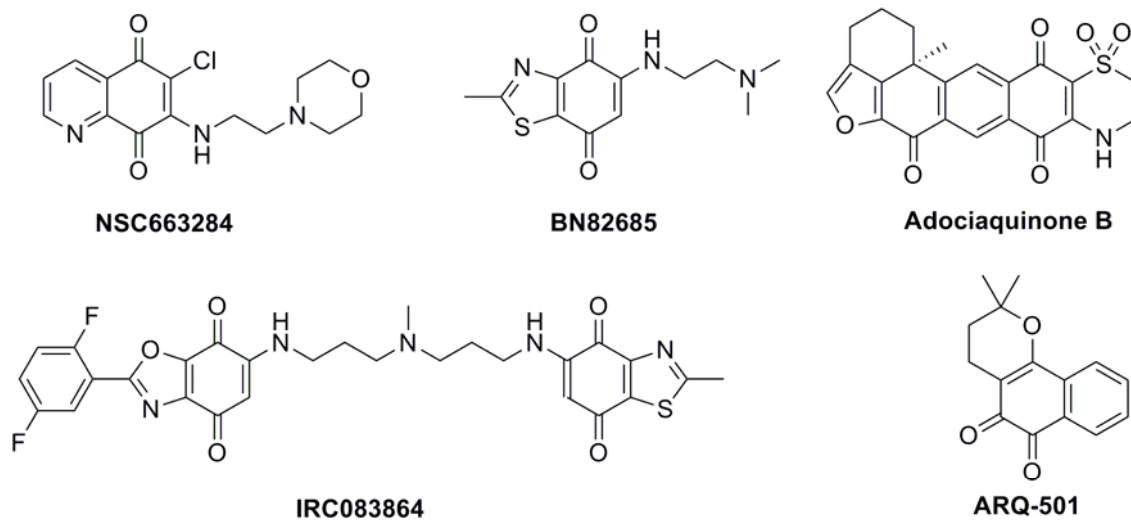


Figure 4. Structures of natural product CDC25 inhibitors.

The biological activities of these natural products inspired total syntheses as well as the preparation of synthetic analogs and chemical libraries. Synthetic inhibitors belong to various chemical classes including phosphate bioisosteres, electrophilic entities, and quinonoids. These compounds act via reversible inhibition with the active site of CDC25s [95-101], irreversible inhibition of CDC25s by electrophilic modification [102-103] or oxidation of the cysteine residue in the catalytic domain (HCX₅R) to sulfinic (Cys-SO₂⁻) or sulfonic (Cys-SO₃⁻) acid by reactive oxygen species (ROS) [104-105] (Figure 5). The number of potent inhibitors of CDC25 phosphatases that efficiently inhibit the proliferation of cancer cells and that are active in vivo on xenografted human tumors is quite limited. Compounds BN82002 [106] and BN82685 [107] impaired the growth of MiaPaCa human pancreatic carcinoma cells; furthermore, BN82685 was reported to retain its activity also when taken orally. The combination of BN82685 and paclitaxel (Taxol®) inhibits the proliferation of colon cancer cells [108],

suggesting that the synergism between CDC25 inhibitors and microtubule-targeting agents may be of therapeutic interest.

Irreversible inhibitors



Reversible inhibitors

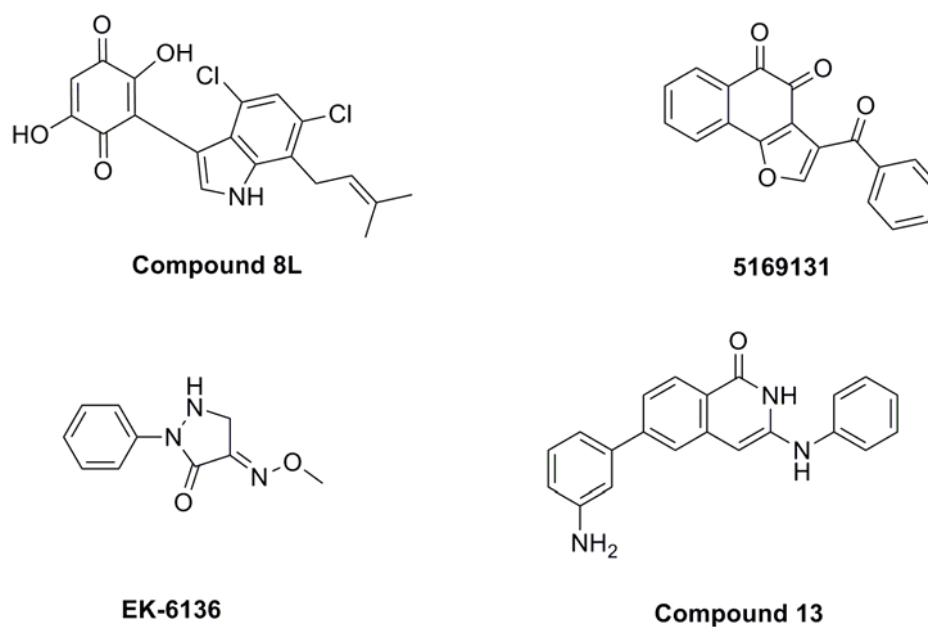


Figure 5. Structures of some representative CDC25 inhibitors

Despite more than 40 patents have been reported for CDC25 inhibitors, spanning over 20 years of drug discovery efforts [109], no therapies targeting CDC25 phosphatase are currently available in the clinic. A potent bis-quinone compound IRC-083864138 under the name Debio0931 entered a phase II clinical trial in 2009, but no data are available yet because the trial was discontinued. Another CDC25 inhibitor, ARQ-501, entered phase I clinical trials in patients with advanced and chemotherapy-unresponsive solid tumors, and is undergoing a phase II trial in patients with leiomyosarcoma and head and neck cancer, having completed an additional trial in combination with the nucleoside analog gemcitabine [110-111]. It is probable, however, that ARQ-501 is not directly a CDC25 inhibitor, but rather functions by some other mechanism. A novel approach to inhibit CDC25 phosphatase activity was recently reported by Cierpicki and co-workers. They identified a small molecule able to disrupt the protein-protein interactions between CDC25B and the Cdk2/CycA complex by fragment-based screening [112]. X-ray crystal structure revealed that this compound binds to a small but well-defined pocket, close to the hot spot region on CDC25B.

1.2 Melanoma

Melanoma is the most dangerous type of skin cancer. It arises from melanocytes, specialized pigmented cells that are found predominantly in the skin. Melanocytes reside in the basal layer of the epidermis and in the hair follicles, and their homeostasis is regulated by epidermal keratinocytes [113]. In response to ultraviolet (UV) radiation, keratinocytes secrete factors that regulate melanocyte survival, differentiation, proliferation and motility, stimulating melanocytes to produce melanin and resulting in the tanning response. Thereby, melanocytes have a key role in protecting our skin from the damaging effects of UV radiation and in preventing skin cancer. Mutations in critical growth regulatory genes, the production of autocrine growth factors and the loss of adhesion receptors all contribute to disrupting the intracellular signalling in melanocytes, allowing them to escape their tight regulation by keratinocytes. Consequently, melanocytes can proliferate and spread, leading to formation of a naevus or common mole [113]. Melanocyte proliferation can be restricted to the epidermis (junctional naevus), the dermis (dermal naevus) or overlapping components of both (compound naevus) [113]. Naevi are generally benign but can progress to the radial-growth-phase (RGP) melanoma, an intra-epidermal lesion that can involve some local microinvasion of the dermis. RGP cells can progress to the vertical-growth phase (VGP), a more dangerous stage in which the cells have metastatic potential, with nodules or nests of cells invading the dermis (Figure 6). Not all melanomas pass through each of these individual phases, as RGP or VGP can both develop directly from isolated melanocytes or naevi, and both can progress directly to metastatic malignant melanoma. Intermittent sun exposure (holiday time) and sunburns are significant risk factors for melanoma development [114].

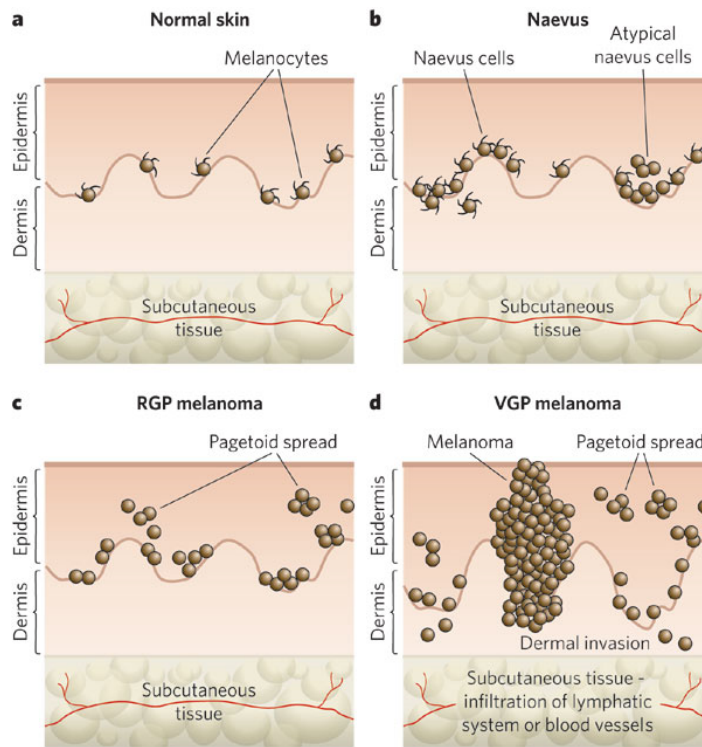


Figure 6. Progression of melanocyte transformation [113].

1.2.1 Mechanisms and pathophysiology

Transformation of melanocytes into melanoma requires a complex interplay of exogenous and endogenous events (Figure 7). Tremendous progress has been made in unravelling the genetic basis of melanoma. Melanomas carry the highest mutational load of all human tumours and harbour an overwhelming number of UV-signature mutations, such as C>T or G>T transitions, which are induced by UVB and UVA, respectively [114]. Current landscape genetic analyses provide compelling evidence for a direct mutagenic role of UVB and UVA light. However, UV-independent secondary cofactors are also involved in melanoma development. In fact, melanomas can develop in non-sun-exposed skin or in internal organs [114]. The mitogen-activated protein kinase (MAPK) cascade is currently the pathway that has the highest oncogenic and therapeutic relevance for melanoma; most mutations in this pathway are not directly attributable to UV damage [114]. The classic MAPK pathway in cutaneous melanoma transmits mitogenic signals from growth factors, such as hepatocyte growth factor (HGF), platelet-derived growth factor (PDGF) and fibroblast growth factor (FGF), via

transmembrane receptor tyrosine kinases (RTKs) to the nucleus and transcriptional targets, such as cyclin D1. The MAPK signalling module comprises the small G protein Ras, which is attached to the inner leaflet of the plasma membrane, Raf, MEK and ERK, cytosolic protein kinases.

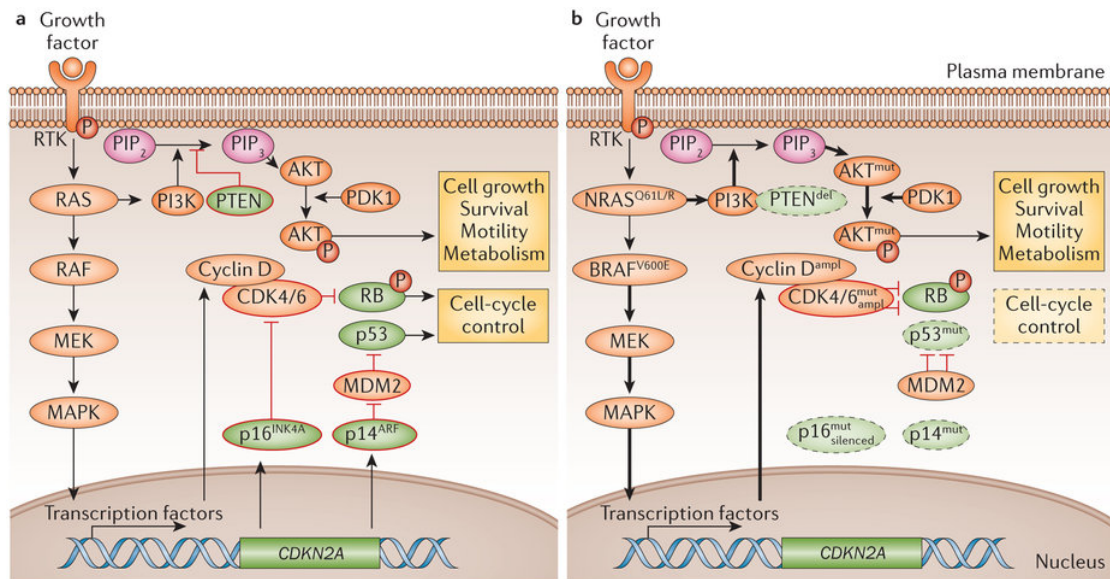


Figure 7. Signalling pathways in melanoma. A) Under normal conditions, mitogen-activated protein kinase (MAPK) and phosphatidylinositol 3-kinase (PI3K)–Akt signalling permit balanced control of basic cellular functions, including cell-cycle regulation, survival, motility and metabolism. B) In melanoma, the depicted genetic alterations are frequently observed, and lead to constitutive pathway activation (indicated by thick arrows) and loss of cellular homeostasis. Adapted from [114].

Common mutations without typical UV signatures include BRAF^{V600E} (detectable in ~50% of all melanomas), NRAS^{Q61L} or NRAS^{Q61R}, KIT^{V559A} and GNA11^{Q209L} mutations in GNAQ and GNA11 (which encode the guanine nucleotide-binding proteins Gαq and Gα11). Genetic evidence in melanoma also supports cooperation between cooperation between the MAPK pathway and the signalling pathway mediated by phosphatidylinositol 3-kinase (PI3K), AKT, PTEN (phosphatidylinositol-3,4,5-trisphosphate 3-phosphatase and dual-specificity protein phosphatase) and mammalian target of rapamycin (mTOR) as a cancer trigger [114]. PI3K can be activated by multiple signals, including RTKs and RAS, and subsequently phosphorylates phosphatidylinositols in the plasma membrane, which attract the RAC serine/threonine-

kinases Akt1, Akt2 and Akt3. The Akts are then activated by phosphorylation through 3-phosphoinositide-dependent protein kinase 1 (PDK1) and mTOR complex 2 (mTORC2). Activated Akts phosphorylate numerous downstream targets that regulate key cellular processes, such as growth, survival, motility and metabolism. The phosphatase PTEN antagonizes the activity of PI3K. The combination of mutated BRAF and focal deletions or mutations of PTEN is observed in most melanoma cell lines and also in up to 40% of human melanomas. It has been suggested that these mutations represent primary steps in the transformation of melanocytes that lead to oncogene-induced senescence. Senescence is a key cellular protection mechanism against cancer that halts aberrant cell proliferation. Cancer cells override senescence by inactivating key pathways such as those regulating p16^{INK4a}/Rb (retinoblastoma protein) and p53. Full development of melanoma might require secondary or tertiary genetic aberrations to overcome senescence. For example, mutations in MAPK signaling and aberrations in cell-cycle control genes, such as CDKN2A (a locus that encodes the tumour suppressors p16^{INK4a} and p14^{ARF}), CDK4 and CCND1 (which encodes for cyclin D1) cooperate efficiently. Wild-type p16^{INK4A} maintains cell-cycle control by inhibiting cyclin-dependent kinase 4 (CDK4) or CDK6-mediated phosphorylation and inactivation of retinoblastoma-associated protein (Rb), whereas functional p14^{ARF} prevents ubiquitylation mediated by the E3 ubiquitin-protein ligase MDM2 and the subsequent degradation of cellular tumour antigen p53 (which is encoded by TP53). Thus, inactivating mutations in CDKN2A promote G1–S cell-cycle transition by loss of two important regulators of cellular homeostasis, Rb and p53. Furthermore, loss of function of other cell cycle inhibitors, such as p21^{CIP1} and p27^{KIP1} results in enhanced cyclin E/CDK2 activity that positively feeds back on itself and on CDK4/6 via CDC25. In particular, CDK2 is significantly and consistently overexpressed in metastatic melanomas (three to eight times more than in benign naevi), with the active and dephosphorylated form of this kinase being detected in metastatic melanoma tissues and melanoma cell lines [115]. CDC25A expression is much higher in the metastatic tumours and melanoma cell lines [115]. It was postulated that abnormal CDC25A expression or function in melanoma might be one of the initial steps in melanoma development [115].

For successful tumour development, melanoma cells modulate the tissue environment and, in particular, the immune response through a myriad of mechanisms. For example, melanomas co-opt immune-checkpoint pathways that normally mediate self-tolerance. By expression of programmed cell death protein 1 ligand 1 (PDL1; also known as B7-H1 and CD274) and PDL2, which are the ligands of the surface receptor programmed cell death protein 1 (PD1), melanoma cells limit T cell effector activity in the tumour tissue [114]. Alongside T cells, B cells and natural killer (NK) cells also express PD1 and are, therefore, also affected. By contrast, cytotoxic T lymphocyte protein 4 (CTLA4) is expressed exclusively on T cells, where it primarily dampens the amplitude of the initial T cell activation that occurs after antigen presentation by dendritic cells in the lymph nodes [114]. Additional mechanisms involved in immunosuppression are downregulation of tumour-associated antigens and MHC class I molecules, as well as immuno-editing and secretion of inhibitory factors such as transforming growth factor- β (TGF- β), interleukin-10 (IL-10) or nitric oxide [114].

1.2.2 Cell cycle alterations in melanoma: the role of CDC25

Full development of melanoma might require secondary or tertiary genetic aberrations to overcome senescence. For example, mutations in MAPK signaling and aberrations in cell-cycle control genes, such as CDKN2A (a locus that encodes the tumour suppressors p16^{INK4a} and p14^{ARF}), CDK4 and CCND1 (which encodes for cyclin D1) cooperate efficiently (Figure 7) [114]. Wild-type p16^{INK4A} maintains cell-cycle control by inhibiting cyclin-dependent kinase 4 (CDK4) or CDK6-mediated phosphorylation and inactivation of retinoblastoma-associated protein (Rb), whereas functional p14^{ARF} prevents ubiquitylation mediated by the E3 ubiquitin-protein ligase MDM2 and the subsequent degradation of cellular tumour antigen p53 (which is encoded by TP53) [114]. Thus, inactivating mutations in CDKN2A promote G1–S cell-cycle transition by loss of two important regulators of cellular homeostasis, Rb and p53. Phosphorylation of Rb leads to release of its associated protein, E2F transcriptional factor, which has the capability to activate the genes necessary for progression through the G1 phase. Loss of function of other cell cycle inhibitors, such as p21^{CIP1} and p27^{KIP1} results in enhanced cyclin E/CDK2 activity that positively feeds back on itself

and on CDK4/6 via CDC25 (Figure 8) [116]. In particular, CDK2 is significantly and consistently overexpressed in metastatic melanomas (three to eight times more than in benign naevi), with the active and dephosphorylated form of this kinase being detected in metastatic melanoma tissues and melanoma cell lines [115]. CDC25A expression is much higher in the metastatic tumours and melanoma cell lines [115]. It was postulated that abnormal CDC25A expression or function in melanoma might be one of the initial steps in melanoma development [115].

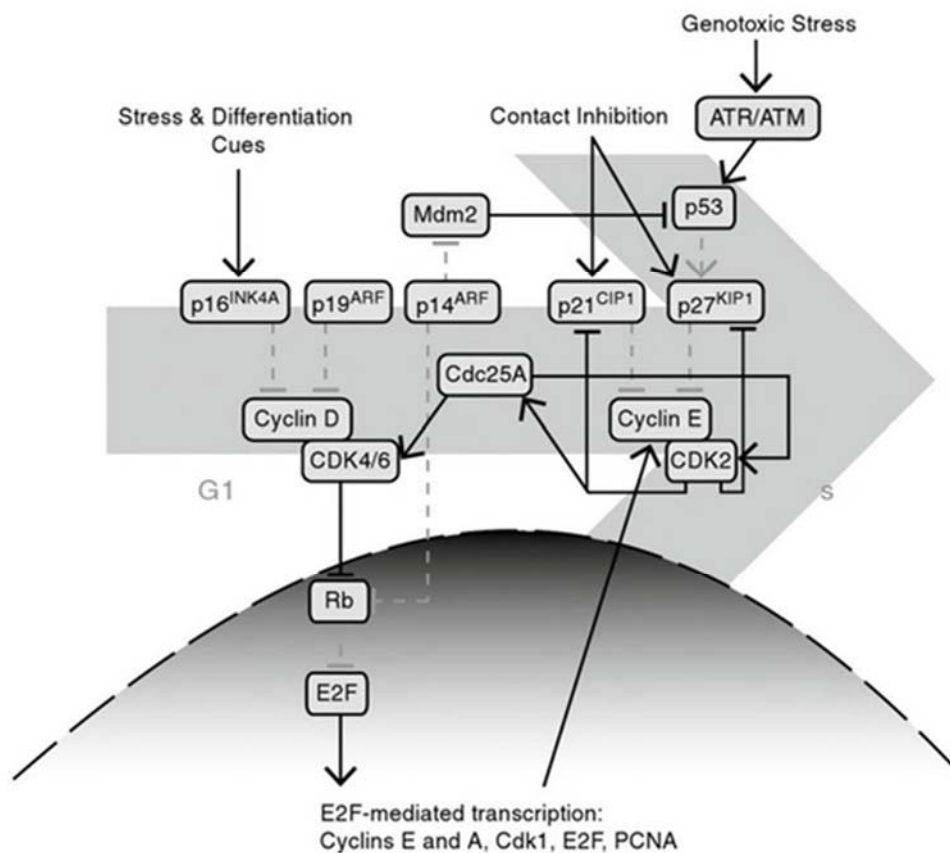


Figure 8. Cell cycle regulation and melanoma. Branches of the cell cycle that are upregulated in melanoma appear in black; downregulated branches appear in dashed gray. Adapted from [115].

1.2.3 Therapeutic treatment of melanoma

If melanoma is diagnosed early, it can be cured by surgical resection, and about 80% of cases are dealt with in this way [113]. More advanced melanomas can be much harder to treat. Over several years, the standard treatment in clinical trials for metastatic

melanoma patients was the use of single-agent chemotherapy (dacarbazine, temozolomide or fotemustine) which offers a marginal clinical benefit [117]. Melanoma treatment options have evolved rapidly and include targeted therapeutics and immune checkpoint inhibitors.

Targeted therapies

After the discovery of the mutation in BRAF as a therapeutic target for those patients with metastatic melanoma, different BRAF inhibitor drugs have been tested in a clinical context with significant benefits in terms of increased response rate, increased progression-free survival (PFS) and increased overall survival (OS) in patients with the presence of a BRAF mutation. Within the classification of these drugs, two groups can be highlighted: non-selective BRAF inhibitors and selective BRAF inhibitors [117].

Non-selective BRAF inhibitors

Sorafenib was the first BRAF inhibitor drug to undergo clinical testing in patients with metastatic melanoma. It has an activity directed toward multiple protein kinases as BRAF, CRAF, VEGF and PDGF in a non-selective manner. The clinical utility of sorafenib in melanoma has been proved to be very limited [117].

Selective BRAF inhibitors

Vemurafenib (PLX4032 and its analog PLX4720) is an oral drug, which inhibits the growth of cells that have mutations in BRAF^{V600E} by blocking the activation of MAPK kinase pathway with subsequent cell senescence in the G1 phase of the cycle and apoptosis. It was approved by the Food and Drug Administration (FDA) and the European Medicines Agency (EMA) for those patients with unresectable or metastatic melanoma BRAF^{V600E} mutation carriers. Dabrafenib is another selective inhibitor of BRAF^{V600E} and BRAF^{V600K} mutations, which has shown comparable results to those, obtained with treatment with vemurafenib. Generally BRAF inhibitors are well tolerated with few potentially serious side effects. The most common side effects include skin changes, fatigue, diarrhea and nausea. The major side effect associated with BRAF inhibitors is the development of cutaneous squamous cell carcinomas and

keratoacanthomas. These lesions, which have a very fast growth, can be managed effectively by surgical removal without further evidence of recurrence [117]. Unfortunately, nearly all patients treated with BRAF inhibitors experience disease progression during the first 1 to 2 years of therapy. Therefore, elucidating mechanisms of acquired resistance has been a major clinical and research focus. Unlike many other cancers, resistance in BRAF-mutant melanoma is not the result of second site mutations in the target gene, BRAF. Instead, a diverse array of resistance mechanisms has been uncovered, largely involving acquired alterations in the MAPK pathway or parallel signaling networks. As such, attention has shifted to BRAF inhibitor–MEK inhibitor combinations targeting distinct MAPK pathway components.

MEK Inhibitors

Single-agent MEK inhibitors also have activity in BRAF^{V600} mutant melanoma. There are several MEK inhibitor drugs that have been tested in clinical trials for patients with metastatic or unresectable melanoma, among which there are selumetinib (AZD6244), PD-0325901, trametinib (GSK1120212), AS703026, cobimetinib (GDC-0973/XL518) and MEK162 [117]. To date, no MEK inhibitor has demonstrated clinical effectiveness such as objectified with BRAF inhibitors. Only the MEK inhibitors trametinib, cobimetinib and MEK 162 have shown, in the clinical setting and in combination with BRAF inhibitors, increased activity in melanomas carriers of BRAF^{V600E} mutations [117]. Although trametinib was approved by the FDA in 2013, it is rarely used as monotherapy because of presumably inferior efficacy compared with single-agent BRAF inhibitors. Newer MEK inhibitors are also being evaluated currently (cobimetinib, binimetinib) [118]. Combination of BRAF and MEK inhibitors has supplanted single-agent BRAF inhibitors as the preferred targeted therapy strategy for patients with BRAF^{V600} mutated melanoma. A phase II clinical trial compared dabrafenib and trametinib, combined at full monotherapy doses, with dabrafenib alone. Progression-free survival was significantly improved with combination therapy. On the basis of this study, dabrafenib and trametinib received FDA approval in early 2014.

Immunotherapies

Immune therapy agents, starting with high-dose interleukin 2 (IL-2) and now with newer immune checkpoint inhibitors, are a cornerstone of melanoma therapeutics [118]. Another agent enhancing the immune system is interferon alpha (IFN- α), that showed a statistically significant improvement in both disease-free survival (DFS) and OS in adjuvant treatment of patients with high-risk cutaneous melanoma.

Anti-CTLA4

Ipilimumab is a monoclonal antibody to cytotoxic T lymphocyte antigen 4 (CTLA4) and was the first agent to demonstrate an OS advantage in melanoma [118]. Ipilimumab blocks this negative regulator of T-cell activation and thus promotes previously inhibited immune responses. Development of tremelimumab is now ongoing in combination with other immune therapies. Ipilimumab received FDA approval in 2011 and is an appropriate first-line treatment option for patients with or without BRAF mutations. The acute toxic effects of ipilimumab therapy are well characterized and quite distinct from those of both IL-2 and cytotoxic chemotherapy.

Anti-PD-1/PD-L1

Antibodies to PD-1 (nivolumab, pembrolizumab) or its ligand (PD-L1; MPDL3280A, MEDI4736) have also been recently tested in melanoma [118]. PD-L1 is frequently expressed by numerous malignant neoplasms as a mediator of immune escape. The interaction between PD-1 and PD-L1 induces T-cell anergy and ineffective antitumor responses in the so-called exhausted T cell. Inhibiting this interaction, therefore, restores T-cell function in the tumor microenvironment. At this time, the most effective target in this axis (PD-1 or PD-L1) is not clear. These agents, however, each have substantial clinical activity. Both pembrolizumab (MK-3475 a fully humanized IgG4 monoclonal antibody) and nivolumab (BMS-936558, a fully human IgG4 monoclonal antibody) have received FDA approval for melanoma therapy following progression after ipilimumab and BRAF-targeted therapy for patients with *BRAF* V600 mutations.

Combined Immune Therapy Strategies

Because ipilimumab and anti-PD-1–directed therapies remove negative T-cell regulators at distinct phases of T-cell activation, combining these therapies was suggested as a synergistic approach [118]. Preclinical studies also demonstrated more effective antitumor activity in mouse models. The encouraging activity of these combination regimens has also led to a number of other anti-PD-1/PD-L1 combination approaches now being evaluated in early-phase trials, largely involving other immune modulators or targeted therapies. In contrast to BRAF and MEK inhibitors, no clearly defined biomarkers exist for predicting the outcome of immune therapies although there are several promising candidate approaches. Developing immune biomarkers will be a critical objective to improve clinical trial design and treatment decision making.

Future strategies

Restoration of disabled cell-cycle control emerges as a prime therapeutic goal for the majority of patients with melanoma [114]. Inhibitors of CDK4/6, MDM2, and ERK1/2 are particularly intriguing, especially in combination with MEK and/or BRAF inhibitors. Over the next years, the focus will be on understanding how resistance to targeted therapies develops and how to overcome potential crosstalk with other signalling pathways, leading to optimized patient selection and enhanced synergy of combination regimens.

1.3 Aim of the work

Recently, Lavecchia *et al.* discovered a new series of CDC25 inhibitors by means of a structure-based virtual screening [38]. Among them, the most promising were

1. Compound **11**, 3-(4,5,6-trihydroxy-3-oxo-3H-xanthen-9-yl)-propanoic acid (NSC 119915), displaying irreversible inhibition kinetics with in vitro K_i values for CDC25A and CDC25B of 0.07 and 0.08 μM , respectively;
2. Compound **19**, 4-(2-carboxybenzoyl)phthalic acid (NSC 28620), displaying reversible inhibition kinetics with in vitro K_i values for CDC25A and CDC25B of 2.3 and 5.3 μM , respectively.

Both compounds arrested cells at the G_0/G_1 and G_2/M phases of the cell cycle, increased Cdk1 hyperphosphorylation in K562 leukemia cells, and significantly suppressed the growth of human MCF-7 breast, PC-3 prostate cancer lines as well as K562 leukemia cells, thus representing novel interesting leads.

The aim of this thesis project was

1. Identification of more active analogs of compound **11** by ligand-based chemoinformatic selection in order to expand our understanding of structure-activity relationships (SARs) within the 6-xanthone class of CDC25 inhibitors and to examine their activity against melanoma cancer cell lines, as well as the mechanism of action involved;
2. Optimization of compound **19** by structure-based drug design in order to improve its binding affinity and pharmacokinetic properties as well as to investigate its anti-melanoma effects.

2. Results and discussion

2.1 Ligand-based chemoinformatic selection of new analogs of compound 11

2.1.1 Similarity search using molecular fingerprints

In order to identify novel structural analogs of lead compound NSC 119915 with increased CDC25 inhibitory potency, we applied different chemoinformatic approaches [119-120] against both the ZINC drug-like library and the NCI lead-like set. The general workflow is presented in Figure 9. The first five VS approaches employed molecular fingerprints, which are binary vectors encoding the presence, or absence, of substructural fragments within the molecule and have been successful in recognizing similar molecules in large databases [121].

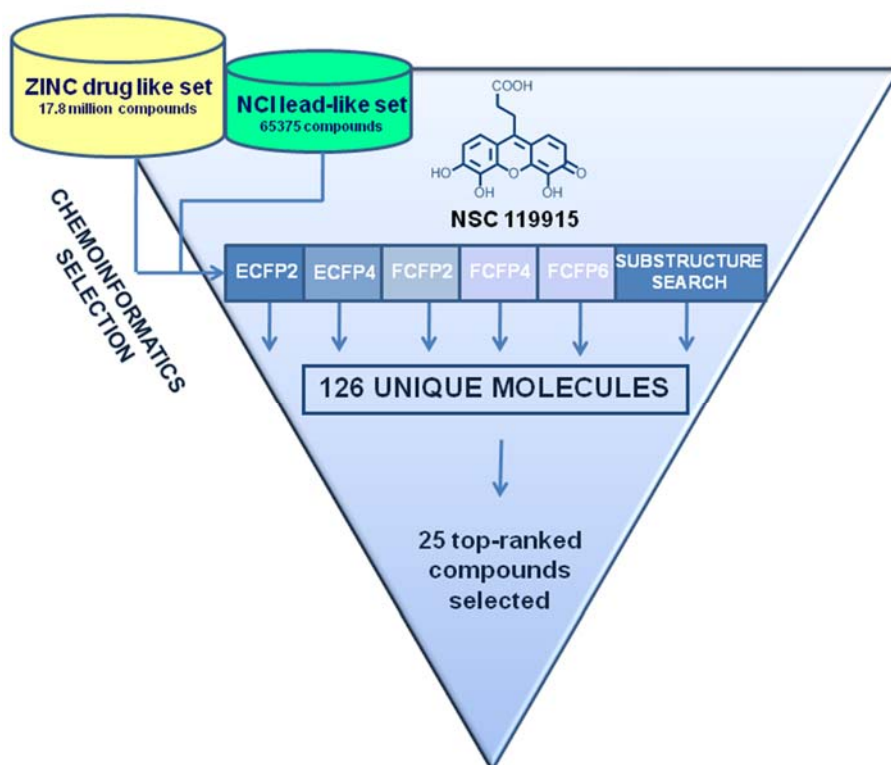


Figure 9. Flow chart of the multiple ligand-based chemoinformatic strategy implemented in this work.

We employed ECFP2, ECFP4, FCFP2, FCFP4, and FCFP6 to identify close active analogs to our lead NSC 119915, using the Tanimoto coefficient as similarity measure. Extended Connectivity Fingerprints (ECFPs) have been shown to have a number of strengths that make them useful for similarity searching. ECFPs are a fingerprint methodology explicitly designed to capture molecular features relevant to molecular activity. They can be quickly calculated, as they are not defined a priori [122]. Functional Class Fingerprints (FCFPs) are a related fingerprint to ECFPs but instead of using a specific atom identifier for the initial atom in the algorithm to generate the fingerprint, FCFPs use a more abstract pharmacophoric set of initial atom identifiers based on properties such as H-bond acceptor (HBA) and donor (HBD), negatively and positively ionizable, aromatic, and halogen [122]. To enhance the probability of finding 50% of all possible actives, we used the threshold values suggested by Muchmore et al. [123]. The entire process was automated in a custom protocol using Pipeline Pilot 9.2 (Figure 10). So, a Tanimoto threshold of 0.52 for ECFP2 allowed the selection of 13 compounds, whereas a Tanimoto threshold of 0.43 for ECFP4 gave 12 compounds. For FCFP2, a Tanimoto threshold of 0.75 provided 16 compounds; for FCFP4, a Tanimoto threshold of 0.60 gave 5 compounds; and for FCFP6, a Tanimoto coefficient of 0.45 highlighted 8 compounds. Thus, the combination of these five FP methods would hopefully maximize the chances of identifying compounds that were sufficiently similar to our lead compound to display inhibition of CDC25 phosphatases.

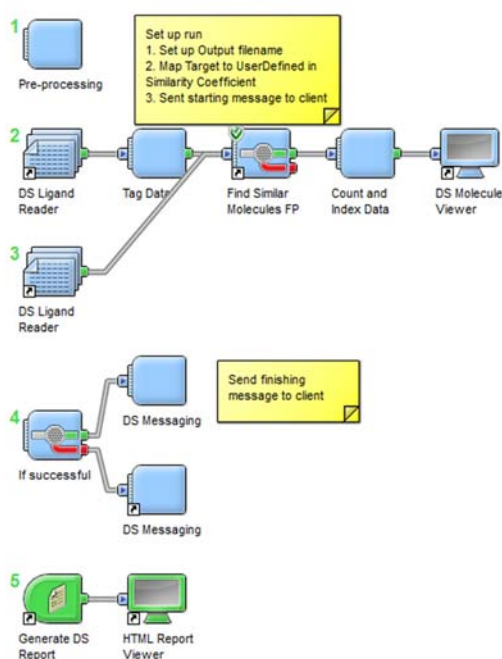


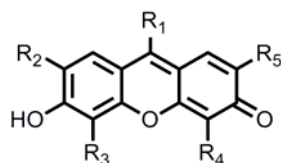
Figure 10. The protocol employed for similarity search by molecular fingerprints.

2.1.2 Substructure search

The sixth method utilized was the substructure search, using the core structure of NSC 119915. By definition, a substructure search identifies molecules that contain a defined molecular fragment, that is, a certain substructure. Of course, such a search will not lead to new scaffolds, but will allow the finding of close analogs and possible variations in the decoration of known molecule classes. A simple substructure searching via SMILES Arbitrary Target Specification (SMARTS) pattern implemented in Schrödinger Canvas 1.9 was used to filter both ZINC drug-like and NCI lead-like collections, using as query the following SMILES notations: [O = c3ccc2cc1cccc1oc2c3], [O = c3ccc2cc1cccc1[nH]c2c3] and [O = c3ccc2cc1cccc1sc2c3]. The substructure search identified 137 scaffold isosteres of our lead core structure. The results of the six VS techniques were combined, and a significant number of identical compounds were removed; this overall strategy led to a final total of 126 unique compounds that were predicted by one or more methods to be similar in some way to our active compound. Then, we selected the top-ranked 25 compounds that were purchased or requested from the NCI Developmental Therapeutics

Program (DTP) (Table 1). Our decision to select the top-ranked compounds was to ensure testing of any highly similar (and therefore likely to be active) compound.

Table 1. Compounds identified by multiple ligand-based chemoinformatic protocol.



Cpd	Code	R ₁	R ₂	R ₃	R ₄	R ₅	Cpd	Code	R ₁	R ₂	R ₃	R ₄	R ₅
1	NSC 158113	CH ₃	H	H	H	H	14	NSC 4202		H	I	I	H
2	ZINC 04015433	CH ₃	OH	H	H	OH	15	NSC 4905		I	I	I	I
3	NSC 158115	COOH	H	H	H	H	16	ZINC 04409973		H	Cl	Cl	H
4	NSC 158112	CH ₂ CH ₂ COOH	H	H	H	H	17	ZINC 04352921		H	Br	Br	H
5	NSC 119894	CH=CHCOOH	H	H	H	H	18	NSC 2087		Br	Br	Br	Br
6	NSC 119911	CH=CHCOOH	H	OH	OH	H	19	ZINC 04261930		NO ₂	Br	Br	NO ₂
7	NSC 119892		H	H	H	H	20	ZINC 03861600		H	OH	OH	H
8	NSC 119910		H	OH	OH	H	21	NSC 119893		H	OH	OH	H
9	ZINC 03860685		OH	H	H	OH	22	ZINC 04822213		OH	H	H	OH
10	ZINC 13597410		OH	H	H	OH	23	ZINC 04582279		H	H	H	H
11	ZINC 05030632		H	H	H	H	24	NSC 119912		H	OH	OH	H
12	NSC 119888		H	H	H	H	25	NSC 119916		H	OH	OH	H
13	ZINC 05030658		H	H	H	H							

2.1.3 Biological evaluation

The inhibitory activity of the twenty-five structures identified from the multiple ligand-based chemoinformatic approach was evaluated by a fluorimetric assay. The residual phosphatase activity of a recombinant form of CDC25B was measured in the presence of two different concentrations of these compounds (Table 2). Eight compounds (**2**, **10**, **12–14**, and **16–18**) were excluded from the analysis, because endowed with a strong fluorescent signal. Compounds **5-9**, **21**, **24**, and **25** exerted a concentration-dependent inhibition of the CDC25B phosphatase activity, with a percentage of inhibition comparable to that exhibited by the lead compound NSC 119915. The rest of the compounds caused a measurable inhibition only at the highest concentration. So, only compound **3** was included in the following analysis.

Table 2. Residual phosphatase activity of CDC25B in the presence of NSC 119915 or its 6-xanthone analogs.

Compound	CDC25B residual activity (%) in the presence of [inhibitor]	
	0.2 μ M	1 μ M
1	76	9
3	85	62
4	90	28
5	12	2
6	14	2
7	44	1
8	10	1
9	9	0
11	89	44
15	79	18
19	86	70
20	91	24
21	13	1
22	80	0
23	80	14
24	22	3
25	24	1
NSC 119915	38	2

Kinetic analyses revealed that these nine compounds inhibited the three different CDC25 proteins in a noncompetitive manner with K_i values comparable to those of the lead compound NSC 119915 (Table 3). The K_i towards CDC25A ranged between 0.01 and 0.80 μM , and the corresponding intervals for CDC25B and CDC25C were 0.12–2.4 μM and 0.30–4.4 μM , respectively.

Table 3. K_i values of NSC 119915 or its 6-xanthone analogs towards CDC25-A, -B and -C phosphatases.

Compound	K_i		
	CDC25A	CDC25B	CDC25C
3	0.28± 0.09	2.4±0.39	4.4±0.62
5	0.38±0.12	0.12±0.05	0.39±0.15
6	0.10±0.03	1.1±0.37	1.0±0.41
7	0.65±0.04	0.78±0.03	3.1±0.22
8	0.17±0.07	0.19±0.08	0.30±0.12
9	0.80±0.31	0.44±0.2	1.5±0.48
21	0.14±0.06	0.14±0.05	0.63±0.14
24	0.01±0.005	0.3±0.08	0.40±0.11
25	0.40±0.15	1.1±0.4	0.96±0.38
NSC 119915	0.34±0.12	0.10±0.04	0.24±0.13

Concerning the mechanism of inhibition, the kinetic measurements showed that the tested compounds behaved similarly to the lead compound NSC 119915 [38], as noncompetitive inhibitors.

As CDC25 phosphatases, in combination with other cell cycle regulators, have been proved to be of determinant significance for melanoma growth and/or transformation [115,124], we evaluated the effects of NSC 119915 and its close analogs on the growth rate of two melanoma cell lines, A2058 and SAN (Figure 11). Although analogs **6** and **24**, and NSC 119915 in some experimental conditions, caused a significant reduction of the cell growth rate in SAN cells, compound **7** [2-(6-hydroxy-3-oxo-3*H*-xanthen-9-yl)cyclohexanecarboxylic acid] resulted as the only common inhibitor of the cell growth rate of both A2058 and SAN melanoma cells. The failure of compounds **3**, **5**, **8**, **9**, **21** and **25** to inhibit cell proliferation despite their potent inhibition of all three CDC25 phosphatases could be due to poor permeability into cells, chemical instability,

unfavorable compartmentalization, active metabolism into inactive compounds, presence of unidentified binding proteins, or a combination of these factors.

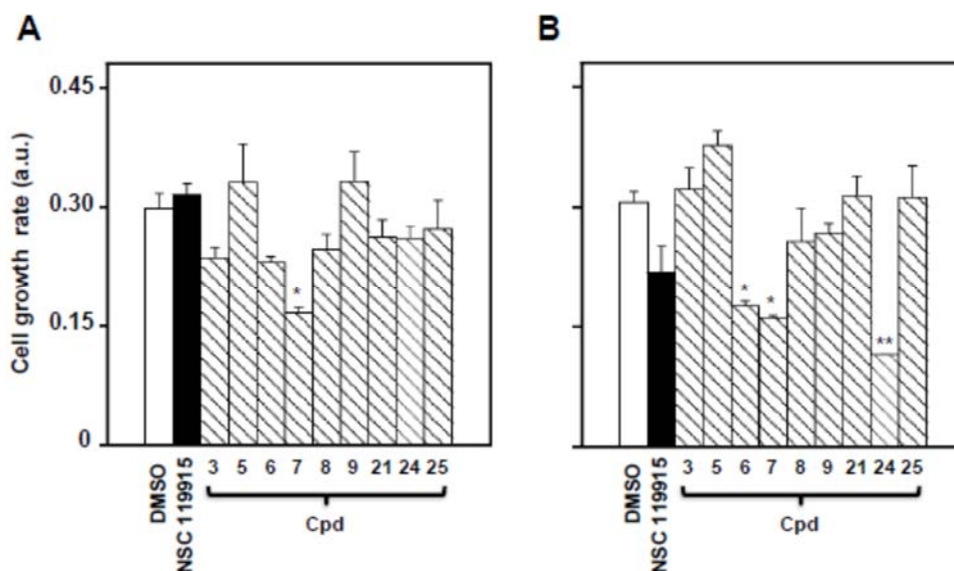


Figure 11. Effect of NSC 119915 and its close analogs on cell growth rate of melanoma cell lines A) A2058 and B) SAN.

Thus, **7** was selected as the most promising compound for further investigation of its anti-melanoma effects. The minimum concentration of inhibitor that caused an evident cytotoxic activity was 100 μ M, as demonstrated for compound **7**. Therefore, this concentration was almost thoroughly used in the following experiments.

As CDC25 phosphatases are key cell cycle regulators, the effect of **7** on cell cycle progression was investigated in detail. To this aim, asynchronously growing A2058 and SAN cells were treated at different times with 100 μ M compound **7**, and then cell cycle analysis was cytofluorimetrically monitored after propidium iodide (PI) incorporation. A significant reduction of the G0/G1 phase and an increase of the G2/M phase occurred in both melanoma cell lines after 16-h treatment and continued up to 24-h (Figure 12). The effect of **7** on cell growth and cycle progression could suggest the beginning of a cell death program, a hypothesis investigated through various methodological approaches.

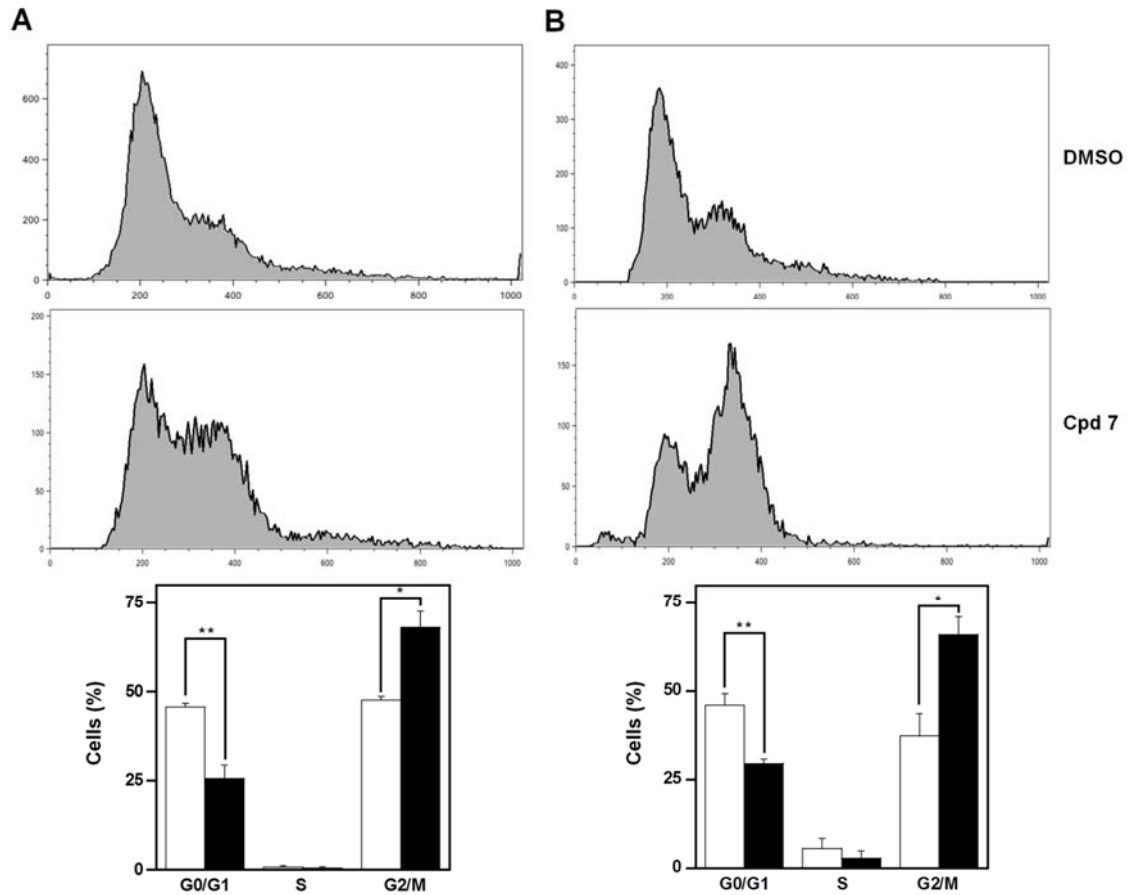


Figure 12. Effect of compound 7 on the distribution of cell cycle phases of A2058 cells after A) 16 h or B) 24 h treatment. Vehicle alone, open bars; compound 7, black bars.

We evaluated if the treatment of A2058 cells with compound 7 affected the protein levels of the three CDC25 isoforms. Compound 7 provoked an early reduction of the CDC25A protein levels up to 4 h, compared to untreated cells (Figure 13). This reduction disappeared under prolonged incubation times. Furthermore, a progressive and significant reduction of CDC25C protein levels was also observed. These overall results suggest that the modulation of the CDC25 protein levels induced by 7, in particular of the -A and more evidently of the -C form, could be related to the arrest of melanoma cells in G2/M observed in the presence of this inhibitor.

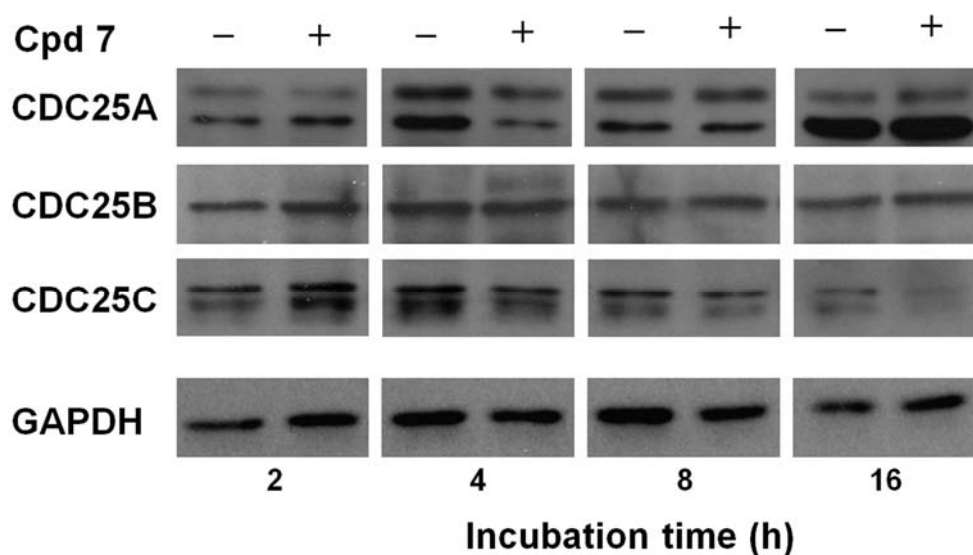


Figure 13. Effect of compound 7 on CDC25A, B and C protein levels.

PI incorporation followed by flow cytometric analysis was used to detect the effect of 7 on the number of nuclei with a sub-diploid content, a typical hallmark of apoptosis. A time-dependent increase of apoptosis was evident in both A2058 and SAN cells and in particular, the effect of 7 on cell death program was already evident after 24-h treatment (Figure 14). In A2058 cells the increase of apoptosis became significant at 48 h, and continued at least up to 72-h incubation (Figure 14A). In SAN cells a similar behaviour was observed and the increase of apoptosis was significant even at 24-h treatment (Figure 14B). To further investigate on the capacity of 7 to induce apoptosis, the enzymatic activity of caspase-3, the final effector of apoptotic program, was monitored. Indeed, this inhibitor provoked a significant increase of the enzymatic activity of caspase-3 in both A2058 (Figure 14C) and SAN cells (Figure 14D). To confirm that the pro-apoptotic effect of 7 was caspase-mediated, the 48-h treatment of A2058 and SAN cells with compound 7 was also carried out in the presence of an irreversible pan-caspase inhibitor, such as Z-VAD-FMK. The level of apoptosis caused by 7 was significantly decreased in the presence of this inhibitor in both A2058 and SAN cells, thus demonstrating that the pro-apoptotic effect of 7 was mainly caspase-dependent. Taken together, all these data support the hypothesis that cell cycle arrest in G2/M phase caused by 7 could evolve in an apoptotic process. It is known that quinonoid

structures, as those of the most active CDC25 inhibitors, are good substrates for the beginning of a redox cycle, and that an increased ROS level may cause severe damages to the CDC25 structure [104,125-126]. Indeed, compound **7** increased the intracellular ROS levels in both A2058 (Figure 15) and SAN cell lines. The oxidant effect of **7** was also evaluated after cell pre-treatment with the antioxidant N-acetyl-cysteine (NAC).

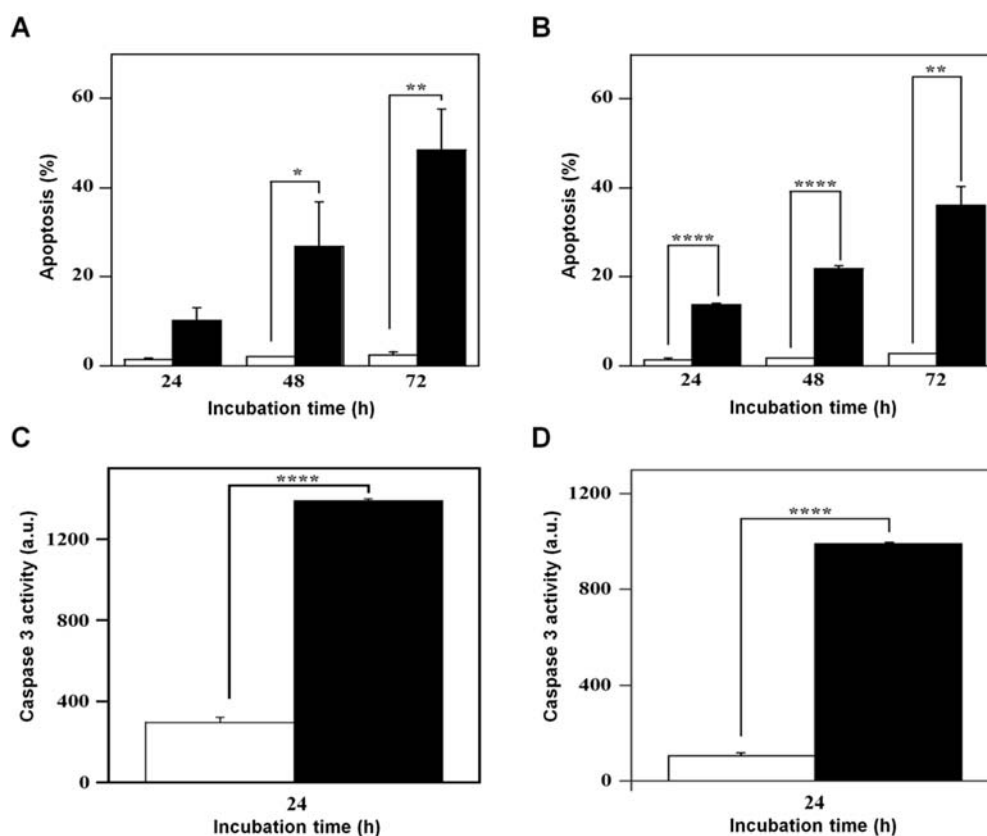


Figure 14. Effect of compound **7** on the apoptosis of A2058 (panels A and C) and SAN cells (panels B and D).

Pre-incubation of A2058 and SAN cells with an anti-oxidant molecule prevented the apoptotic process; indeed, the apoptosis was in a great part reverted by the cellular pre-treatment with NAC. Taken together, all these findings suggest that **7** altered the intracellular redox state of melanoma cells, thus mediating the observed cytotoxicity.

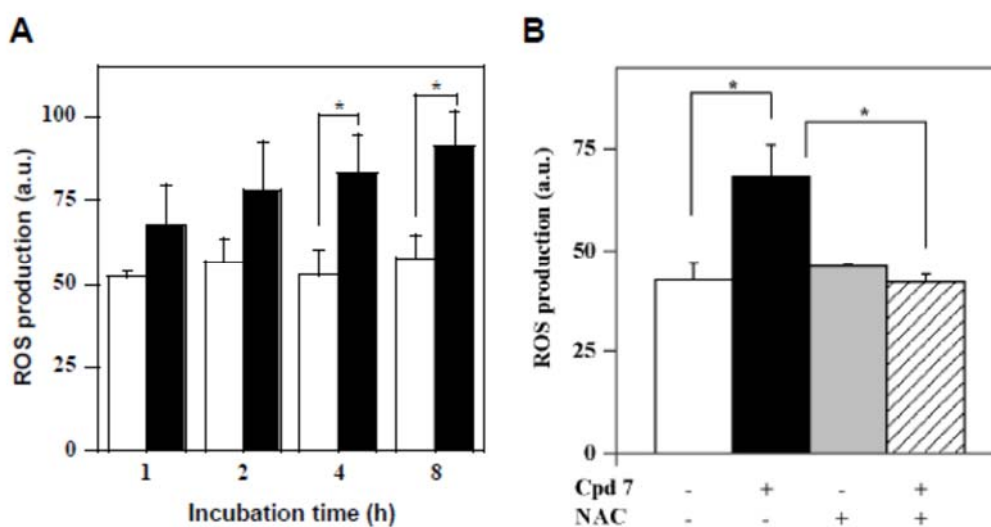


Figure 15. A) Time-dependent measurement of ROS production. B) Effect of the antioxidant NAC on ROS production.

Mitochondria represent the primary source of ROS, as well as the target of ROS action, and therefore, compound **7** could affect their functionality in melanoma cells. A decrease of the fluorescent signal, corresponding to a reduction of the mitochondrial membrane potential, was already evident after 24-h treatment of A2058 cells with **7** and then continued at least up to 72 h (Figure 16A). Proteins belonging to the B-cell lymphoma-2 (Bcl-2) family are involved in the modulation of the mitochondrial functionality [127-128]. Therefore, we have evaluated the levels of the anti-apoptotic protein Bcl-2, as well as that of the pro-apoptotic Bcl-2-associated X protein (Bax), after incubation of A2058 cells with **7** (Figure 16B). We observed a clear reduction of the Bcl-2 level and an increase of Bax level. Moreover, the densitometric analysis also revealed a significant reduction of the Bcl-2/Bax ratio after 8 and 16 h of incubation with **7**, a useful index to evaluate apoptosis (Figure 16C). To further investigate the occurrence of a mitochondrial-mediated apoptosis induced by **7**, the caspase-9 activity was assayed. A clear increase of caspase-9 activity was measured in A2058 cells after 24-h incubation with **7** (Figure 16D). The observed increase of ROS levels, as well as the decrease of the crucial parameter for controlling life and death of a cell, *i.e.* the Bcl-2/Bax ratio, are clear markers of an involvement of the mitochondrion in the apoptotic program triggered by **7** in melanoma cells.

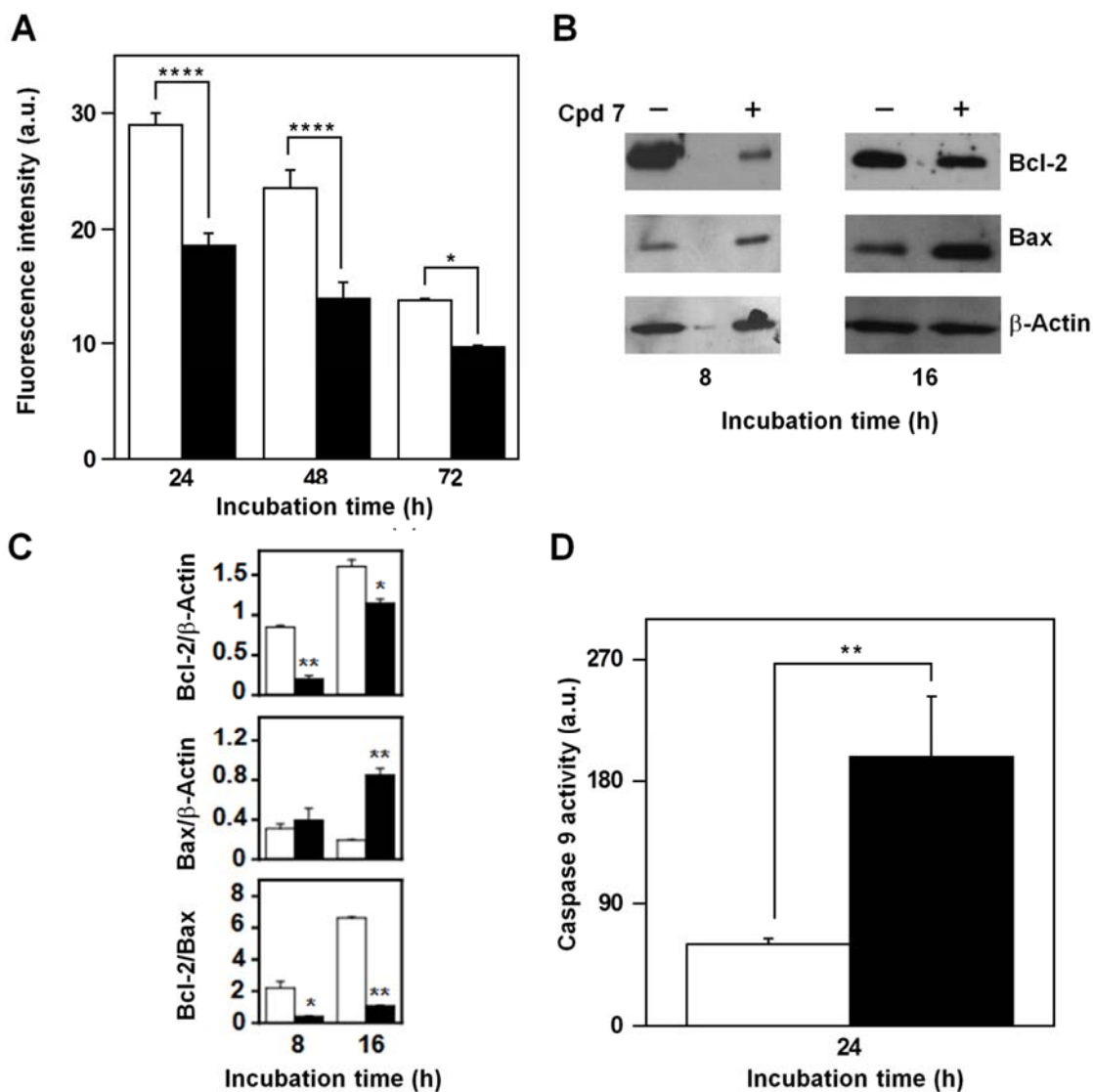


Figure 16. Effect of compound 7 on some apoptotic mitochondrial markers in A2058 cells. A) Measurement of the mitochondrial membrane depolarization. B) Evaluation of Bcl-2 and Bax protein levels. C) Densitometric analysis of the Bcl-2 and Bax protein levels, and Bcl-2/Bax ratio. D) Determination of the caspase-9 enzymatic activity.

The molecular mechanisms that regulate the cytotoxic potential of 7 in melanoma cells were further investigated through the evaluation of the activation state of protein kinase B (pAkt), one of the key proteins involved in the control and regulation of cell survival [129-130]. Compound 7 provoked an early reduction of the protein level of pAkt with respect to total Akt in A2058 cells, which was already evident after 2-h and remained detectable until 4-h incubation (Figure 17A). Interestingly, it has been demonstrated that CDC25B mediates the activation of Akt, probably through a dephosphorylation

mechanism of specific protein kinases [67,131]. We suggest that the early reduction of pAkt levels could be related to a concomitant impairment of CDC25 functions. It is known that Akt regulates the process of cell survival by phosphorylating different substrates, directly or indirectly involved in the apoptotic program [132]. One of these targets is p53, a protein with a tumor-suppressor activity that regulates the cell cycle, as well as the expression of several genes involved in the apoptosis [132]. In particular, Akt negatively regulates the apoptosis, by enhancing the degradation of p53 via its phosphorylation, as well as by promoting the nuclear localization and binding of this factor to human murine double-minute 2 (MDM2) protein, a negative regulator of p53 [132]; therefore, we tested if the CDC25 inhibitor 7 affected the protein levels of p53. We observed an increase of p53 protein level in A2058 cells treated with compound 7, already evident after 8-h, that became significant after 16-h treatment (Figure 17B).

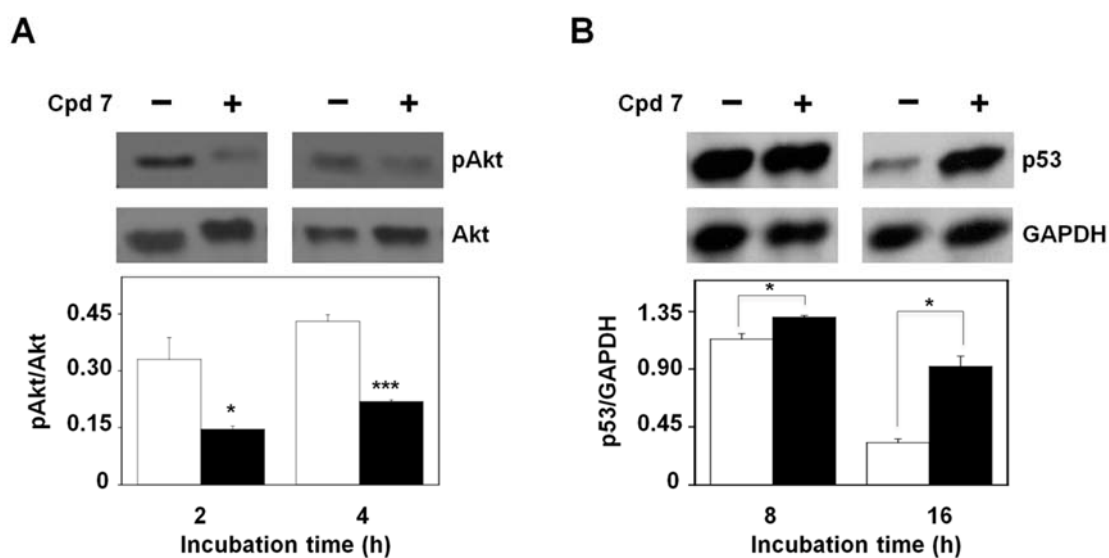


Figure 17. Effect of compound 7 on pAkt and p53 protein levels. A) Evaluation of pAkt protein levels. B) Evaluation of p53 protein levels.

We can suggest that the modulation of p53 protein levels represents one of the molecular events linked to the early decrease of pAkt caused by 7.

Chemoresistance represents a typical hallmark of advanced melanomas. It has been reported that the aggressive nature of melanoma is related to an accumulation of

mutations in several key proliferation- regulating mechanisms, as well as in apoptosis-controlling pathways [113]. Defects in Akt expression occur in a significant proportion of malignant melanomas [133]. Under this concern, the early reduction of the pAkt protein levels caused by **7** was very interesting, because it has been demonstrated that CDC25B mediates the activation of Akt, probably through a dephosphorylation mechanism of specific protein kinases [67,131]. A key molecule involved in the regulation of cell cycle and apoptosis pathway is p53. Frequently, in melanoma this protein is not mutated, but its impaired functions depend on high levels of the phosphorylated form of MDM2, a typical inhibitor of p53 [134]. The time-dependent decrease of the basal level of p53 observed in both melanoma cells, and its higher level measured in treated cells mainly after a late incubation with **7**, suggest that this compound could affect the p53 protein stability. Indeed, higher levels of p53 in treated compared to untreated cells could be ascribable to a reduced activation of Akt, because this protein is responsible for the MDM2 phosphorylation [135-136]. On the other hand, it is likely that the reduced activation of Akt modulates the functions of other downstream proteins; under this concern, one possible candidate seems to be Bax, because of the increased levels of this pro-apoptotic factor observed upon treatment of A2058 with **7**. In conclusion, we suggest that the early reduction of pAkt levels could be related to a concomitant impairment of CDC25 functions. In turn, the reduced activation of Akt could cause the deregulation of other downstream pathways leading to an increase of ROS level and later on of p53 levels.

2.2 Lead optimization of compound 19

2.2.1 Structure-based drug design strategy

Optimization of compound **19** began with the analysis of its binding mode into the CDC25B catalytic domain, predicted by docking experiments [38]. As depicted in Figure 18, the carboxylate group of the benzoyl moiety binds deep in the active site pocket of CDC25B, making a salt-bridge with the R479 guanidinium group and a H-bond with the catalytic backbone NHs of R479 and E478. This moiety approximates the binding mode of the sulfate ion bound to the catalytic site of the CDC25B crystal structure. The two carboxylate groups of the phthalic moiety (positions 1 and 2) bind in the “swimming pool” and form salt-bridges with both R482 and R544 side chains. Furthermore, the carbonyl group of the inhibitor accepts a H-bond from the Y428 OH group.

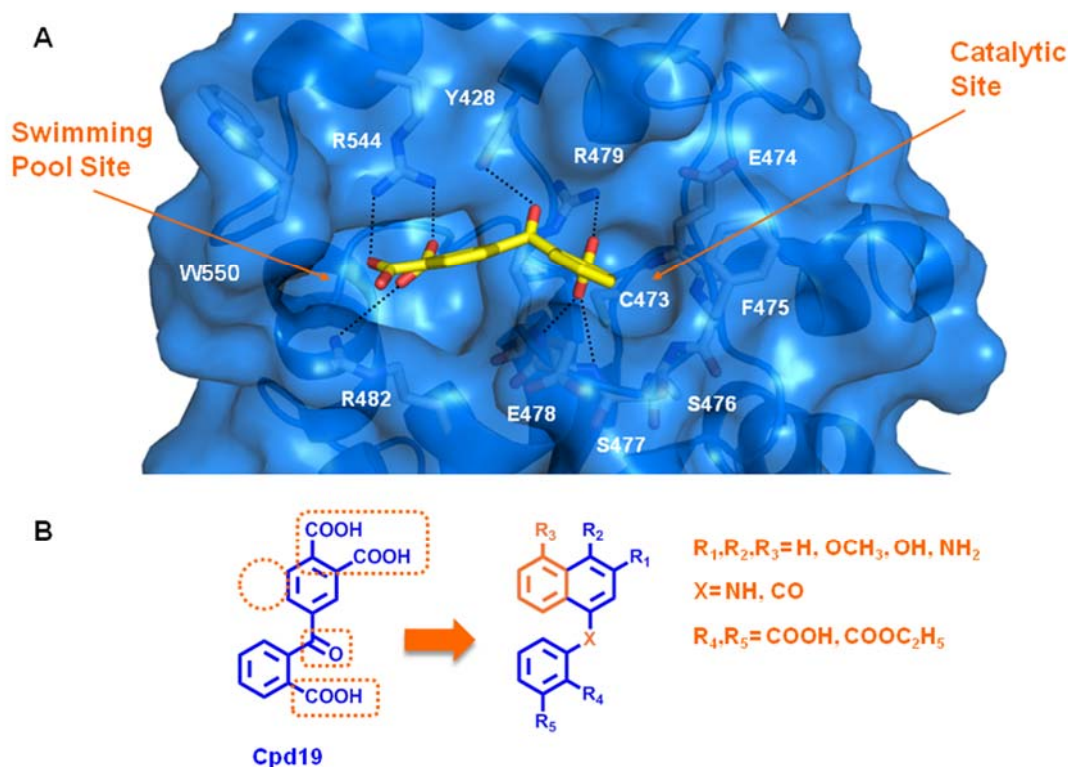
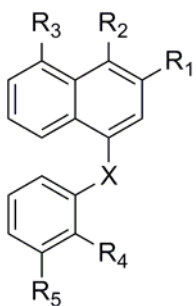


Figure 18. Structure-based optimization of compound **19**. A) Predicted binding mode of compound **19** (yellow sticks) within CDC25 catalytic domain (blue marine surface). Protein residues are highlighted as white sticks. Key H-bonding interactions are shown as dotted lines. B) Schematic overview of the rationally designed compounds illustrated in Table 4.

Structural analysis identified potential areas where both lipophilic and polar groups could be incorporated to make improved contacts with the enzyme. On the basis of these premises, the phthalic system of **19** was replaced with a bulkier naphthalene moiety, strategically directed into the upper inner wall of the swimming pool that is composed by both hydrophobic (F543, L445, M483, W550, P444, and L545) and polar residues (Y428, R479, R482, E446, R544, T547, and S549). Then, the naphthalene system was decorated with hydroxyl, methoxy or amino groups at positions 1, 2 and 3 in the attempt to establish potential H-bonds with Y428, R479, R482, E446, R544, T547, and S549 side chains, resulting in improved activity. The replacement of the carbonyl bridge with an amino group was also explored, to evaluate the H-bonding acceptor or donor capability at this position. Finally, in order to investigate the importance of the 2-carboxy function of the benzoyl moiety, 2- or 3-carboxy derivatives and their corresponding ethyl esters were synthesized (Table 4).

Table 4. Rationally designed compounds.

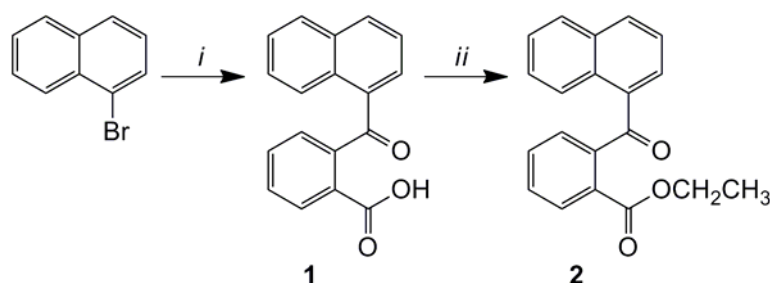


Cpd	R ₁	R ₂	R ₃	R ₄	R ₅	X
1	H	H	H	COOH	H	CO
1a	OCH ₃	H	H	COOH	H	CO
1b	H	OCH ₃	H	COOH	H	CO
1c	OH	H	H	COOH	H	CO
2	H	H	H	COOC ₂ H ₅	H	CO
3	H	H	H	COOH	H	NH
3a	OCH ₃	H	H	COOH	H	NH
3b	H	OCH ₃	H	COOH	H	NH
3c	OH	H	H	COOH	H	NH
3d	H	OH	H	COOH	H	NH
4	H	H	H	COOC ₂ H ₅	H	NH
4a	OCH ₃	H	H	COOC ₂ H ₅	H	NH
4b	H	OCH ₃	H	COOC ₂ H ₅	H	NH
5	H	H	H	H	COOH	NH
5a	OCH ₃	H	H	H	COOH	NH
5b	H	OCH ₃	H	H	COOH	NH
5c	OH	H	H	H	COOH	NH
5d	H	OH	H	H	COOH	NH
5e	H	NH ₂	H	H	COOH	NH
5f	H	H	NH ₂	H	COOH	NH
6	H	H	H	H	COOC ₂ H ₅	NH
6a	OCH ₃	H	H	H	COOC ₂ H ₅	NH
6b	H	OCH ₃	H	H	COOC ₂ H ₅	NH
7	H	H	H	H	H	NH

2.2.2 Synthesis of rationally designed compounds

The general synthetic strategy followed for the preparation of derivatives with a carbonylic group as linker between the two aromatic systems is outlined in Scheme 1 and Scheme 2. Grignard's reagent was prepared *in situ* starting from the commercially available 1-bromonaphthalene in the presence of magnesium turnings. The organomagnesium halide was added to a solution of phthalic anhydride in dry tetrahydrofuran to afford compound **1**. The subsequent Fischer esterification of the carboxylic group in ethanol with sulfuric acid as catalyst provided the final ester **2**.

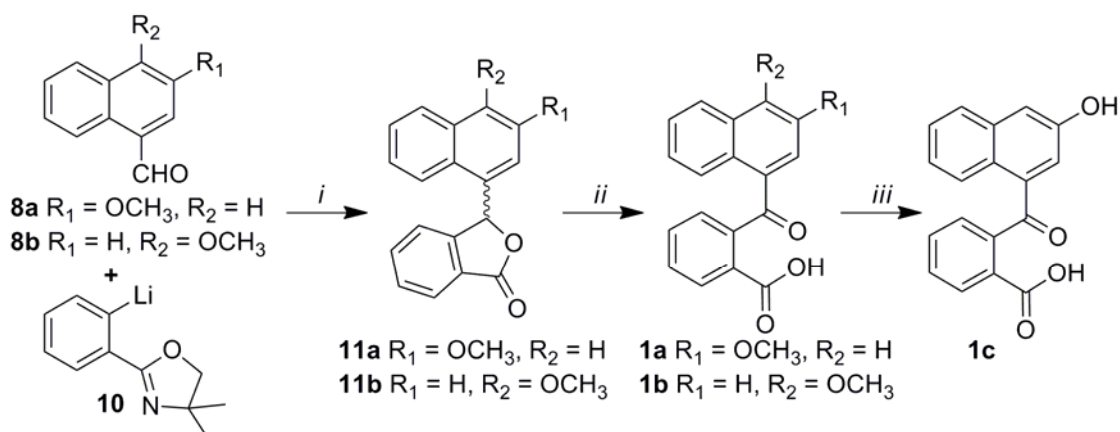
Scheme 1



Reagents and conditions: *i*) a. Mg, dry THF, N₂, reflux, 1h; b. phthalic anhydride, dry THF, N₂, reflux, 48h; *ii*) EtOH, H₂SO₄, reflux, 24h.

Otherwise, in order to obtain the same class of compounds described in Scheme 1 having an hydroxyl group on the naphthalene ring, a second synthetic approach was developed. The key intermediate **10**, which was synthesized following the four-step procedure depicted in Scheme 9, reacted with the appropriate substituted naphthaldehydes **8a,b** and the acid-catalyzed deprotection of the carboxylic moiety lead to the desired lactones **11a,b** in alkaline condition. The oxidation of these last with potassium permanganate and 25% aqueous solution of KOH in pyridine affords the 2-(methoxy-1-naphthyl)benzoic acids **1a** and **1b**. Finally, the cleavage of the methyl ether of **1a** with a 1M solution of boron tribromide in dichloromethane provides the final products **1c**.

Scheme 2



Reagents and conditions: *i*) a. dry Et₂O, N₂, rt, overnight; b. 3N HCl, reflux, 4.5h; c. 10% NaOH, reflux, 1h; *ii*) 25% KOH, KMnO₄, Py, reflux, 5h; *iii*) BBr₃ (1M in DCM), dry DCM, N₂, rt, 30-210min.

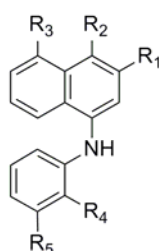
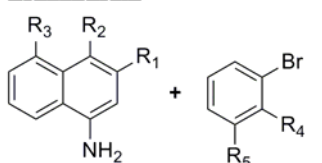
In parallel, the synthesis of another class of derivatives, bearing an amino group in replacement of the carbonylic one between the two aromatic system was carried out. The appropriate substituted aryl halide and aryl amine underwent a Buchwald palladium catalyzed amination reaction (compounds **4**, **4a,b**, **6**, **6a,b,g,h** and **7**) using a mixture of palladium acetate (Pd(OAc)₂) and racemic 2,2'-bis(diphenylphosphino)-1,1'-binaphthyl (BINAP) as catalysts, in the presence of Cs₂CO₃ as base. Although the yield of the aryl amination reaction was critically hindered by the electron deficiency of the amine, the combination of the more nucleophilic amine and more electrophilic aryl bromo was used (procedure a and b in Scheme 3). A basic hydrolysis of the ester group was then performed and this led to the formation of the corresponding acids **3**, **3a,b**, **5**, **5a,b,g,h**. The cleavage of methoxy protection was performed with a 1M solution of boron tribromide in dichloromethane to afford compounds **3c,d**, **5c,d**. The N-Boc protecting group was hydrolyzed with HCl (4M in 1,4-dioxane) to obtain compounds **5e,f**.

Scheme 3

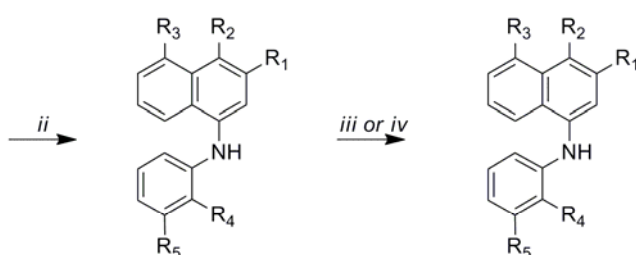
Procedure a



Procedure b



- 4** $R_1 = R_2 = R_3 = R_5 = H, R_4 = COOC_2H_5$
4a $R_1 = OCH_3, R_2 = R_3 = R_5 = H, R_4 = COOC_2H_5$
4b $R_1 = R_3 = R_5 = H, R_2 = OCH_3, R_4 = COOC_2H_5$
6 $R_1 = R_2 = R_3 = R_4 = H, R_5 = COOC_2H_5$
6a $R_1 = OCH_3, R_2 = R_3 = R_4 = H, R_5 = COOC_2H_5$
6b $R_1 = R_3 = R_4 = H, R_2 = OCH_3, R_5 = COOC_2H_5$
6g $R_1 = R_3 = R_4 = H, R_2 = NHBoc, R_5 = COOC_2H_5$
6h $R_1 = R_2 = R_4 = H, R_3 = NHBoc, R_5 = COOC_2H_5$
7 $R_1 = R_2 = R_3 = R_4 = R_5 = H$

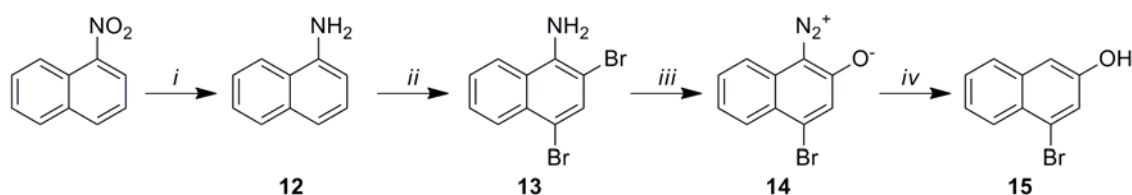


- 3** $R_1 = R_2 = R_3 = R_5 = H, R_4 = COOH$
3a $R_1 = OCH_3, R_2 = R_3 = R_5 = H, R_4 = COOH$
3b $R_1 = R_3 = R_5 = H, R_2 = OCH_3, R_4 = COOH$
5 $R_1 = R_2 = R_3 = R_4 = H, R_5 = COOH$
5a $R_1 = OCH_3, R_2 = R_3 = R_4 = H, R_5 = COOH$
5b $R_1 = R_3 = R_4 = H, R_2 = OCH_3, R_5 = COOH$
5g $R_1 = R_3 = R_4 = H, R_2 = NHBoc, R_5 = COOH$
5h $R_1 = R_2 = R_4 = H, R_3 = NHBoc, R_5 = COOH$
- 3c** $R_1 = OH, R_2 = R_3 = R_5 = H, R_4 = COOH$
3d $R_1 = R_3 = R_5 = H, R_2 = OH, R_4 = COOH$
5c $R_1 = OH, R_2 = R_3 = R_4 = H, R_5 = COOH$
5d $R_1 = R_3 = R_4 = H, R_2 = OH, R_5 = COOH$
5e $R_1 = R_3 = R_4 = H, R_2 = NH_2, R_5 = COOH$
5f $R_1 = R_2 = R_4 = H, R_3 = NH_2, R_5 = COOH$

Reagents and conditions: *i*) $Pd(OAc)_2$, (\pm)-BINAP, Cs_2CO_3 , dry toluene, Ar, $80^\circ C$, 17-40h; *ii*) 1M NaOH, THF/EtOH (1:1), reflux, 30-90min; *iii*) HCl (4M in 1,4-dioxane), dry 1,4-dioxane, rt, 24h; *iv*) BBr_3 (1M in DCM), dry DCM, N_2 , rt, 30-210min.

The key intermediates **8a,b** and **16a,b** used in the previously reactions were synthesized as outlined in Scheme 4. The reduction of the nitro-group of the commercial available 1-nitronaphthalene required the use of organosilicon reagent (Et_3SiH) in the presence of a catalytic amount of $PdCl_2$ to afford compound **12**. The subsequent halogenation with bromine in acetic acid provided intermediate **13** whose treatment with sodium nitrite led to the formation of the diazonium salt **14**, which was isolated and characterized. The conversion of **14** into the 4-bromo-2-hydroxynaphthalene **15** was accomplished with sodium borohydrid.

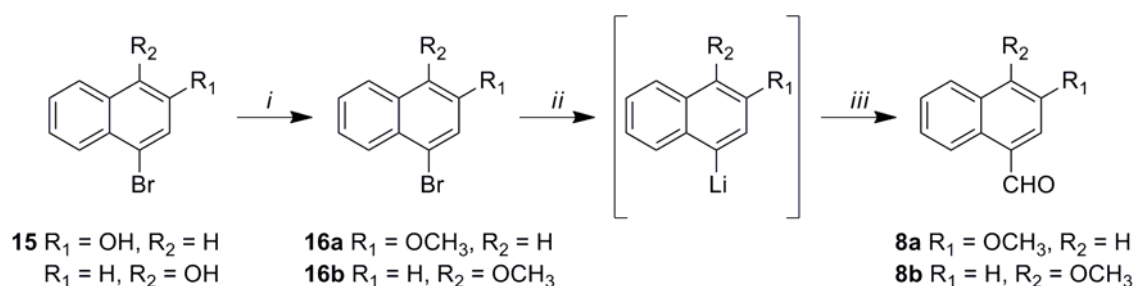
Scheme 4



Reagents and conditions: *i*) Et₃SiH, PdCl₂ cat., EtOH, N₂, rt, 10 min; *ii*) Br₂, AcOH, 60°C, 15 min; *iii*) NaNO₂, AcOH, 8-10°C, 10 min; *iv*) NaBH₄, EtOH, 0-10°C, 2-3 h.

Intermediate **15** or of the commercial available 4-bromo-1-hydroxynaphthalene (Scheme 5) were subsequently protected as methyl ether in the presence of iodomethane provide the intermediates **16a,b**. Finally, the exchange of the halogen atom with lithium by treatment with a solution of *n*-butyllithium in dry THF at -78°C, followed by the formylation with *N,N*-dimethylformamide, led to the final products **8a,b**.

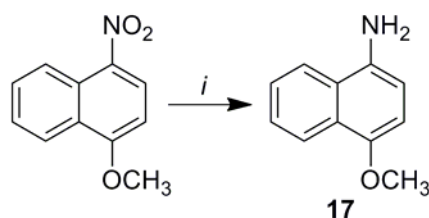
Scheme 5



Reagents and conditions: *i*) a. NaH, dry DMF, N₂, rt, 15 min; b. CH₃I, dry DMF, N₂, rt, 3h; *ii*) *n*BuLi, dry THF, N₂, -78°C, 1h; *iii*) dry DMF, dry THF, N₂, -78°C, 1h.

The synthesis of intermediate **17** was performed using the same reaction conditions applied for the synthesis of the intermediate **12**, as shown in Scheme 6.

Scheme 6



Reagents and conditions: *i*) Et₃SiH, PdCl₂ cat., EtOH, N₂, rt, 10 min.

As depicted in Scheme 7, the appropriate bromonaphthylamine was *N*-protected with di-*tert*-butyl dicarbonate to obtain compounds (**18g,h**).

2.2.3 Inhibitory activities of rationally designed compounds toward CDC25B

The inhibition properties exerted by the rationally designed compounds showed in Table 4 on the recombinant form of CDC25B were investigated, using a fluorimetric assay. In a preliminary screening aimed at assessing their inhibition power, the residual phosphatase activity of CDC25B was measured in the presence of two increasing concentrations of the various compounds. The data presented in Table 5 show that ten molecules (compounds **2**, **3d**, **4**, **4a**, **4b**, **5f**, **6**, **6a**, **6b**, **7**) cause a well measurable inhibition, thus acting as powerful inhibitors of CDC25B. Conversely, six molecules (compounds **1**, **1a**, **1c**, **3**, **3a** and **5b**) were judged essentially ineffective, because the residual phosphatase activity measured in the presence of the highest concentration tested, i.e. 100 μM , was higher than 70%. The remaining eight molecules (compounds **1b**, **3b**, **3c**, **5**, **5a**, **5c-e**) showed an intermediate behaviour of weak inhibitors, being able to cause a significant inhibition only when added at the highest concentration.

An insight on the properties of the powerful CDC25B inhibitors (compounds **2**, **3d**, **4**, **4a**, **4b**, **5f**, **6**, **6a**, **6b**, **7**) was carried out through kinetic measurements of the corresponding K_i values, because this parameter better evaluates the inhibition power of these molecules; furthermore, the usage of the kinetic approach gives an information on the inhibition mechanism exerted by these compounds on CDC25B. The measured values of K_i reported in Table 5 range in the interval 2.8–20.1 μM , thus confirming that all these molecules act as powerful inhibitors of CDC25B; moreover, some of them (*i.e.* compounds **6** and **6a**) seem to act as more powerful inhibitors compared to the lead compound **19**. The mechanism of inhibition was evaluated through Lineweaver-Burk plots of CDC25B phosphatase activity performed in the absence or in the presence of fixed concentrations of each inhibitor. Preliminary studies revealed that the group of ten powerful inhibitors could be splitted in two subgroups on the basis of the observed effects on K_M for the substrate OMFP and V_{max} of reaction. In particular, two of them (compounds **3d** and **5f**) caused a reduction of the K_M without altering the V_{max} value, thus allowing their ranking as competitive inhibitors of CDC25B. On the other hand, the remaining eight compounds (**2**, **4**, **4a**, **4b**, **6**, **6a**, **6b** and **7**) caused a significant decrease of the V_{max} and in most cases an alteration of the K_M . Therefore, these inhibitors cannot be ranked as competitive inhibitors, as they probably act as noncompetitive or mixed inhibitors. Interestingly, a look on the structure of these powerful inhibitors indicated

that both compounds **3d** and **5f** possess a free carboxylic group at position R₄ and R₅, respectively; conversely, compounds **2**, **4**, **4a**, **4b**, **6**, **6a**, and **6b** have the carboxylic group at R₄ or R₅ masked as ethyl ester, whereas the remaining inhibitor **7** represents the scaffold structure of the lead compound **19**, without any carboxylic group.

Table 5. Residual phosphatase activity in the presence of Compound **19** or rationally designed compounds.

Cpd	CDC25B residual activity (%) in the presence of [inhibitor]			K _i (μM)
	1 μM	3 μM	100 μM	
1	-	96	110	-
1a	-	96	89	-
1b	-	-	-	-
1c	-	65	71	-
2	87	-	1	11.2
3	95	-	78	-
3a	-	81	81	-
3b	97		49	-
3c	-	92	67	-
3d	83	-	5	20.1
4	93	-	1	13.8
4a	-	-	-	5.7
4b	99	-	2	7.3
5	-	-	-	-
5a	-	72	57	-
5b	90	-	79	-
5c	95	-	44	-
5d	73	-	14	-
5e	-	-	-	-
5f	-	-	-	7.4
6	-	-	-	2.8
6a	-	-	-	3.4
6b	-	-	-	7.7
7	-	-	-	15.5
Cpd 19		82	13	5.3

2.2.4 Docking studies and SAR rationalization

In order to rationalize the obtained biochemical data, docking studies were carried out for those compounds showing the lowest K_i values: compound **5f**, the most active derivative of the series bearing the free carboxylic function, and compound **6**, the most active derivative among the ethyl esters. Furthermore, to gain further insights into the nature of the inhibition exhibited by **5f** and **6**, we explored possible positions and orientations of the synthetic substrate 3-O-methylfluorescein phosphate (OMFP) with the catalytic domain of CDC25B. The phosphate group of OMFP was positioned to occupy the same location as the sulfate ion bound to the catalytic site of the crystal structure and the fluorescein moiety occupying the swimming pool. This binding mode is similar to that reported in previous studies [99,101]. As depicted in Figure 19A, the carboxylate group of **5f** was bound deeply into the active site pocket of CDC25B, similar to the natural pTyr substrate, while the naphthalene group extended into the “swimming pool”. In particular, the carboxylate made a salt-bridge with the R479 guanidinium group and engaged several H-bonds with the catalytic backbone NHs of E474, F475, S477 and E478. The naphthalene group formed a cation- π interaction with R544 side chain within the “swimming pool” with a distance between the cation center and the ring center of 4.2 Å. Superposition of the models for **5f** and OMFP (Figure 19C) revealed a steric interference at the catalytic site of the enzyme, which could explain the competitive nature of **5f** seen in the kinetic studies. It is noteworthy that the acid derivatives bearing -NH₂ and -OH substituents on the naphthalene ring displayed better inhibitory activity, while the insertion of methoxy groups was detrimental for the activity. Additionally, derivatives bearing the naphthalene ring without substituents showed little or no inhibitory activity. It is well-known that the interaction between the cation and the ring π cloud is electrostatic in nature and can be greatly affected by the nature of the attached substituents due to inductive and resonance effects. We can hypothesize that the electron-donating groups such as -NH₂ and -OH at position R₂ of the naphthalene ring enhance the cation- π interaction through the resonance effect, which results in an increase of the π electron density cloud of the naphthalene ring. On the other hand, the presence of the methoxy group, which is electron-withdrawing via induction, but becomes overall electron-releasing when resonance effects come into play, weakens the cation- π interaction due to steric hindrance, when it is inserted at

position R₂, or due to the dominant electron-withdrawing inductive effect, when this group is placed on R₁.

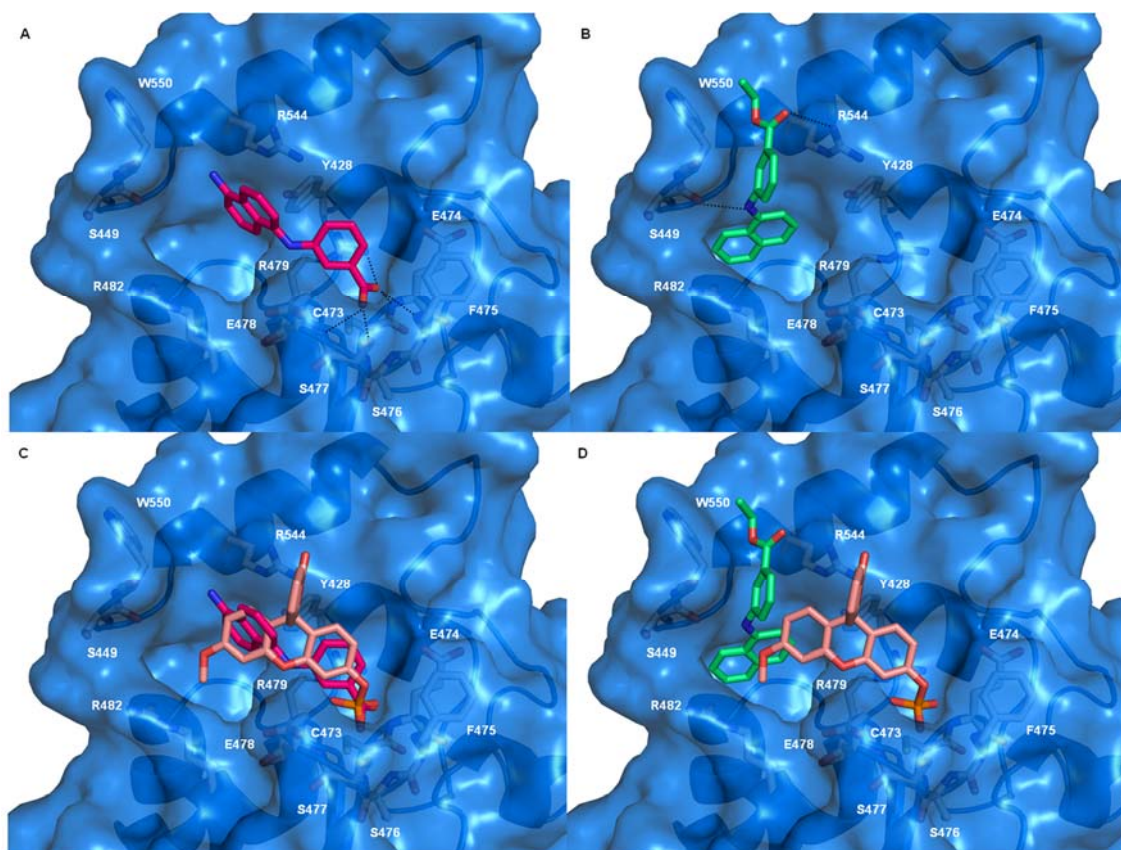


Figure 19. Proposed binding modes of A) **5f** (magenta sticks) and B) **6** (green sticks) within CDC25B catalytic domain (blue marine surface). Comparisons of the predicted binding mode of OMFP substrate (salmon sticks) with **5f** C) and **6** D), obtained independently. Protein residues are highlighted as white sticks. Key H-bonding interactions are shown as dotted lines.

Curiously, when the ethyl ester derivative **6** was docked to CDC25B, a different binding mode was found. It bound deeply into the swimming pool with the carbonyl ester accepting an H-bond from the side chain of R544, while the amino group established a further H-bond with the CO backbone of S549 (Figure 19B). Moreover, **6** was engaged in several hydrophobic interactions with the residues on the C-terminal helix, in particular with W550. Superposition of the model for **6** and OMFP (Figure 19D) didn't show significant overlap, consistent with the observed noncompetitive inhibition. A

very similar binding mode was observed also for the other ester derivatives **2**, **4a**, **4b**, **6**, **6a**, and **6b**.

2.2.5 Antiproliferative effects of compounds **2**, **4**, **4a**, **4b**, **6**, **6a**, **6b** and **7**

We selected a first group of compounds possessing the carboxylic group in R₄ or R₅ masked by ethyl ester (**2**, **4**, **4a**, **4b**, **6**, **6a** and **6b**) and showing similar kinetic parameters. Indeed, the presence of an ester group makes these molecules more lipophilic, thus enhancing their cellular uptake. Furthermore, the analysis was extended to the lead compound **19** and its scaffold structure (compound **7**). Hence, the effects of these molecules on the cell growth rate of A2058 melanoma cell line were investigated. A preliminary MTT assay was carried out after different times of treatment, in the presence of different concentrations of inhibitor (Figure 20). After 24-h, only compound **6a** caused an evident cytotoxicity at 50 μ M, whereas at 100 μ M also compounds **2** and **7** were active. When the incubation time was prolonged to 48 or 72 h, both compounds **2** and **6a** were cytotoxic at 50 μ M concentration and, at 100 μ M concentration, cytotoxicity was extended also to compounds **6**, **6b** and **7**.

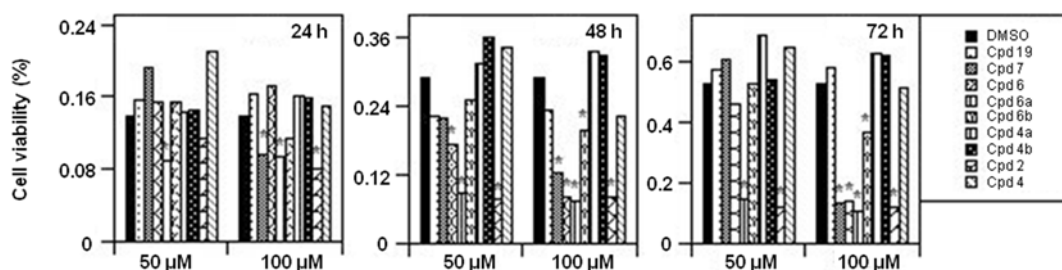


Figure 20. Effect of the rationally designed compounds and compound **19** and on cell growth rate of melanoma cells A2058.

In order to check the minimum cytotoxic concentration of the more active compounds (compounds **2** and **6a**), the MTT assay was repeated at different incubation times using lower concentrations (1.25, 2.5 or 5 μ M) of these inhibitors. The data of Figure 21 indicate that only compound **6a** exerted a significant reduction of proliferation, being cytotoxic at 5 μ M after 48-h, and even at 2.5 μ M after 72-h incubation. Future

investigations will be mainly focused on compounds **2** and **6a** because of their cytotoxicity observed in a reasonable concentration range.

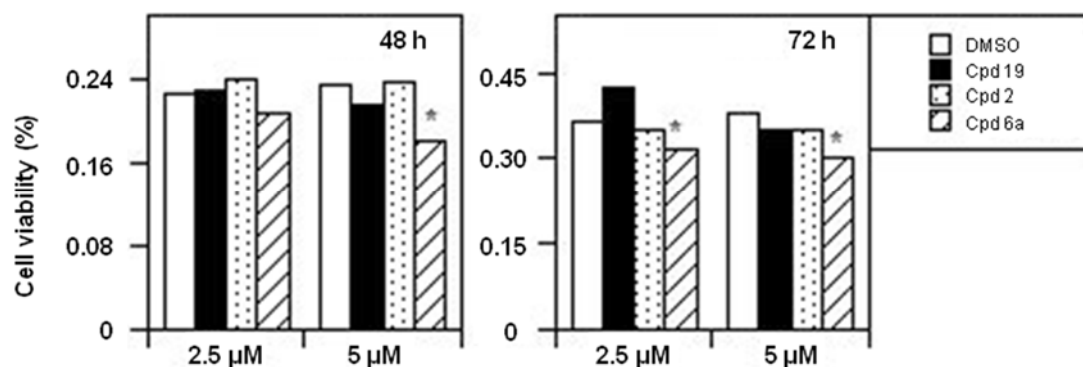


Figure 21. Evaluation of the antiproliferative effects of compounds **19**, **2** and **6a** using different concentrations.

In conclusion, the careful analysis of CDC25B catalytic domain in complex with the lead compound **19** offered precious insight for structural optimization, allowing to disclose a novel series of potent derivatives. The described SARs and the very useful synthetic approach constitute important guidelines for the design of further improved inhibitors.

2.3 Conclusions

CDC25 phosphatases have a central role in the complex regulation of signalling pathways that are involved in cell stress responses, proliferation and death. Considered their biological importance, this enzyme family has been the target of several drug discovery efforts. This research project has been mainly addressed to the discovery of novel CDC25 inhibitors, starting from two promising lead compounds identified in a previous virtual screening campaign. By using a range of ligand- and structure-based computational methods we have identified two major classes of inhibitors. The first one is a series of 6-xanthone derivatives, structural analogs of the lead compound **11** (NSC 119915), which was identified by a ligand-based chemoinformatic approach. Nine compounds (**3**, **5–9**, **21**, **24**, and **25**) were identified with K_i values for CDC25A, -B and -C ranging from 0.01 to 4.4 μM . One of these analogs, **7**, showed a high antiproliferative effect on human melanoma cell lines, A2058 and SAN. Compound **7** arrested melanoma cells in G2/M, causing a reduction of the protein levels of CDC25A and, more consistently, of CDC25C. Furthermore, an intrinsic apoptotic pathway was induced, which was mediated by ROS, because it was reverted in the presence of antioxidant N-acetyl-cysteine (NAC). Finally, **7** decreased the protein levels of phosphorylated Akt and increased those of p53, thus contributing to the regulation of chemosensitivity through the control of downstream Akt pathways in melanoma cells. On the other hand, a series of novel derivatives of the second lead compound **19** was rationally designed using a structure-based approach. Ten molecules (compounds **2**, **3d**, **4**, **4a**, **4b**, **5f**, **6**, **6a**, **6b**, **7**) acted as powerful inhibitors of CDC25B, with K_i values towards CDC25B ranging between 2.8-20.1 μM , thus confirming the validity of the design strategy. Among them, compounds **3d** and **5f**, bearing a free carboxylic group, acted as competitive inhibitors of CDC25B, whereas compounds **2**, **4**, **4a**, **4b**, **6**, **6a**, **6b**, bearing the carboxylic group at R4 or R5 masked as ethyl ester, acted as noncompetitive or mixed inhibitors. Compound **7**, containing only the “scaffold structure”, also showed a noncompetitive or mixed inhibition profile. The distinct inhibition profiles of these inhibitors were also reflected in their different binding modes, as predicted by the docking experiments carried out for compounds **5f** and **6**. The effects of compounds **2**, **4**, **4a**, **4b**, **6**, **6a**, **6b** and **7** on the cell growth rate of A2058 melanoma cell line were also

investigated. Compounds **2** and **6a** significantly reduced the proliferation of A2058 cells, being cytotoxic at 5 μ M and 2.5 μ M, respectively, after 72-h incubation.

Overall, our data indicate that the reduced viability of melanoma cells observed after treatment with both the reported classes of inhibitors is probably related to the inhibition potency exhibited by these molecules on the CDC25 phosphatase activity. Therefore, the deregulation of CDC25 in melanoma cells suggests that this crucial element of cell cycle could be considered as a possible oncotarget *in vivo*. It is known that the success of advanced anti-melanoma strategies, for example therapies based on the usage of BRAF inhibitors, that selectively inhibit the proliferation of melanoma cells harbouring the BRAF^{V600E} mutation, is not definitive. In fact, the patients usually relapse because of acquired drug resistance, possibly due to the activation of others survival pathways. An alternative strategy could be represented by the combination of two different drugs, co-targeting independent survival pathways that are critical for development and maintenance of melanoma. Hence, the study of the effects of CDC25 inhibitors in melanoma cells could be helpful for finding other molecular pathways, as possible targets for melanoma treatment.

3. Experimental section

3.1 Computational chemistry

3.1.1 Chemoinformatic methods

All of the approaches below were performed in parallel against the full ZINC drug-like subset (~17.8 million drug-like compounds) and the NCI lead-like set.

Database: lead-like selection and preparation

The NCI Open Database (<http://ntp.cancer.gov/>) with 260,071 compounds was obtained from ZINC [137-138]. The compound database was processed with FILTER version 2.0.2 (OpenEye Scientific Software Inc., Santa Fe, USA, <http://www.eyesopen.com/>) to select a subset of lead-like compounds. We used the default parameters in the lead-like filter without further modifications. The resulting database, referred in this work as the NCI lead-like set, contained 65,375 compounds.

Molecular fingerprints

Five types of molecular FPs ECFP2, ECFP4, FCFP2, FCFP4, and FCFP6 [122] were calculated using Pipeline Pilot (Accelrys Inc., San Diego, USA, <http://accelrys.com/products/pipeline-Pilot/>). The similarity between the lead compound NSC 119915 and our compound libraries was assessed using the Tanimoto coefficient. The Tanimoto coefficient (T_c) is given by eq. 1:

$$T_c(A, B) = \frac{c}{a+b-c}$$

where a and b are the number of bits set in the fingerprints of molecules A and B , respectively, and c is the number of bits set in both fingerprints. The T_c ranges between 0 and 1, with 0 corresponding to no fingerprint overlap and 1 to identical fingerprints. It should be noted that, identical fingerprints do not necessarily correspond to identical molecules (as fingerprints are only abstractions of molecular structures). Furthermore, as defined by the above formula, the T_c only takes into account bits set to 1 (i.e., features present in the molecule). Hence, the magnitude of the T_c value will be greatly influenced by the bit density in the underlying fingerprint, which on the other hand, increases with molecular size and complexity [139]. The calculation of T_c translates

structural similarity into numerical values and can be interpreted as the “percentage of structural features shared between two compounds”, yet it is debatable which T_c value corresponds to “significant similarity”. There is no generally applicable T_c threshold for the indication of structural similarity, which is dependent on the molecular fingerprint applied [140]. In this work, we applied threshold values of 0.52, 0.43, 0.75, 0.60, 0.45 in combination with ECFP2, ECFP4, FCFP2, FCFP4, and FCFP6 fingerprints, respectively, because they give much higher confidence in correlating structural similarity [123].

Substructure search

ZINC drug-like and NCI lead-like collections were exposed to substructure 2D searching using as query the following SMILES notations: [O = c3ccc2cc1ccccc1oc2c3], [O = c3ccc2cc1ccccc1[nH] c2c3] and [O = c3ccc2cc1ccccc1sc2c3]. Canvas version 1.9 (Schrödinger, LLC, New York, USA) was used in this process by using SMILES Arbitrary Target Specification (SMARTS) filter module to carry out substructure search. All structures retrieved from both molecular fingerprints and substructure search were combined and duplicates were removed, thus obtaining a single database of 126 unique compounds. Out of these compounds, we selected the top-ranked 25 compounds for CDC25 inhibitory assay.

3.1.2 Molecular modeling

Protein and ligand preparation

Docking experiments were carried out employing the crystal structure of 1QB0 [24]. All crystallographic water molecules and other chemical components were omitted, the right bond orders as well as charges and atom types were assigned, and hydrogen atoms were added to the crystal structure. Arg, Lys, Glu, and Asp residues were considered ionized, while His was considered as neutral. Then the protein was submitted to a series of restrained, partial minimizations using the OPLS-AA force field [141] within the “Protein Preparation” module of Schrödinger’s Maestro version 10.5

(Schrödinger, LLC, New York, NY, 2016). The initial structures of the inhibitors were created, modified and energy-minimized with Maestro.

Docking

Docking of **5f** and **6** into the catalytic domain of CDC25B was performed with the Gold software, which uses a genetic algorithm (GA) for determining the docking modes of ligands and proteins. The coordinates of the cocrystallized sulfate were chosen as active-site origin. The active-site radius was set equal to 13 Å. The Goldscore-CS docking protocol was adopted in this study [142]. In this protocol, the poses obtained with the original GoldScore function are rescored and reranked with the GOLD implementation of the ChemScore function [142]. To perform thorough and unbiased search of the conformation space, each docking run was allowed to produce 200 poses without the option of early termination, using standard default settings. The top solution obtained after re-ranking of the poses with ChemScore was selected.

3.2 Biology

Materials and reagents

Compounds retrieved by ligand-based chemoinformatic selection protocol were purchased from commercial vendors or kindly provided from the NCI/DTP. Compounds were dissolved in DMSO, and stock solutions at 10 mM concentration were prepared. Recombinant forms of the catalytic domains of CDC25A, -B and -C were obtained through the vectors pET28a-CDC25A-cd, pET28a-CDC25B-cd and pET28a-CDC25C-cd, kindly provided by H. Bhattacharjee (Florida International University, Herbert Wertheim College of Medicine, Miami, Florida). Protein purification was obtained essentially as previously described [38]. The synthetic substrate for CDC25 phosphatase activity, OMFP, was purchased from Sigma-Aldrich. Dulbecco's modified Eagle's medium (DMEM), Roswell Park Memorial Institute (RPMI) 1640 medium, fetal bovine serum (FBS), L-glutamine, penicillin G, streptomycin, and trypsin were purchased from Lonza (Milano, Italy). Propidium iodide (PI), dichlorofluorescein diacetate (DCFH-DA), Rhodamine 123 (R123), N-acetyl-L-cysteine (NAC) and

apocynin were purchased from Sigma-Aldrich. A protease inhibitor cocktail was obtained from Roche Diagnostics S.p.A. (Monza, Italy). Caspase-3 and caspase-9 fluorimetric assay kits were purchased from BioVision (Milpitas, CA, USA). The pan-caspase inhibitor Z-VAD-FMK was purchased from Selleckchem (USA). Rabbit monoclonal antibody against glyceraldehyde 3-phosphate dehydrogenase (GAPDH) was obtained from Cell Signaling (Boston, MA, USA); mouse monoclonal antibody against CDC25A, CDC25C, or Bcl-2, rabbit polyclonal antibody against CDC25B, pAkt (Ser473) or Bax, and each secondary antibody conjugated to horseradish peroxidase were obtained from Santa Cruz Biotechnology (Heidelberg, Germany). All other chemicals were of analytical grade and were purchased from Sigma-Aldrich.

In vitro assays of CDC25 phosphatase activity

The enzymatic activity of the catalytic domains of CDC25A, -B and -C were determined through a fluorimetric method, which monitored the dephosphorylation of the synthetic substrate OMFP, essentially as previously described [38]. In steady-state enzyme kinetic studies, the residual phosphatase activity of purified recombinant CDC25B was measured at 30°C in the presence of different concentrations of the various inhibitors, using a computer-assisted Cary Eclipse spectrofluorimeter (Varian) equipped with an electronic temperature controller. Excitation and emission wavelengths were set at 485 and 530 nm, respectively; both excitation and emission slits were set at 10 nm. The reaction mixture contained 10 nM CDC25B and different concentrations of the various inhibitors in 500 µL final volume of 20 mM Tris-HCl, pH 7.8, 1 mM DTT. DMSO was used as vehicle control. The reaction started by the addition of 25 µM OMFP, and the formation of the fluorescent product *o*-methylfluorescein was monitored continuously. The rate of OMFP hydrolysis was expressed as arbitrary units per min (a.u./min). The comparison of the rates determined in the absence and in the presence of the various inhibitors allowed the calculation of the residual phosphatase activity, expressed as a percentage. The K_m for OMFP and the maximum rate of OMFP hydrolysis ($\Delta AU/\text{min}_{\text{max}}$) were obtained from Lineweaver–Burk plots, carried out in the absence or in the presence of different inhibitor concentrations. For the calculation of the inhibition constant (K_i), the equation used depended on the type of inhibition. In the reversible competitive inhibition, K_i was

averaged from the increase of K_m for OMFP in the presence of the inhibitor, according to $K_m' = K_m\{1 + ([I]/K_i)\}$, where K_m' represents the K_m for OMFP measured in the presence of the concentration $[I]$ of the inhibitor. In the irreversible inhibition, K_i was averaged from the decrease of $\Delta AU/\min_{\max}$ in the presence of the inhibitor, according to $\Delta AU/\min_{\max}' = \Delta AU/\min_{\max}/\{1 + ([I]/K_i)\}$, where $\Delta AU/\min_{\max}'$ represents the maximum rate of OMFP hydrolysis measured in the presence of the concentration $[I]$ of the inhibitor.

Cell culture

The human melanoma cell line A2058, kindly provided by CEINGE (Naples, Italy), and SAN cells [143] were derived from lymph nodal metastases and grown in DMEM and RPMI 1640, respectively, supplemented with 10% FBS, 2 mM L-glutamine, 100 IU/mL penicillin G, and 100 $\mu\text{g}/\text{mL}$ streptomycin in humidified incubator at 37°C under 5% CO₂ atmosphere. All cells were split and seeded every three days and used during the exponential phase of growth. Cell treatments were always carried after 24 h from plating.

3-(4,5-Dimethylthiazole-2-yl)-2,5- biphenyltetrazolium bromide (MTT) assay

The MTT assay was used to detect cell proliferation essentially as previously described [144]. Briefly, A2058 and SAN cells were plated in 96-well microtiter plates (100 $\mu\text{L}/\text{well}$) at 4000 and 6000 cells/well, respectively. After 24-h seeding, cells were treated with the selected compounds added at 25, 50 or 100 μM concentration, or with 0.5% (v/v) DMSO as a vehicle control. After 24-h, 48-h or 72-h treatment, and upon the addition of 10 μL of MTT solution in the dark, the plate was incubated for 3 h at 37°C under CO₂ atmosphere. After medium aspiration and solubilization of formazan crystals, absorbance was measured at 570 nm, using an ELISA plate reader (Bio- Rad, Milano, Italy).

Cell cycle analysis and evaluation of apoptosis

Cells were seeded into 6-well plates at 3×10^5 cells/ well for 24 h at 37°C; after the addition of 100 μM **7** or 0.5% DMSO as a vehicle control, the incubation of treated cells continued for 16 or 24 h. After each treatment, cells were harvested with trypsin,

centrifuged and the pellet was resuspended in phosphate-buffered saline (PBS). For cell cycle analysis, cells were fixed with 70% (v/v) cold ethanol and stored at -20°C for 1 h. Then, cells were washed with cold PBS, centrifuged and the pellets were resuspended in 200 μL of a non-lysis solution containing 50 $\mu\text{g}/\text{mL}$ PI. For the evaluation of apoptosis, cells were not fixed in ethanol and directly resuspended in 200 μL of a hypotonic lysis solution containing 50 $\mu\text{g}/\text{mL}$ PI. After incubation at 4°C for 30 min, cells were analyzed with a FACScan flow cytometer (Becton Dickinson) for evaluating the distribution in cell cycle phases or the presence of nuclei with a DNA content lower than the diploid.

Measurements of caspase-3 and caspase-9 activity

To estimate caspase-3 and caspase-9 activity during the treatment with compound 7, the respective enzymatic activities were measured by using caspase-3 and -9 fluorimetric assay kits, according to the manufacturer's protocol, essentially as previously described [145]. Briefly, cells were seeded into 75 cm^2 plates (2×10^6 cells/plate) for 24 h at 37°C and then treated with 100 μM 7 or 0.5% DMSO. At the end of each incubation, cells were collected, washed with PBS, and finally lysed at 4°C in the cell lysis buffer. Cell lysates were incubated with 50 μM DEVD-AFC or LEHD-AFC substrates at 37°C for 2 h, to detect caspase-3 or caspase-9 activity, respectively, using a Cary Eclipse fluorescence spectrophotometer (Varian). Excitation and emission wavelengths were set at 400 nm and 505 nm, respectively; both excitation and emission slits were set at 10 nm.

Measurement of intracellular ROS content

The intracellular ROS level was monitored using the oxidation-sensitive fluorescence probe DCFH-DA. Cells were seeded into 6-well-plates (3×10^5 cells/plate) for 24 h at 37°C and then treated at various times with 100 μM compound 7 or 0.5% DMSO. DCFH-DA was added in the dark at 10 μM final concentration 30-min before the end of each incubation; then, cells were collected, washed in PBS, and finally resuspended in 500 μL PBS for fluorimetric analysis. Measurements were realized in a Cary Eclipse fluorescence spectrophotometer (Varian); excitation and emission wavelengths were set at 485 nm and 530 nm, respectively; both excitation and emission

slits were set at 10 nm. The effect of **7** on ROS production was also estimated after pretreatment of cells with 10 mM NAC for 1 h.

Evaluation of mitochondrial membrane potential

Cells were seeded into 6-well-plates (3×10^5 cells/well) for 24 h at 37°C, and then incubated at 37°C for 1 h in the presence of 5 μ M R123, washed twice with PBS, and placed in medium containing 100 μ M compound **7** or 0.5% DMSO. After various times from treatment, cells were harvested, washed and centrifuged for 10 min at 4°C. The cellular pellet was resuspended in 500 μ L PBS. The fluorescence of cell-associated R123 was detected in the above-mentioned fluorescence spectrophotometer, using excitation and emission wavelengths of 490 and 520 nm, respectively; both excitation and emission slits were set at 10 nm.

Western blotting

A2058 cells were seeded into 6-well-plates (3×10^5 cells/plate) for 24 h at 37°C and then treated at different times with 100 μ M compound **7** or 0.5% DMSO. After treatment, cells were harvested, washed with PBS and then lysed in ice-cold modified radio immunoprecipitation assay (RIPA) buffer (50 mM Tris-HCl, pH 7.4, 150 mM NaCl, 1% Nonidet P-40, 0.25% sodium deoxycholate, 1 mM Na₃VO₄ and 1 mM NaF), supplemented with protease inhibitors and incubated for 30 min on ice. The supernatant obtained after centrifugation at 12,000 rpm for 30 min at 4°C constituted the total protein extract. The protein concentration was determined by the method of Bradford, using bovine serum albumin (BSA) as standard [146]. Equal amounts of total protein extracts were used for Western blot analysis. Briefly, protein samples were dissolved in SDS-reducing loading buffer, run on 12% SDS/PAGE and then transferred to Immobilon P membrane (Millipore). The filter was incubated with the specific primary antibody at 4°C overnight and then with the secondary antibody at room temperature for 1 h. Membranes were then analysed by an enhanced chemiluminescence reaction, using Super Signal West Pico kit (Pierce) according to manufacturer's instruction; signals were visualized by autoradiography.

Statistical analysis

Data are reported as average and standard error. The statistical significance of differences among groups was evaluated using ANOVA, with the Bonferroni correction as post hoc test or the Student *t* test where appropriate. The significance was accepted at the level of $p < 0.05$.

3.3 Chemistry

Reagents and solvents were purchased from Sigma-Aldrich and used without further purification. Some reactions involving air-sensitive reagents were performed under nitrogen atmosphere and anhydrous solvents were used when necessary. The Biotage-initiator microwave synthesizer was used. Reactions were monitored by thin layer chromatography analysis on aluminium-backed Silica Gel 60 plates (70-230 mesh, Merck), using a ultraviolet fluorescent lamp at 254 nm and 365 nm. Visualization was aided by opportune staining reagents. Purification of intermediates and the final compounds was performed by flash chromatography using Geduran® Si 60 (40-63 μm , Merck). ^1H - and ^{13}C - NMR spectra were recorded at room temperature on a Variant 300 MHz Oxford instrument using TMS as internal standard. CDCl_3 , CD_3OD , acetone- d_6 and $\text{DMSO-}d_6$ were used as deuterated solvents for all the spectra run. Chemical shift are expressed as δ (ppm). Multiplicity is reported as *s* (singlet), *br s* (broadened singlet), *d* (double), *t* (triplet), *q* (quartet), *m* (multiplet), *dd* (double of doublets), *dt* (doublet of triplets). The coupling constants (J-values) are given in Hertz (Hz). All spectroscopic data match the assigned structures. The melting points were determined on a Buchi Melting Point B540 instrument.

General procedure for the synthesis of aminonaphthalene derivatives (12, 17).

To a solution of the suitable 1-nitronaphthalene (200 mg, 1.155 mmol) and triethylsilane (0.74 mL, 4.633 mmol) in ethanol (5 mL) a catalytic amount of palladium (II) chloride (10 mol %) was added under an N_2 atmosphere [147]. The resulting mixture was kept under stirring and a change of color was observed. The solvent was

evaporated and then water was added and decanted. The aqueous phase was extracted with diethyl ether (3x2mL). The organic phase was firstly treated with HCl 3N (2mL) and then the collected acidic aqueous solution, which contained the hydrochloride salt of naphthylamina, was basified with NaOH 25% (2mL) and extracted with diethyl ether (6x2mL). The organic phase was dried over anhydrous sodium sulfate and the solvent was evaporated under reduced pressure.

1-aminonaphthalene **12**. Starting compound: 1-nitronaphthalene. Reaction time: 10 minutes. Purple solid (melting point: 47-50°C), 74 % yield. Molecular formula: C₁₀H₉N. Molecular Weight: 143.19 g/mol. R_f = 0.47 (cyclohexane/ethyl acetate 7:3). Eluent for chromatography: cyclohexane/ethyl acetate from (8:2) to (7:3). ¹H NMR (300 MHz, CDCl₃) δ 7.80-8.00 (m, 2H, ArH), 7.40-7.60 (m, 4H, ArH), 6.82 (d, *J* = 6 Hz, 1H, ArH), 4.10 (br s, 2H, NH₂, exchangeable with D₂O) ppm.

1-methoxy-4-aminonaphthalene **17**. Starting compound: 1-methoxy-4-nitronaphthalene. Reaction time: 60 minutes. Light tan solid (melting point: 38-40°C), 49 % yield. Molecular formula: C₁₁H₁₁NO. Molecular Weight: 173.21 g/mol. R_f = 0.43 (cyclohexane/ethyl acetate 8:2). Compound **17** was used in the next reaction without any further purification. ¹H NMR (300 MHz, CDCl₃) δ 8.27-8.24 (m, 1H, ArH), 7.84-7.81 (m, 1H, ArH), 7.52-7.49 (m, 2H, ArH), 6.74-6.66 (m, 2H, ArH), 3.95 (s, 3H, OCH₃), 3.85 (br s, 2H, NH₂, exchangeable with D₂O) ppm.

Synthesis of 1-amino-2,4-dibromonaphthalene 13.

To a solution of compound **12** (250 mg, 1.745 mmol) in acetic acid (1 mL) was added a 0-5°C solution of Br₂ (0.27 mL, 5.235 mmol) in acetic acid (2 mL) [148]. Another 1 mL of acetic acid was added and the mixture was warmed at 60°C for 15 min, during which the color solution changes from purple to orange. Then the mixture was cooled with and the salt was filtered, washed with acetic acid, and suspended in an excess of 1M NaOH. The product was collected by filtration, washed with water and dried to give a purple solid. The crude residue was purified by flash chromatography (cyclohexane/ethyl acetate 9:1) to provide compound **13**. Violet solid (melting point: 114-116 °C), 86 % yield. Molecular formula: C₁₀H₇Br₂N. Molecular Weight: 300.98

g/mol. Rf = 0.33 (cyclohexane/ethyl acetate 8:2). Compound **17** was used in the next reaction without any further purification. ¹H NMR (300 MHz, CDCl₃) δ 8.17 (dd, $J_1 = 12$ Hz, $J_2 = 3$ Hz, ArH) 7.77-7.83 (m, 1H, ArH), 7.79 (s, 1H, ArH), 7.50-7.62 (m, 2H, ArH), 4.63 (br s, 2H, NH₂, exchangeable with D₂O).

Synthesis of 1-diazo-4-bromo-2-naphthol 14.

To a stirred solution of compound **13** (250 mg, 0.831 mmol) in acetic acid (4 mL) and propionic acid (0.67 mL) at 8-10°C was gradually added sodium nitrite (86 mg, 1.246 mmol) [148]. After stirring for 10 min the yellow-brown solution was poured into 6 mL of ice water and the resulting mixture was rapidly filtered to remove a black tar. The aqueous phase was extracted with dichloromethane (6x2 mL). The collected organic phase was dried over anhydrous sodium sulfate, filtered and the solvent was evaporated under reduced pressure to give compound **14**. Yellow-orange solid (melting point: 118-125°C), 98 % yield. Molecular formula: C₁₀H₅BrN₂O. Molecular Weight: 249.06 g/mol. ¹H NMR (300 MHz, CDCl₃) δ 8.08 (d, $J = 9$ Hz, 1H, ArH), 7.58 (t, $J = 9$ Hz, 1H, ArH), 7.37 (t, $J = 9$ Hz, 1H, ArH), 7.28 (d, $J = 9$ Hz, 1H, ArH), 7.18 (s, 1H, ArH) ppm.

Synthesis of 4-bromo-2-naphthol 15.

To a suspension of compound **14** (200 mg, 0.803 mmol) in ethanol (3.5 mL), NaBH₄ (30.4 mg, 0.803 mmol) was added at 0-10°C [148]. The solution was stirred until gas evolution ceased and the mixture appeared darker. After evaporating ethanol, the remaining residue poured into water, basified with 10% NaOH and then extracted with dichloromethane (2x2 mL), in order to purify the reaction mixture from the unreacted materials and impurities. Then the collected alkaline aqueous solution, which contains the sodium salt of compound **15**, was acidified with 3M HCl and extracted with ethyl acetate (2x2 mL). The organic layer was dried over anhydrous sodium sulfate and evaporated under reduced pressure, to afford a crude brown solid. The residue was purified by flash chromatography (cyclohexane/ethyl acetate 9:1 - Rf =

0.18) to provide the intermediate **15**. Brown solid (melting point: 118-119°C), 75 % yield. Molecular formula: C₁₀H₇BrO. Molecular Weight: 223.07 g/mol. ¹H NMR (300 MHz, CDCl₃) δ 8.14 (d, *J* = 7.8 Hz, 1H, ArH), 7.67 (d, *J*₁ = 6.9 Hz, *J*₂ = 1.8 Hz, 1H, ArH), 7.41-7.50 (m, 3H, ArH), 7.14 (d, *J* = 1.8 Hz, 1H, ArH), 4.98 (s, 1H, OH, exchangeable with D₂O) ppm.

General procedure for the synthesis of 4-bromo-methoxynaphthalene derivatives (16a,b).

To a solution of the required bromonaphthol (150 mg, 0.672 mmol) in dry N,N-dimethylformamide (1 mL) sodium hydride (60% dispersion in mineral oil, 29.6 mg, 0.739 mmol) was added under N₂. After the evolution of H₂ ceased, iodomethane (0.17 mL, 2.688 mmol) was added and then the reaction mixture stirred at room temperature for 3 hours. After the evaporation of N,N-dimethylformamide, the resultant residue was extracted with ethyl acetate (3x2 mL). The collected organic phase was dried over anhydrous sodium sulfate and the solvent was evaporated under reduced pressure to give the desired derivatives. The crude oils were purified by flash chromatography (cyclohexane/ethyl acetate 9:1) to provide compounds **16a** and **16b**.

4-bromo-2-methoxynaphthalene 16a. Starting compound: **15**. Brown oil, 97 % yield. Molecular formula: C₁₁H₉BrO. Molecular Weight: 237.09 g/mol. R_f = 0.66 (cyclohexane/ethyl acetate 9:1). ¹H NMR (300 MHz, CDCl₃) δ 8.15 (d, *J* = 7.5 Hz, 1H, ArH), 7.72 (d, *J* = 7.5 Hz, 1H, ArH), 7.41-7.52 (m, 3H, ArH), 7.12 (d, *J* = 2.4 Hz, 1H, ArH), 3.91 (s, 3H, OCH₃) ppm.

4-bromo-1-methoxynaphthalene 16b. Starting compound: 4-bromo-1-naphthol. Brown oil, 98 % yield. Molecular formula: C₁₁H₉BrO. Molecular Weight: 237.09 g/mol. R_f = 0.56 (cyclohexane/ethyl acetate 9:1). ¹H NMR (300 MHz, CDCl₃) δ 8.28 (d, *J* = 8.4 Hz, 1H, ArH), 8.18 (d, *J* = 8.4 Hz, 1H, ArH), 7.50-7.67 (m, 3H, ArH), 6.67 (d, *J* = 8.4 Hz, 1H, ArH), 3.98 (s, 3H, OCH₃) ppm.

General procedure for the synthesis of methoxy-1-naphthaldehyde derivatives (8a,b).

To a solution of the proper bromomethoxynaphthalene (100 mg, 0.422 mmol) in anhydrous THF (4 mL) cooled to -78°C under N_2 was added *n*BuLi (2.7M in eptane, 0.39 mL, 1.055 mmol) and stirred for 1 hour. Anhydrous N,N-dimethylformamide (0.20 mL, 2.532 mmol) was added and the reaction stirred for a further 1 hour at -78°C . The reaction was quenched by slowly addition of cold water (0.5 mL), in order to neutralize the unreacted *n*BuLi, and THF and DMF were evaporated. The residue was poured into 3N HCl (3 mL) and extracted with diethyl ether (6x2 mL). The combined organic layer were washed firstly with water, then with a saturated sodium hydrogen carbonate solution and, finally, with a saturated sodium chloride solution. The organic phase was dried, filtered and concentrated. The crude oils were purified by flash chromatography (cyclohexane/ethyl acetate 9:1) to provide compounds **8a** and **8b**.

3-methoxy-1-naphthaldehyde 8a. Starting compound: **16a**. Yellow-brown oil, 56 % yield. Molecular formula: $\text{C}_{12}\text{H}_{10}\text{O}_2$. Molecular Weight: 186.21 g/mol. $R_f = 0.38$ (cyclohexane/ethyl acetate 9:1). ^1H NMR (300 MHz, CDCl_3) δ 10.36 (s, 1H, CHO), 9.16-9.02 (m, 1H, ArH), 7.84-7.75 (m, 1H, ArH), 7.68-7.60 (m, 1H, ArH), 7.57-7.47 (m, 2H, ArH), 7.38 (d, $J = 2.5$ Hz, 1H, ArH), 3.95 (s, 3H, OCH_3) ppm.

4-methoxy-1-naphthaldehyde 8b. Starting compound: **16b**. Yellow-brown oil, 89 % yield. Molecular formula: $\text{C}_{12}\text{H}_{10}\text{O}_2$. Molecular Weight: 186.21 g/mol. $R_f = 0.25$ (cyclohexane/ethyl acetate 9:1). ^1H NMR (300 MHz, CDCl_3) δ 10.18 (s, 1H, CHO), 9.30 (d, $J = 8.6$ Hz, 1H, ArH), 8.32 (d, $J = 7.8$ Hz, 1H, ArH), 7.88 (d, $J = 8.0$ Hz, 1H, ArH), 7.69 (t, $J = 7$ Hz, 1H, ArH), 7.56 (t, $J = 8.3$ Hz, 1H, ArH), 6.88 (d, $J = 8.0$ Hz, 1H, ArH), 4.04 (s, 3H, OCH_3) ppm.

General procedure for formation of Boc-protected amines (18g,h).

To a solution of the proper bromo-1-naphthalenamine (300 mg, 1.351 mmol) in ethanol (2.5 mL) di-*tert*-butyl dicarbonate (442.3 mg, 2.026 mmol) was added [149]. The resulting mixture was kept under stirring for 24 hours at 30°C . Then the solvent was evaporated under reduced pressure and the crude oil was purified by flash

chromatography eluting with cyclohexane/ethyl acetate (9:1) to afford compound **18g** or **18h**.

tert-butyl-4-bromonaphthylcarbamate **18g**. Starting compound: 1-amino-4-bromonaphthalene. Foam, 98 % yield. Molecular formula: C₁₅H₁₆BrNO₂. Molecular Weight: 322.20 g/mol. R_f = 0.33 (cyclohexane/ethyl acetate 9:1). ¹H NMR (300 MHz, CDCl₃) δ 8.25 (d, *J* = 7.5 Hz, 1H, ArH), 7.86 (d, *J* = 8.1 Hz, 1H, ArH), 7.71-7.77 (m, 2H, ArH), 7.51-7.62 (m, 2H, ArH), 6.89 (br s, 1H, NH, exchangeable with D₂O), 1.56 (s, 9H, CH₃) ppm.

tert-butyl-5-bromonaphthylcarbamate **18h**. Starting compound: 1-amino-5-bromonaphthalene. Light pink foam, 85 % yield. Molecular formula: C₁₅H₁₆BrNO₂. Molecular Weight: 322.20 g/mol. R_f = 0.53 (cyclohexane/ethyl acetate 8:2). ¹H NMR (300 MHz, CDCl₃) δ 7.99 (d, *J* = 8.7 Hz, 1H, ArH), 7.79-7.87 (m, 2H, ArH), 7.73 (d, *J* = 7.5 Hz, 1H, ArH), 7.50 (t, *J* = 8.1 Hz, 1H, ArH), 7.28 (t, *J* = 8.1 Hz, 1H, ArH), 6.73 (br s, 1H, NH, exchangeable with D₂O), 1.49 (s, 9H, CH₃) ppm.

Synthesis of 4,4-dimethyl-2-(2-bromophenyl)oxazoline **9**.

Thionyl chloride (1.09 mL, 14.924 mmol) was added to 2-bromobenzoic acid (1000 mg, 4.975 mmol) under N₂ and the mixture was refluxed for 6 hours. Then the excess of thionyl chloride was removed under vacuum. The ice-cold solution of the remaining acyl chloride in dry dichloromethane (2 mL) was added dropwise to a solution of 2-amino-2-methyl-1-propanol (886.9 mg, 9.950 mmol) in dichloromethane (2 mL) at 0°C. The mixture was stirred at room temperature for 2 hours. In order to purify the reaction mixture from the unreacted 2-amino-2-methyl-1-propanol, the organic phase was washed with 3N HCl (3x1 mL), dried over anhydrous sodium sulfate, filtered and the solvent was evaporated under reduced pressure. The crude **19** was used in the following reaction without further purification. White foam, 98 % yield. Molecular formula: C₁₁H₁₄BrNO₂. Molecular weight: 272.14 g/mol. R_f = 0.67 (dichloromethane/methanol 9:1). ¹H NMR (300 MHz, CDCl₃) δ 7.51 (dd, *J*₁ = 8.1 Hz, *J*₂ = 1.1 Hz, 1H, ArH), 7.43 (dd, *J*₁ = 7.7 Hz, *J*₂ = 1.8 Hz, 1H, ArH), 7.29 (dt, *J*₁ = 8.1 Hz, *J*₂ = 1.1 Hz, 1H, ArH), 7.20 (dt, *J*₁ = 7.7 Hz, *J*₂ = 1.8 Hz, 1H, ArH), 5.97 (br s, 1H,

exchangeable with D₂O), 3.96 (br s, 1H, exchangeable with D₂O), 3.63 (s, 2H, CH₂), 1.35 (s, 6H, CH₃) ppm.

In order to obtain the final compound **9**, thionyl chloride (1.07 mL, 14.625 mmol) was added dropwise to benzamide **19** (1326.8 mg, 4.875 mmol). When the vigorous reaction had subsided, 6 mL of dry diethyl ether was added to the yellow solution. The excess of thionyl chloride was evaporated under reduce pressure to provide white crystals of the hydrochloride salt which was neutralized with cold 20% sodium hydroxide (2 mL) and extracted with diethyl ether (3x2 mL). The organic phase was dried over anhydrous sodium sulfate and the solvent was evaporated under reduced pressure. The crude brown oil was purified by flash chromatography eluting firstly with cyclohexane/ethyl acetate (98:2) and then with cyclohexane/ethyl acetate (9:1) to afford compound **9**. Pale yellow oil, 79 % yield. Molecular formula: C₁₁H₁₂BrNO. Molecular weight: 254.12 g/mol. R_f = 0.15 (cyclohexane / ethyl acetate 9:1). ¹H NMR (300 MHz, CDCl₃) δ 7.62-7.54 (m, 2H, ArH), 7.18-7.31 (m, 2H, ArH), 4.08 (s, 2H, CH₂), 1.35 (s, 6H, CH₃) ppm.

General procedure for the synthesis of ethyl-bromobenzoate derivates (20, 21, 2).

To a solution of the suitable bromobenzoic acid (500 mg, 2.487 mmol) in ethanol (1mL) a catalytic amount of concentrated sulfuric acid was added dropwise. The resulting mixture was kept under stirring at reflux overnight and, after cooling, the solvent was evaporated under reduced pressure. Ethyl acetate (3 mL) was added and the organic layer was firstly wash with a saturated solution of sodium bicarbonate (1x2 mL) and then with water (2x2 mL). The organic solvent was dried over anhydrous sodium sulfate and evaporated. Purification with flash chromatography (eluent: cyclohexane/ethyl acetate 9:1) was performed.

Ethyl-2-bromobenzoate **20**. Starting compound: 2-bromobenzoic acid. Pail brown oil, 56 % yield. Molecular formula: C₉H₉BrO₂. Molecular Weight: 229.07 g/mol. R_f = 0.63 (cyclohexane/ethyl acetate 9:1). ¹H NMR (300 MHz, CDCl₃) δ 7.73 (dd, *J*₁ = 7 Hz, *J*₂ = 2 Hz, 1H, ArH), 7.60 (dd, *J*₁ = 8 Hz, *J*₂ = 1.5 Hz, 1H, ArH), 7.28 (m, 2H, ArH), 4.36 (q, *J* = 7.2 Hz, 2H, CH₂), 1.36 (t, *J* = 7.2 Hz, 3H, CH₃) ppm.

Ethyl-3-bromobenzoate **21**. Starting compound: 3-bromobenzoic acid. Pail brown oil, 65 % yield. Molecular formula: C₉H₉BrO₂. Molecular Weight: 229.07 g/mol. R_f = 0.72 (cyclohexane/ethyl acetate 9:1). ¹H NMR (300 MHz, CDCl₃) δ 8.18 (t, *J* = 1.8 Hz, 1H, ArH), 7.97 (dt, *J*₁ = 8.1 Hz, *J*₂ = 1.2 Hz, 1H, ArH), 7.67 (ddd, *J*₁ = 8.1 Hz, *J*₂ = 1.8 Hz, *J*₃ = 1.2 Hz, 1H, ArH), 7.30 (t, *J* = 8.1 Hz, 1H, ArH), 4.37 (q, *J* = 7.2 Hz, 2H, CH₂), 1.39 (t, *J* = 7.2 Hz, 3H, CH₃) ppm.

Ethyl-2-naphthoylebenzoate **2**. Starting compounds: **1**. Yellow oil, 60 % yield. Molecular formula: C₂₀H₁₆O₃. Molecular Weight: 304.34 g/mol. R_f = 0.38 (cyclohexane/ethyl acetate 9:1). ¹H NMR (300 MHz, CDCl₃) δ 9.07 (d, *J* = 8.4 Hz, 1H, ArH), 7.99 (m, 2H, ArH), 7.90 (d, *J* = 8.4 Hz, 1H, ArH), 7.50-7.60 (m, 5H, ArH), 7.45 (d, *J* = 7.5 Hz, 1H, ArH), 7.36 (t, *J* = 8.4 Hz, 1H, ArH), 3.90 (q, *J* = 7.2 Hz, 2H, CH₂), 0.91 (t, *J* = 7.2 Hz, 3H, CH₃) ppm.

General procedure for the synthesis of synthesis of 3-(methoxy-1-naphthyl)phthalide derivatives (11a,b)

To a solution of compound **9** (200 mg, 0.787 mmol) in dry diethyl ether (1 mL) at -78 °C was added dropwise 0.58 mL of a 2.7 M solution of *n*BuLi in heptane (1.574 mmol), under N₂ [150]. The solution was stirred at -78°C for 1 hour, then the suitable methoxy-1-naphthaldehyde **8a** or **8b** (146.5 mg, 0.787 mmol) was added and the reaction mixture was stirred at room temperature overnight. To quench the unreacted *n*BuLi, cold water (1 mL) was dropped in the reaction mixture and then the aqueous phase extracted with ethyl acetate (3x2 mL). The organic phase was dried over anhydrous sodium sulfate and the solvent was evaporated under reduced pressure. The obtained oil (284.3 mg) was dissolved in a solution of 3N HCl (1.5 mL), and the mixture was heated at reflux for 4.5 hours. After cooling, the solid was collected and washed with water, in order to be taken up in aqueous 10% NaOH (1.5 mL) and heated at reflux for 1 hour. The product was collected on acidification with 3N HCl (2 mL), extracted into ethyl acetate, washed with water and dried over sodium sulfate anhydrous. The solvent was evaporated under reduced pressure to give a crude solid

which was purified by flash chromatography eluting with cyclohexane/ethyl acetate (8:2).

3-(3-methoxy-1-naphthoyl)phthalide 11a. Starting compounds: compound **8a** and **9**. Foam, 52 % yield. Molecular formula: C₁₉H₁₄O₃. Molecular Weight: 290.31 g/mol. R_f = 0.37 (cyclohexane/ethyl acetate 8:2). ¹H NMR (300 MHz, CDCl₃) δ 8.15 (d, *J* = 8 Hz, 1H, ArH), 8.00 (d, *J* = 8 Hz, 1H, ArH), 7.81 (d, *J* = 7.7 Hz, 1H, ArH), 7.40-7.67 (m, 5H, ArH), 7.13-7.20 (m, 2H, ArH), 6.95 (d, *J* = 2.5 Hz, 1H, ArH), 3.86 (s, 3H, OCH₃) ppm.

3-(4-methoxy-1-naphthoyl)phthalide 11b. Starting compounds: compound **8b** and **9**. Oil, 21 % yield. Molecular formula: C₁₉H₁₄O₃. Molecular Weight: 290.31 g/mol. R_f = 0.41 (cyclohexane/ethyl acetate 8:2). ¹H NMR (300 MHz, CDCl₃) δ 8.29 (d, *J* = 8.1 Hz, 1H, ArH), 8.09 (d, *J* = 8.4 Hz, 1H, ArH), 7.94 (d, *J* = 7.2 Hz, 1H, ArH), 7.46-7.62 (m, 4H, ArH), 7.36 (d, *J* = 7.8 Hz, 1H, ArH), 7.06-7.09 (m, 2H, ArH), 6.63 (d, *J* = 8.1 Hz, 1H, ArH), 3.91 (s, 3H, OCH₃) ppm.

Synthesis of 2-(1-naphthyl)benzoic acid 1.

A mixture of 1-bromonaphthalene (200 mg, 0.966 mmol), magnesium turnings (47 mg, 1.931 mmol), and a catalytic amount of iodine in dry THF (2 mL) was refluxed under N₂ until the formation of the Grignard reagent. Hence it was added dropwise, under N₂, to a solution of phthalic anhydride (143.1 mg, 0.966 mmol) in dry THF (1.5 mL) and the resulting mixture was heated under reflux for 48 hours. The reaction mixture was quenched with 0.5 mL of a saturated aqueous solution of ammonium chloride. The solvent was evaporated and then the aqueous layer was extracted with ethyl acetate (3x2 mL). In order to purify the reaction mixture from the unreacted starting material, the organic phase was firstly treated with saturated solution of sodium bicarbonate (1 mL) and then the collected alkaline aqueous layer, which contained the sodium salt of compound **1**, was acidified by 3N HCl and extracted with ethyl acetate (3x2 mL). The organic phase was dried over anhydrous sodium sulfate, filtrated and the solvent was evaporated under reduced pressure. The crude oil was purified by flash chromatography eluting firstly with cyclohexane/ethyl acetate (8:2) and then with dichloromethane/methanol (95:5) to afford compound **1**. Pale green oil, 73 % yield.

Molecular formula: C₁₈H₁₂O₃. Molecular Weight: 276.29 g/mol. R_f = 0.28 (dichloromethane/methanol 95:5). ¹H NMR (300 MHz, CD₃OD) δ 8.94 (d, *J* = 8.1 Hz, 1H, ArH), 7.98 (d, *J* = 8.1 Hz, 1H, ArH), 7.82-7.94 (m, 2H, ArH), 7.30-7.62 (m, 7H, ArH) ppm.

General procedure for the synthesis of 2-(methoxy-1-naphthyl)benzoic acids (1a,b).

To a stirred mixture of the proper lactone **11a** or **11b** (50 mg, 0.172 mmol) in 25% KOH (1 mL) and pyridine (0.5 mL) powdered KMnO₄ (43.5 mg, 0.275 mmol) was added, and the mixture was heated at reflux for 5 hours. The hot mixture was filtered and the residue was washed with water. Then the filtrate was extracted with diethyl ether (2x2 mL) to remove any unreacted lactone. The aqueous phase was acidified with 3N HCl (2 mL), extracted with ethyl acetate (3x2 mL), washed with water and the organic layer was dried over sodium sulfate anhydrous. The organic solvent was evaporated under reduced pressure to give a crude oil which was purified by flash chromatography eluting firstly with cyclohexane/ethyl acetate (8:2) and then (1:9) to afford compound **1a** or **1b**.

2-(3-methoxy-1-naphthoyl)benzoic acid 1a. Oil, 71 % yield. Molecular formula: C₁₉H₁₄O₄. Molecular Weight: 306.31 g/mol. R_f = 0.31 (dichloromethane/methanol 95:5). ¹H NMR (300 MHz, CD₃OD) δ 8.81 (d, *J* = 9 Hz, 1H, ArH), 7.89 (dd, *J*₁ = 6 Hz, *J*₂ = 3 Hz, 1H, ArH), 7.80 (d, *J* = 9 Hz, 1H, ArH), 7.40-7.60 (m, 6H, ArH), 6.99 (d, *J* = 3 Hz, 1H, ArH), 3.82 (s, 3H, OCH₃) ppm.

2-(4-methoxy-1-naphthoyl)benzoic acid 1b. Brown foam, 36 % yield. Molecular formula: C₁₉H₁₄O₄. Molecular Weight: 306.31 g/mol. R_f = 0.20 (dichloromethane/methanol 95:5). ¹H NMR (300 MHz, CD₃OD) δ 9.12 (d, *J* = 8.4 Hz, 1H, ArH), 8.28 (d, *J* = 8.7 Hz, 1H, ArH), 7.87-7.90 (m, 1H, ArH), 7.62 (dt, *J*₁ = 7.2 Hz, *J*₂ = 1.5 Hz, 1H, ArH), 7.45-7.54 (m, 4H, ArH), 7.36-7.39 (m, 1H, ArH), 6.76 (d, *J* = 8.1 Hz, 1H, ArH), 4.02 (s, 3H, OCH₃) ppm.

General procedure for the synthesis of ethyl-(naphthylamino)benzoates (4, 4a,b, 6, 6a,b,g,h, 7).

Procedure a. A dried flask was purged with argon, charged with (±)-BINAP (3% mmol) and toluene (2.7 mL) was added [151]. The mixture was heated to 80 °C under stirring until the BINAP was dissolved. The solution was cooled to room temperature, and Pd(OAc)₂ (2% mmol) was added. The mixture was stirred at room temperature for 1 minute, then a solution of the proper 1-bromonaphthalene (1.0 mmol) and the corresponding ethyl aminobenzoate (0.8 mmol) in toluene (0.5 mL) was added. Finally, Cs₂CO₃ (1.14 mmol) and other toluene (2 mL) were added to the reaction mixture. The solution was heated at 80 °C under stirring, then was cooled to room temperature, diluted with diethyl ether, filtered, and concentrated. The obtained crude product was purified by column chromatography to provide the desired adduct.

Procedure b. A dried flask was purged with argon, charged with (±)-BINAP (3% mmol) and toluene (2.7 mL) was added. The mixture was heated to 80 °C under stirring until the BINAP was dissolved. The solution was cooled to room temperature, and Pd(OAc)₂ (2% mmol) was added. After stirring of the mixture at room temperature for 1 minute, a solution of proper ethyl bromobenzoate (1.0 mmol) with appropriate naphthylamine (0.8 mmol) in toluene (0.5 mL) was added. Cs₂CO₃ (1.14 mmol) was introduced within the mixture and toluene (2 mL) was added. The mixture was heated to 80 °C under stirring, then was cooled to room temperature, diluted with diethyl ether, filtered, and concentrated. The crude product that was obtained was purified by column chromatography to obtain the desired adduct.

Ethyl-2-(naphthylamino)benzoate 4. Procedure a: starting from 1-bromonaphthalene and ethyl-2-amino-benzoate. Reaction time: 17 hours. Silver foam, quantitative yield. Molecular formula: C₁₉H₁₇NO₂. Molecular Weight: 291.34 g/mol. R_f = 0.47 (cyclohexane/ethyl acetate 98:2). Eluent for chromatography: firstly only cyclohexane, then cyclohexane/ ethyl acetate from (98:2) to till (9:1). ¹H NMR (300 MHz, CDCl₃) δ 9.85 (br s, 1H, NH, exchangeable with D₂O), 8.10-8.13 (m, 1H, ArH), 8.05 (dd, J₁ = 7.8 Hz, J₂ = 1.2 Hz 1H, ArH), 7.88-7.91 (m, 1H, ArH), 7.71 (d, J = 7.8 Hz, 1H, ArH), 7.45-7.55 (m, 4H, ArH), 7.22-7.27 (m, 1H, ArH), 6.96 (dd, J₁ = 8.7 Hz, J₂ = 0.9 Hz, 1H,

ArH), 6.73 (dt, $J_1 = 7.8$ Hz, $J_2 = 1.2$ Hz, 1H, ArH), 4.43 (q, $J = 7.2$ Hz, 2H, CH₂), 1.45 (t, $J = 7.2$ Hz, 3H, CH₃) ppm.

Ethyl-2-(3-methoxy-1-naphthylamino)benzoate 4a. Procedure a: starting from **16a** and ethyl-2-aminobenzoate. Reaction time: 18 hours. Yellow oil, 71% yield. Molecular formula: C₂₀H₁₉NO₃. Molecular Weight: 321.37 g/mol. Rf = 0.62 (cyclohexane/ethyl acetate 9:1). Eluent for chromatography: cyclohexane/ethyl acetate (9:1). ¹H NMR (300 MHz, CDCl₃) δ 9.98 (br s, 1H, NH, exchangeable with D₂O), 8.08 (d, $J = 8.1$ Hz, 2H, ArH), 7.79 (d, $J = 8.1$ Hz, 1H, ArH), 7.50 (t, $J = 8.1$ Hz, 1H, ArH), 7.28-7.41 (m, 3H, ArH), 7.19 (d, $J = 8.4$ Hz, 1H, ArH), 7.02 (d, $J = 2.4$ Hz, 1H, ArH), 6.79 (t, $J = 7.8$ Hz, 1H, ArH), 4.45 (q, $J = 6.9$ Hz, 2H, CH₂), 3.95 (s, 3H, OCH₃), 1.47 (t, $J = 6.9$ Hz, 3H, CH₃) ppm.

Ethyl-2-(4-methoxy-1-naphthylamino)benzoate 4b. Procedure b: starting from **20** and **17**. Reaction time: 18 hours. Yellow oil, 98% yield. Molecular formula: C₂₀H₁₉NO₃. Molecular Weight: 321.37 g/mol. Rf = 0.40 (cyclohexane/ethyl acetate 98:2). Eluent for chromatography: cyclohexane/ethyl acetate (98:2). ¹H NMR (300 MHz, CDCl₃) δ 9.49 (br s, 1H, NH, exchangeable with D₂O), 8.30 (d, $J = 8.8$ Hz, 1H, ArH), 8.06-7.89 (m, 2H, ArH), 7.55-7.42 (m, 2H, ArH), 7.37 (d, $J = 8.2$ Hz, 1H, ArH), 7.15 (t, $J = 8.4$ Hz, 1H, ArH), 6.82 (d, $J = 8.3$ Hz, 1H, ArH), 6.64 (t, $J = 7.6$ Hz, 1H, ArH), 6.58 (d, $J = 8.6$ Hz, 1H, ArH), 4.41 (q, $J = 7.1$ Hz, 2H, CH₂), 4.03 (s, 3H, OCH₃), 1.44 (t, $J = 7.1$ Hz, 3H, CH₃) ppm.

Ethyl-3-(naphthylamino)benzoate 6. Procedure a: starting from 1-bromonaphthalene and ethyl-3-amino-benzoate. Reaction time: 17 hours. Yellow-brown oil, 83% yield. Molecular formula: C₁₉H₁₇O₂. Molecular Weight: 291.34 g/mol. Rf = 0.39 (cyclohexane/ethyl acetate 9:1). Eluent for chromatography: cyclohexane/ethyl acetate (95:5). ¹H NMR (300 MHz, CDCl₃) δ 8.01 (dd, $J_1 = 8.4$ Hz, $J_2 = 1.2$ Hz, 1H, ArH), 7.88 (dd, $J_1 = 7.0$ Hz, $J_2 = 2.5$ Hz, 1H, ArH), 7.67-7.71 (m, 1H, ArH), 7.36-7.64 (m, 6H, ArH), 7.28 (t, $J = 8.1$ Hz, 1H, ArH), 7.12 (ddd, $J_1 = 8.1$ Hz, $J_2 = 2.4$ Hz, $J_3 = 1.0$ Hz, 1H, ArH), 6.06 (br s, 1H, NH, exchangeable with D₂O), 4.36 (q, $J = 7.1$ Hz, 2H, CH₂), 1.38 (t, $J = 7.1$ Hz, 3H, CH₃) ppm.

Ethyl-3-(3-methoxy-1-naphthylamino)benzoate 6a. Procedure a: starting from **16a** and ethyl-3-aminobenzoate. Reaction time: 18 hours. Yellow oil, 85% yield. Molecular formula: C₂₀H₁₉NO₃. Molecular Weight: 321.37 g/mol. R_f = 0.36 (cyclohexane/ethyl acetate 9:1). Eluent for chromatography: cyclohexane/ethyl acetate (98:2). ¹H NMR (300 MHz, CDCl₃) δ 7.91 (d, *J* = 8.1 Hz, 1H, ArH), 7.74-7.78 (m, 2H, ArH), 7.63 (dt, *J*₁ = 7.5 Hz, *J*₂ = 1.2 Hz, 1H, ArH), 7.46 (dt, *J*₁ = 7.8 Hz, *J*₂ = 1.2 Hz, 1H, ArH), 7.21-7.36 (m, 3H, ArH), 7.04 (d, *J* = 2.4 Hz, 1H, ArH), 6.90 (d, *J* = 2.1 Hz, 1H, ArH), 6.13 (br s, 1H, NH, exchangeable with D₂O), 4.37 (q, *J* = 6.9 Hz, 2H, CH₂), 3.90 (s, 3H, OCH₃), 1.39 (t, *J* = 7.2 Hz, 3H, CH₃) ppm.

Ethyl-3-(4-methoxy-1-naphthylamino)benzoate 6b. Procedure a: starting from **16b** and ethyl-3-aminobenzoate. Reaction time: 40 hours, 40% yield. Procedure b: starting from **21** and **17**. Reaction time: 24 hours, 94% yield. Brown oil. Molecular formula: C₂₀H₁₉NO₃. Molecular Weight: 321.37 g/mol. R_f = 0.25 (cyclohexane/ethyl acetate 9:1). Eluent for chromatography: cyclohexane/ethyl acetate (9:1). ¹H NMR (300 MHz, CO(CD₃)₂) δ 8.13-8.16 (m, 1H, ArH), 7.88-7.91 (m, 1H, ArH), 7.33-7.40 (m, 3H, ArH), 7.21-7.26 (m, 1H, NH, exchangeable with D₂O; 2H, ArH), 7.10 (t, *J* = 7.8 Hz, 1H, ArH), 6.82-6.25 (m, 2H, ArH), 4.14 (q, *J* = 7.2 Hz, 2H, CH₂), 3.91 (s, 3H, OCH₃), 1.17 (t, *J* = 7.2 Hz, 3H, CH₃) ppm.

Ethyl-3-(4-((tert-butoxycarbonyl)amino)-1-naphthylamino)benzoate 6g. Procedure a: starting from **18g** and ethyl-3-aminobenzoate. Reaction time: 18 hours. Silver foam, 83% yield. Molecular formula: C₂₄H₂₆N₂O₄. Molecular Weight: 406.47 g/mol. R_f = 0.40 (cyclohexane/ethyl acetate 8:2). Eluent for chromatography: cyclohexane/ethyl acetate (8:2). ¹H NMR (300 MHz, CD₃OD) δ 8.09 (d, *J* = 8.1 Hz, 1H, ArH), 8.02 (d, *J* = 8.4 Hz, 1H, ArH), 7.41-7.57 (m, 5H, ArH), 7.34 (d, *J* = 8.1 Hz, 1H, ArH), 7.25 (t, *J* = 7.8 Hz, 1H, ArH), 7.11 (dd, *J*₁ = 8.1 Hz, *J*₂ = 2.1 Hz, 1H, ArH), 4.30 (q, *J* = 7.2 Hz, 2H, CH₂), 1.55 (s, 9H, CH₃), 1.34 (t, *J* = 7.2 Hz, 3H, CH₃) ppm.

Ethyl-3-(5-((tert-butoxycarbonyl)amino)-1-naphthylamino)benzoate 6h. Procedure a: starting from **18h** and ethyl-3-aminobenzoate. Reaction time: 18 hours. Foam, 85% yield. Molecular formula: C₂₄H₂₆N₂O₄. Molecular Weight: 406.47 g/mol. R_f = 0.33 (cyclohexane/ethyl acetate 8:2). Eluent for chromatography: cyclohexane/ethyl acetate (8:2). ¹H NMR (300 MHz, CDCl₃) δ 7.82 (d, *J* = 7.5 Hz, 1H, ArH), 7.70 (d, *J* = 8.4 Hz,

1H, ArH), 7.59 (t, $J = 1.8$ Hz, 1H, ArH), 7.47-7.54 (m, 2H, ArH), 7.26-7.35 (m, 3H, ArH), 7.18 (t, $J = 7.5$ Hz, 1H, ArH), 7.02 (dd, $J_1 = 8.4$ Hz, $J_2 = 1.5$ Hz, 1H, ArH), 6.83 (br s, 1H, NH, exchangeable with D₂O), 6.02 (br s, 1H, NH, exchangeable with D₂O), 4.26 (q, $J = 6.9$ Hz, 2H, CH₂), 1.48 (s, 9H, CH₃), 1.28 (t, $J = 6.9$ Hz, 3H, CH₃) ppm.

1-(N-phenylamino)naphthalene **7**. Procedure a: starting from 1-bromonaphthalene and aniline. Yellow-brown oil, 34 % yield. Molecular formula: C₁₆H₁₃N. Molecular Weight: 219.28 g/mol. R_f = 0.58 (cyclohexane/ethyl acetate 9:1). Eluent for chromatography: firstly only cyclohexane and then cyclohexane/ ethyl acetate (95:5). ¹H NMR (300 MHz, CDCl₃) δ 8.04 (dd, $J_1 = 7.2$ Hz, $J_2 = 2.1$ Hz, 1H, ArH), 7.89 (dd, $J_1 = 7.2$ Hz, $J_2 = 2.1$ Hz, 1H, ArH), 7.59 (dd, $J_1 = 7.2$ Hz, $J_2 = 2.1$ Hz, 1H, ArH), 7.40-7.53 (m, 4H, ArH), 7.26-7.31 (m, 2H, ArH), 7.00-7.03 (m, 2H, ArH), 6.94 (t, $J_1 = 7.2$ Hz, $J_2 = 1.2$ Hz, 1H, ArH), 5.95 (br s, 1H, NH, exchangeable with D₂O) ppm.

General procedure for the ester hydrolysis to obtain (naphthylamino)benzoic acid derivates (3, 3a,b, 5, 5a,b,g,h).

To a solution of the suitable ethyl-(naphthylamino)-benzoate (0.15 mmol) in 2 mL of THF/EtOH (1:1), 1M NaOH (0.375 mmol) was added [152]. The resulting mixture was refluxed for a period of time different for each substrate. The solvent was evaporated and then water (2 mL) was added. The aqueous phase was firstly washed with diethyl ether in order to purify the reaction mixture from the unreacted starting material, and then treated with 1N HCl (0.5 mL). The acid was extracted with ethyl acetate (3x1 mL), then the organic phase was dried over anhydrous sodium sulfate and the solvent was evaporated under reduced pressure. The crude was purified by flash chromatography eluting dichloromethane/methanol (95:5) to afford the desired derivates.

2-(naphthylamino)benzoic acid **3**. Starting compound: compound **4**. Reaction time: 60 minutes. Yellow oil, 98 % yield. Molecular formula: C₁₇H₁₃NO₂. Molecular Weight: 263.29 g/mol. R_f = 0.39 (dichloromethane/methanol 95:5). ¹H NMR (300 MHz, CO(CD₃)₂) δ 10.09 (br s, 1H, NH, exchangeable with D₂O), 8.07-8.09 (m, 2H, ArH),

7.95-7.97 (m, 1H, ArH), 7.77 (d, $J = 7.5$ Hz, 1H, ArH), 7.51-7.58 (m, 4H, ArH), 7.33 (t, $J = 8.7$ Hz, 1H, ArH), 6.97 (d, $J = 8.7$ Hz, 1H, ArH), 6.78 (t, $J = 7.5$ Hz, 1H, ArH) ppm.

2-(3-methoxy-1-naphthylamino)benzoic acid 3a. Starting compound: compound **4a**. Reaction time: 30 minutes. Yellow foam, quantitative yield. Molecular formula: $C_{18}H_{15}NO_3$. Molecular Weight: 293.32 g/mol. $R_f = 0.34$ (dichloromethane/methanol 95:5). 1H NMR (300 MHz, $CO(CD_3)_2$) δ 10.15 (br s, 1H, NH, exchangeable with D_2O), 7.96 (d, $J = 8.4$ Hz, 1H, ArH), 7.85 (d, $J = 8.4$ Hz, 1H, ArH), 7.71 (d, $J = 8.1$ Hz, 1H, ArH), 7.35 (t, $J = 7.2$ Hz, 1H, ArH), 7.20-7.244 (m, 2H, ArH), 7.08 (d, $J = 2.1$ Hz, 1H, ArH), 6.99-7.02 (m, 2H, ArH), 6.68 (d, $J = 7.2$ Hz, 1H, ArH), 3.80 (s, 3H, OCH_3) ppm.

2-(4-methoxy-1-naphthylamino)benzoic acid 3b. Starting compound: compound **4b**. Reaction time: 90 minutes. Oil, 53 % yield. Molecular formula: $C_{18}H_{15}NO_3$. Molecular Weight: 293.32 g/mol. $R_f = 0.54$ (dichloromethane/methanol 95:5). 1H NMR (300 MHz, $CO(CD_3)_2$) δ 9.72 (br s, 1H, NH, exchangeable with D_2O), 8.25-8.34 (m, 1H, ArH), 8.03 (dd, $J_1 = 8.0$ Hz, $J_2 = 1.6$ Hz, 1H, ArH), 7.89-7.96 (m, 1H, ArH), 7.48-7.58 (m, 2H, ArH), 7.44 (d, $J = 8.1$ Hz, 1H, ArH), 7.23 (dt, $J_1 = 8.4$ Hz, $J_2 = 1.6$ Hz, 1H, ArH), 7.01 (d, $J = 8.1$ Hz, 1H, ArH), 6.69 (t, $J = 7.6$ Hz, 1H, ArH), 6.58 (d, $J = 8.5$ Hz, 1H, ArH), 4.07 (s, 3H, OCH_3) ppm.

(naphthylamino)benzoic acid 5. Starting compound: compound **6**. Reaction time: 60 minutes. Oil, 96 % yield. Molecular formula: $C_{17}H_{13}NO_2$. Molecular Weight: 263.29 g/mol. $R_f = 0.25$ (dichloromethane/methanol 95:5). 1H NMR (300 MHz, CD_3OD) δ 8.12 (d, $J = 7.5$ Hz, 1H, ArH), 7.82 (d, $J = 7.5$ Hz, 1H, ArH), 7.64 (s, 1H, ArH), 7.32-7.52 (m, 6H, ArH), 7.20 (t, $J = 7.5$ Hz, 1H, ArH), 7.08 (d, $J = 7.5$ Hz, 1H, ArH) ppm.

3-(3-methoxy-1-naphthylamino)benzoic acid 5a. Starting compound: compound **6a**. Reaction time: 40 minutes. Oil, 96 % yield. Molecular formula: $C_{18}H_{15}NO_3$. Molecular Weight: 293.32 g/mol. $R_f = 0.19$ (dichloromethane/methanol 95:5). 1H NMR (300 MHz, $CO(CD_3)_2$) δ 7.95 (d, $J = 8.4$ Hz, 1H, ArH), 7.64-7.68 (m, 2H, ArH), 7.59 (br s, 1H, NH, exchangeable with D_2O), 7.41-7.44 (m, 1H, ArH), 7.14-7.33 (m, 4H, ArH), 6.91 (d, $J = 2.1$ Hz, 1H, ArH), 6.87 (d, $J = 2.1$ Hz, 1H, ArH), 3.74 (s, 3H, OCH_3) ppm.

3-(4-methoxy-1-naphthylamino)benzoic acid 5b. Starting compound: compound **6b**. Reaction time: 60 minutes. Oil, 73 % yield. Molecular formula: $C_{18}H_{15}NO_3$. Molecular

Weight: 293.32 g/mol. Rf = 0.16 (dichloromethane/methanol 95:5). ¹H NMR (300 MHz, CO(CD₃)₂) δ 8.25–8.31 (m, 1H, ArH), 7.99–8.07 (m, 1H, ArH), 7.45–7.55 (m, 3H, ArH), 7.36–7.42 (m, 2H, ArH), 7.34 (bs, 1H, NH, exchangeable with D₂O), 7.24 (t, *J* = 7.8 Hz, 1H, ArH), 7.00 (dd, *J* = 8.1, *J*₂ = 1.6 Hz, 1H, ArH), 6.96 (d, *J* = 8.2 Hz, 1H, ArH), 4.04 (s, 3H, OCH₃) ppm.

3-(4-((tert-butoxycarbonyl)amino)-1-naphthylamino)benzoic acid **5g**. Starting compound: compound **6g**. Reaction time: 30 minutes. Silver foam, quantitative yield. Molecular formula: C₂₂H₂₂N₂O₄. Molecular Weight: 378.42 g/mol. Rf = 0.17 (dichloromethane/methanol 95:5). ¹H NMR (300 MHz, CD₃OD) δ 8.09 (d, *J* = 7.8 Hz, 1H, ArH), 8.01 (d, *J* = 8.7 Hz, 1H, ArH), 7.42–7.59 (m, 5H, ArH), 7.32 (d, *J* = 8.1 Hz, 1H, ArH), 7.24 (t, *J* = 7.8 Hz, 1H, ArH), 7.10 (dq, *J*₁ = 7.8 Hz, *J*₂ = 1.5 Hz, 1H, ArH), 1.54 (s, 9H, CH₃) ppm.

3-(5-((tert-butoxycarbonyl)amino)-1-naphthylamino)benzoic acid **5h**. Starting compound: compound **6h**. Reaction time: 30 minutes. Green-brown oil, 79 % yield. Molecular formula: C₂₂H₂₂N₂O₄. Molecular Weight: 378.42 g/mol. Rf = 0.20 (dichloromethane/methanol 95:5). ¹H NMR (300 MHz, CO(CD₃)₂) δ 8.19 (br s, 1H, NH, exchangeable with D₂O), 7.84 (d, *J* = 8.7 Hz, 1H, ArH), 7.75 (dd, *J*₁ = 6.9 Hz, *J*₂ = 3 Hz, 1H, ArH), 7.70 (d, *J* = 7.5 Hz, 1H, ArH), 7.58 (t, *J* = 2.1 Hz, 1H, ArH), 7.55 (br s, 1H, NH, exchangeable with D₂O), 7.28–7.40 (m, 4H, ArH), 7.20 (t, *J* = 7.5 Hz, 1H, ArH), 7.12 (dq, *J*₁ = 8.1 Hz, *J*₂ = 1.2 Hz, 1H, ArH), 1.39 (s, 9H, CH₃) ppm.

General procedure for the demethoxylation of α,β-naphthol-methyl ethers.

To a solution of the proper methoxynaphthalene (0.180 mmol) in dry dichloromethane (2 mL), BBr₃ (1M in dichloromethane, 0.945 mmol) was added dropwise under N₂ [151]. The reaction takes place at room temperature for all the synthesized compounds except from **5c** and **3d**, indeed, the starting solution was firstly, cooled at -78°C and BBr₃ was carefully added dropwise to the reaction mixture. After 20 minutes, the resulting solution was warmed to room temperature and the stirring was continued for further 3 hours. The reaction was then quenched at 0°C with water (4 mL), and extracted with ethyl acetate (3x2 mL). The combined organic phases were

washed with brine (3x1 mL) and dried over anhydrous sodium sulfate. The subsequent filtration and evaporation of the organic solvent provide a crude product, which was purified by flash chromatography eluting firstly with dichloromethane/methanol (95:5) and then with dichloromethane/ methanol (8:2) to afford the final naphthol.

2-(3-hydroxy-1-naphthoyl)benzoic acid 1c. Starting compound: compound **1a**. Reaction time: 60 minutes. Foam, 6 % yield. Molecular formula: C₁₈H₁₂O₄. Molecular Weight: 292.29 g/mol. R_f = 0.10 (dichloromethane/methanol 95:5). ¹H NMR (300 MHz, CD₃OD) δ 8.78 (d, *J* = 8.1 Hz, 1H, ArH), 8.01 (dd, *J*₁ = 7.5 Hz, *J*₂ = 1.2 Hz, 1H, ArH), 7.64-7.72 (m, 3H, ArH), 7.37-7.53 (m, 3H, ArH), 7.28 (d, *J* = 2.4 Hz, 1H, ArH), 7.00 (d, *J* = 2.7 Hz, 1H, ArH) ppm.

2-(3-hydroxy-1-naphthylamino)benzoic acid 3c. Starting compound: compound **3a**. Reaction time: 30 minutes. Brown-purple foam, 90 % yield. Molecular formula: C₁₇H₁₃NO₃. Molecular Weight: 279.29 g/mol. R_f = 0.17 (dichloromethane/methanol 95:5). ¹H NMR (300 MHz, CO(CD₃)₂) δ 10.00 (br s, 1H, exchangeable with D₂O), 7.95 (dd, *J*₁ = 7.8 Hz, *J*₂ = 1.5 Hz, 1H, ArH), 7.81 (d, *J* = 8.4 Hz, 1H, ArH), 7.59 (d, *J* = 7.8 Hz, 1H, ArH), 7.10-7.32 (m, 4H, ArH), 6.99 (d, *J* = 8.4 Hz, 1H, ArH), 6.93 (d, *J* = 1.8 Hz, 1H, ArH), 6.67 (t, *J* = 7.5 Hz, 1H, ArH) ppm.

2-(4-hydroxy-1-naphthylamino)benzoic acid 3d. Starting compound: compound **3b**. Reaction time: 90 minutes. Dark foam, 98 % yield. Molecular formula: C₁₇H₁₃NO₃. Molecular Weight: 279.29 g/mol. R_f = 0.18 (dichloromethane/methanol 95:5). ¹H NMR (300 MHz, CO(CD₃)₂) δ 9.66 (br s, 1H, exchangeable with D₂O), 9.14 (br s, 1H, exchangeable with D₂O), 8.25-8.38 (m, 1H, ArH), 8.02 (dd, *J*₁ = 8.0 Hz, *J*₂ = 1.7 Hz, 1H, ArH), 7.85-7.94 (m, 1H, ArH), 7.43-7.58 (m, 2H, ArH), 7.32 (d, *J* = 7.9 Hz, 1H, ArH), 7.22 (dt, *J*₁ = 7.7 Hz, *J*₂ = 1.5 Hz, 1H, ArH), 6.98 (d, *J* = 8.0 Hz, 1H, ArH), 6.67 (t, *J* = 7.5 Hz, 1H, ArH), 6.55 (d, *J*₁ = 8.3 Hz, 1H, ArH) ppm.

3-(3-hydroxy-1-naphthylamino)benzoic acid 5c. Starting compound: compound **5a**. Reaction time: 210 minutes. Oil, 91 % yield. Molecular formula: C₁₇H₁₃NO₃. Molecular Weight: 279.29 g/mol. R_f = 0.17 (dichloromethane/methanol 95:5). ¹H NMR (300 MHz, CO(CD₃)₂) δ 7.93 (d, *J* = 8.0 Hz, 1H, ArH), 7.67 (s, 1H, ArH), 7.53-7.60 (m, 2H,

ArH), 7.40-7.44 (m, 1H, ArH), 7.22-7.30 (m, 3H, ArH, NH, exchangeable with D₂O), 7.08-7.14 (m, 1H, ArH), 6.96 (d, *J* = 2.7 Hz, 1H, ArH), 6.81 (s, 1H, ArH) ppm.

3-(4-hydroxy-1-naphthylamino)benzoic acid 5d. Starting compounds: compound **5b**. Reaction time: 60 minutes. Yellow oil, 89 % yield. Molecular formula: C₁₇H₁₃NO₃. Molecular Weight: 279.29 g/mol. R_f = 0.13 (dichloromethane/methanol 95:5). ¹H NMR (300 MHz, CO(CD₃)₂) δ 8.99 (br s, 1H, exchangeable with D₂O), 8.26-8.32 (m, 1H, ArH), 7.96-8.03 (m, 1H, ArH), 7.44-7.51 (m, 3H, ArH), 7.33-7.39 (m, 1H, ArH), 7.18-7.30 (m, 2H, ArH), 6.90-6.99 (m, 2H, ArH) ppm.

General procedure for Boc-deprotection to obtain the corresponding amines as hydrochloride salts (5e,f).

To an ice-cold solution of the proper tert-butyl-naphthylcarbamate (632 mg, 1.67 mmol) in dry 1,4-dioxane (1 mL), HCl (4M in 1,4-dioxane, 1 mL) was added dropwise, under N₂. The reaction was stirred at room temperature for 24 hours. After completion of the reaction, monitored by TLC, diethyl ether was added to the reaction mixture and it was stirred. After cooling at 0°C, the formed precipitate was collected by filtration, washed with cold diethyl ether and dried to afford hydrochloride acid salt of compound **5e** or **5f**.

3-(4-amino-1-naphthylamino)benzoic acid hydrochloride 5e. Starting compound: compound **5g**. Foam, 58 % yield. Molecular formula: C₁₇H₁₄N₂O₂ · HCl. Molecular Weight: 314.77 g/mol. ¹H NMR (300 MHz, CD₃OD) δ 8.33 (d, *J* = 9 Hz, 1H, ArH), 7.94 (d, *J* = 9 Hz, 1H, ArH), 7.72-7.78 (m, 2H, ArH), 7.66 (t, *J* = 8.1, 1H, ArH), 7.57-7.60 (m, 1H, ArH), 7.49 (d, *J* = 8.1 Hz, 1H, ArH), 7.33-7.40 (m, 3H, ArH) ppm.

3-(5-amino-1-naphthylamino)benzoic acid hydrochloride 5f. Starting compound: compound **5h**. Foam, 66 % yield. Molecular formula: C₁₇H₁₄N₂O₂ · HCl. Molecular Weight: 314.77 g/mol. ¹H NMR (300 MHz, CD₃OD) δ 8.28 (dd, *J*₁ = 8.1 Hz, *J*₂ = 1.2 Hz, 1H, ArH), 7.66 (t, *J* = 2.1 Hz, 1H, ArH), 7.49-7.63 (m, 6H, ArH), 7.34 (t, *J* = 7.8 Hz, 1H, ArH), 7.26 (dq, *J*₁ = 8.1 Hz, *J*₂ = 1.2 Hz, 1H, ArH) ppm.

References

- 1 Gunawardena, J. (2005) Multisite protein phosphorylation makes a good threshold but can be a poor switch. *Proceedings of the National Academy of Sciences of the United States of America* 102 (41), 14617-14622
- 2 Hunter, T. (1995) Protein kinases and phosphatases: The Yin and Yang of protein phosphorylation and signaling. *Cell* 80 (2), 225-236
- 3 Novak, B. et al. (2010) Regulated protein kinases and phosphatases in cell cycle decisions. *Current opinion in cell biology* 22 (6), 801-808
- 4 Tautz, L. et al. (2013) Protein tyrosine phosphatases: structure, function, and implication in human disease. *Phosphatase Modulators*, 179-221
- 5 Olsen, J.V. et al. (2006) Global, In Vivo, and Site-Specific Phosphorylation Dynamics in Signaling Networks. *Cell* 127 (3), 635-648
- 6 Egloff, M.-P. et al. (1995) Crystal Structure of the Catalytic Subunit of Human Protein Phosphatase 1 and its Complex with Tungstate. *Journal of Molecular Biology* 254 (5), 942-959
- 7 Barford, D. (1996) Molecular mechanisms of the protein serine/threonine phosphatases. *Trends in Biochemical Sciences* 21 (11), 407-412
- 8 Barford, D. et al. (1998) THE STRUCTURE AND MECHANISM OF PROTEIN PHOSPHATASES: Insights into Catalysis and Regulation. *Annual Review of Biophysics and Biomolecular Structure* 27 (1), 133-164
- 9 Denu, J.M. et al. (1996) Form and Function in Protein Dephosphorylation. *Cell* 87 (3), 361-364
- 10 Alonso, A. et al. (2004) Protein Tyrosine Phosphatases in the Human Genome. *Cell* 117 (6), 699-711
- 11 Russell, P. and Nurse, P. (1986) cdc25+ functions as an inducer in the mitotic control of fission yeast. *Cell* 45 (1), 145-153
- 12 Boudolf, V. et al. (2006) What if higher plants lack a CDC25 phosphatase? *Trends in Plant Science* 11 (10), 474-479
- 13 Galaktionov, K. and Beach, D. (1991) Specific activation of cdc25 tyrosine phosphatases by B-type cyclins: Evidence for multiple roles of mitotic cyclins. *Cell* 67 (6), 1181-1194
- 14 Sadhu, K. et al. (1990) Human homolog of fission yeast cdc25 mitotic inducer is predominantly expressed in G2. *Proceedings of the National Academy of Sciences of the United States of America* 87 (13), 5139-5143
- 15 Nagata, A. et al. (1991) An additional homolog of the fission yeast cdc25+ gene occurs in humans and is highly expressed in some cancer cells. *The new biologist* 3 (10), 959-968
- 16 Brenner, A.K. et al. (2014) Therapeutic targeting the cell division cycle 25 (CDC25) phosphatases in human acute myeloid leukemia—the possibility to target several kinases through inhibition of the various CDC25 isoforms. *Molecules* 19 (11), 18414-18447
- 17 Lyon, M.A. et al. (2002) Dual-specificity phosphatases as targets for antineoplastic agents. *Nature Reviews Drug Discovery* 1 (12), 961-976
- 18 Wegener, S. et al. (2000) Alternative splicing in the regulatory region of the human phosphatases CDC25A and CDC25C. *European journal of cell biology* 79 (11), 810-815
- 19 Baldin, V. et al. (1997) Alternative splicing of the human CDC25B tyrosine phosphatase. Possible implications for growth control? *Oncogene* 14 (20), 2485-2495
- 20 Forrest, A. et al. (1999) Multiple splicing variants of cdc25B regulate G2/M progression. *Biochemical and biophysical research communications* 260 (2), 510-515

- 21 Bureik, M. et al. (2000) An additional transcript of the *cdc25C* gene from A431 cells encodes a functional protein. *International journal of oncology* 17 (6), 1251-1259
- 22 Boutros, R. et al. (2006) The when and wheres of CDC25 phosphatases. *Current Opinion in Cell Biology* 18 (2), 185-191
- 23 Fauman, E.B. et al. (1998) Crystal structure of the catalytic domain of the human cell cycle control phosphatase, *Cdc25A*. *Cell* 93 (4), 617-625
- 24 Reynolds, R.A. et al. (1999) Crystal structure of the catalytic subunit of *Cdc25B* required for G2/M phase transition of the cell cycle. *J Mol Biol* 293 (3), 559-568
- 25 Rudolph, J. (2007) *Cdc25* phosphatases: structure, specificity, and mechanism. *Biochemistry* 46 (12), 3595-3604
- 26 Sohn, J. et al. (2004) Remote hot spots mediate protein substrate recognition for the *Cdc25* phosphatase. *Proceedings of the National Academy of Sciences of the United States of America* 101 (47), 16437-16441
- 27 Rudolph, J. (2004) Targeting the neighbor's pool. *Mol Pharmacol* 66 (4), 780-782
- 28 Hobiger, K. and Friedrich, T. (2015) Voltage sensitive phosphatases: emerging kinship to protein tyrosine phosphatases from structure-function research. *Frontiers in pharmacology* 6
- 29 Jackson, M.D. and Denu, J.M. (2001) Molecular reactions of protein phosphatases insights from structure and chemistry. *Chemical Reviews* 101 (8), 2313-2340
- 30 McCain, D.F. et al. (2002) The catalytic mechanism of *Cdc25A* phosphatase. *Journal of Biological Chemistry* 277 (13), 11190-11200
- 31 Chen, W. et al. (2000) Dual-specific *Cdc25B* phosphatase: in search of the catalytic acid. *Biochemistry* 39 (35), 10781-10789
- 32 Rudolph, J. (2002) Catalytic mechanism of *Cdc25*. *Biochemistry* 41 (49), 14613-14623
- 33 Parks, J.M. et al. (2009) Mechanism of *Cdc25B* phosphatase with the small molecule substrate *p*-nitrophenyl phosphate from QM/MM-MFEP calculations. *The Journal of Physical Chemistry B* 113 (15), 5217-5224
- 34 Malumbres, M. and Barbacid, M. (2005) Mammalian cyclin-dependent kinases. *Trends in biochemical sciences* 30 (11), 630-641
- 35 Hoffmann, I. et al. (1994) Activation of the phosphatase activity of human *cdc25A* by a *cdk2*-cyclin E dependent phosphorylation at the G1/S transition. *The EMBO journal* 13 (18), 4302
- 36 Chen, M.-S. et al. (2001) Absence of apparent phenotype in mice lacking *Cdc25C* protein phosphatase. *Molecular and cellular biology* 21 (12), 3853-3861
- 37 Ferguson, A.M. et al. (2005) Normal cell cycle and checkpoint responses in mice and cells lacking *Cdc25B* and *Cdc25C* protein phosphatases. *Molecular and cellular biology* 25 (7), 2853-2860
- 38 Lavecchia, A. et al. (2012) Discovery of new inhibitors of *Cdc25B* dual specificity phosphatases by structure-based virtual screening. *J Med Chem* 55 (9), 4142-4158
- 39 Ren, S. and Rollins, B.J. (2004) Cyclin C/*cdk3* promotes Rb-dependent G0 exit. *Cell* 117 (2), 239-251
- 40 Frazer, C. and Young, P. (2012) *Phosphorylation mediated regulation of Cdc25 activity, localization and stability*, INTECH Open Access Publisher
- 41 Turowski, P. et al. (2003) Functional *cdc25C* dual-specificity phosphatase is required for S-phase entry in human cells. *Molecular biology of the cell* 14 (7), 2984-2998
- 42 Gabrielli, B.G. et al. (1996) Cytoplasmic accumulation of *cdc25B* phosphatase in mitosis triggers centrosomal microtubule nucleation in HeLa cells. *Journal of Cell Science* 109 (5), 1081-1093
- 43 Lindqvist, A. et al. (2005) *Cdc25B* cooperates with *Cdc25A* to induce mitosis but has a unique role in activating cyclin B1-Cdk1 at the centrosome. *The Journal of cell biology* 171 (1), 35-45
- 44 Donzelli, M. et al. (2002) Dual mode of degradation of *Cdc25 A* phosphatase. *The EMBO journal* 21 (18), 4875-4884

- 45 Karlsson-Rosenthal, C. and Millar, J.B.A. (2006) Cdc25: mechanisms of checkpoint inhibition and recovery. *Trends in Cell Biology* 16 (6), 285-292
- 46 Salaun, P. et al. (2008) Cdk1, Plks, Auroras, and Neks: the mitotic bodyguards. In *Hormonal Carcinogenesis V*, pp. 41-56, Springer
- 47 Boutros, R. et al. (2007) CDC25 phosphatases in cancer cells: key players? Good targets? *Nat Rev Cancer* 7 (7), 495-507
- 48 Macurek, L. et al. (2009) Aurora-A and hBora join the game of Polo. *Cancer research* 69 (11), 4555-4558
- 49 Seki, A. et al. (2008) Bora and the kinase Aurora a cooperatively activate the kinase Plk1 and control mitotic entry. *Science* 320 (5883), 1655-1658
- 50 Kotani, S. et al. (1998) PKA and MPF-activated polo-like kinase regulate anaphase-promoting complex activity and mitosis progression. *Molecular cell* 1 (3), 371-380
- 51 Barré, B. et al. (2005) The STAT3 transcription factor is a target for the Myc and riboblastoma proteins on the Cdc25A promoter. *Journal of Biological Chemistry* 280 (16), 15673-15681
- 52 Dalvai, M. et al. (2011) Cdc25B is negatively regulated by p53 through Sp1 and NF-Y transcription factors. *Oncogene* 30 (19), 2282-2288
- 53 Clair, S.S. et al. (2004) DNA Damage-Induced Downregulation of Cdc25C Is Mediated by p53 via Two Independent Mechanisms: One Involves Direct Binding to the cdc25C Promoter. *Molecular Cell* 16 (5), 725-736
- 54 Didier, C. et al. (2008) G2/M checkpoint stringency is a key parameter in the sensitivity of AML cells to genotoxic stress. *Oncogene* 27 (27), 3811-3820
- 55 Reinhardt, H.C. and Yaffe, M.B. (2009) Kinases that control the cell cycle in response to DNA damage: Chk1, Chk2, and MK2. *Current opinion in cell biology* 21 (2), 245-255
- 56 Niida, H. and Nakanishi, M. (2006) DNA damage checkpoints in mammals. *Mutagenesis* 21 (1), 3-9
- 57 Falck, J. et al. (2001) The ATM-Chk2-Cdc25A checkpoint pathway guards against radioresistant DNA synthesis. *Nature* 410 (6830), 842-847
- 58 Uto, K. et al. (2004) Chk1, but not Chk2, inhibits Cdc25 phosphatases by a novel common mechanism. *The EMBO journal* 23 (16), 3386-3396
- 59 Krämer, A. et al. (2004) Centrosome-associated Chk1 prevents premature activation of cyclin-B-Cdk1 kinase. *Nature cell biology* 6 (9), 884-891
- 60 Schmitt, E. et al. (2006) CHK1 phosphorylates CDC25B during the cell cycle in the absence of DNA damage. *Journal of cell science* 119 (20), 4269-4275
- 61 Yarden, R.I. et al. (2002) BRCA1 regulates the G2/M checkpoint by activating Chk1 kinase upon DNA damage. *Nature genetics* 30 (3), 285-289
- 62 Busino, L. et al. (2004) Cdc25A phosphatase: combinatorial phosphorylation, ubiquitylation and proteolysis. *Oncogene* 23 (11), 2050-2056
- 63 Smits, V.A. et al. (2000) Polo-like kinase-1 is a target of the DNA damage checkpoint. *Nature cell biology* 2 (9), 672-676
- 64 Kumagai, A. and Dunphy, W.G. (2000) Claspin, a novel protein required for the activation of Chk1 during a DNA replication checkpoint response in *Xenopus* egg extracts. *Molecular cell* 6 (4), 839-849
- 65 Reinhardt, H.C. et al. (2007) p53-deficient cells rely on ATM-and ATR-mediated checkpoint signaling through the p38MAPK/MK2 pathway for survival after DNA damage. *Cancer cell* 11 (2), 175-189
- 66 Zeng, Y. and Piwnica-Worms, H. (1999) DNA damage and replication checkpoints in fission yeast require nuclear exclusion of the Cdc25 phosphatase via 14-3-3 binding. *Molecular and cellular biology* 19 (11), 7410-7419
- 67 Chen, R.-q. et al. (2009) CDC25B mediates rapamycin-induced oncogenic responses in cancer cells. *Cancer research* 69 (6), 2663-2668

- 68 Li, G.-Y. et al. (2013) A novel imidazopyridine derivative, HS-106, induces apoptosis of breast cancer cells and represses angiogenesis by targeting the PI3K/mTOR pathway. *Cancer letters* 329 (1), 59-67
- 69 Liang, J. and Slingerland, J.M. (2003) Multiple roles of the PI3K/PKB (Akt) pathway in cell cycle progression. *Cell cycle* 2 (4), 336-342
- 70 Puc, J. et al. (2005) Lack of PTEN sequesters CHK1 and initiates genetic instability. *Cancer cell* 7 (2), 193-204
- 71 Hirose, Y. et al. (2005) Akt activation suppresses Chk2-mediated, methylating agent-induced G2 arrest and protects from temozolomide-induced mitotic catastrophe and cellular senescence. *Cancer research* 65 (11), 4861-4869
- 72 Tonic, I. et al. (2010) Akt activation emulates Chk1 inhibition and Bcl2 overexpression and abrogates G2 cell cycle checkpoint by inhibiting BRCA1 foci. *Journal of Biological Chemistry* 285 (31), 23790-23798
- 73 Xu, N. et al. (2010) Akt/PKB suppresses DNA damage processing and checkpoint activation in late G2. *The Journal of cell biology* 190 (3), 297-305
- 74 Feng, X. et al. (2008) Discovery and characterization of a novel inhibitor of CDC25B, LGH00045. *Acta Pharmacol Sin* 29 (10), 1268-1274
- 75 Bugler, B. et al. (2006) Genotoxic-activated G2-M checkpoint exit is dependent on CDC25B phosphatase expression. *Molecular cancer therapeutics* 5 (6), 1446-1451
- 76 Cangi, M.G. et al. (2000) Role of the Cdc25A phosphatase in human breast cancer. *The Journal of clinical investigation* 106 (6), 753-761
- 77 Takemasa, I. et al. (2000) Overexpression of CDC25B phosphatase as a novel marker of poor prognosis of human colorectal carcinoma. *Cancer research* 60 (11), 3043-3050
- 78 Galaktionov, K. et al. (1995) CDC25 phosphatases as potential human oncogenes. *Science* 269 (5230), 1575-1577
- 79 Galaktionov, K. et al. (1996) Cdc25 cell-cycle phosphatase as a target of c-myc. *Nature* 382 (6591), 511-517
- 80 Fernandez-Vidal, A. et al. (2006) Cell adhesion regulates CDC25A expression and proliferation in acute myeloid leukemia. *Cancer research* 66 (14), 7128-7135
- 81 Ding, X.-L. et al. (2000) The cell cycle Cdc25A tyrosine phosphatase is activated in degenerating postmitotic neurons in Alzheimer's disease. *The American journal of pathology* 157 (6), 1983-1990
- 82 Vincent, I. et al. (2001) Constitutive Cdc25B tyrosine phosphatase activity in adult brain neurons with M phase-type alterations in Alzheimer's disease. *Neuroscience* 105 (3), 639-650
- 83 Hernández, S. et al. (2001) Differential Expression of cdc25 Cell-Cycle-Activating Phosphatases in Human Colorectal Carcinoma. *Laboratory investigation* 81 (4), 465-473
- 84 Wang, Z. et al. (2010) Overexpression of CDC25B, CDC25C and phospho-CDC25C (Ser216) in vulvar squamous cell carcinomas are associated with malignant features and aggressive cancer phenotypes. *BMC cancer* 10 (1), 233
- 85 Kristjansdottir, K. and Rudolph, J. (2004) Cdc25 phosphatases and cancer. *Chemistry & biology* 11 (8), 1043-1051
- 86 Albert, H. et al. (2011) Differential expression of CDC25 phosphatases splice variants in human breast cancer cells. *Clinical Chemistry and Laboratory Medicine* 49 (10), 1707-1714
- 87 Donzelli, M. and Draetta, G.F. (2003) Regulating mammalian checkpoints through Cdc25 inactivation. *EMBO reports* 4 (7), 671-677
- 88 Löffler, H. et al. (2003) Distinct modes of deregulation of the proto-oncogenic Cdc25A phosphatase in human breast cancer cell lines. *Oncogene* 22 (50), 8063-8071
- 89 Lazo, J.S. and Wipf, P. (2008) Is Cdc25 a druggable target? *Anti-cancer agents in medicinal chemistry* 8 (8), 837

- 90 Horiguchi, T. et al. (1994) Dnacin A1 and dnacin B1 are antitumor antibiotics that inhibit cdc25B phosphatase activity. *Biochemical pharmacology* 48 (11), 2139-2141
- 91 Gunasekera, S.P. et al. (1996) Dysidiolide: a novel protein phosphatase inhibitor from the Caribbean sponge *Dysidea etheria* de Laubenfels. *Journal of the American Chemical Society* 118 (36), 8759-8760
- 92 Ham, S.W. et al. (1997) Studies on menadione as an inhibitor of the cdc25 phosphatase. *Bioorganic Chemistry* 25 (1), 33-36
- 93 Cebula, R.E. et al. (1997) Synthesis and phosphatase inhibitory activity of analogs of sulfircin. *Bioorganic & Medicinal Chemistry Letters* 7 (15), 2015-2020
- 94 Loukaci, A. et al. (2001) Coscinosulfate, a CDC25 phosphatase inhibitor from the sponge *Coscinoderma mathewsi*. *Bioorganic & medicinal chemistry* 9 (11), 3049-3054
- 95 Kolb, S. et al. (2009) Development of novel thiazolopyrimidines as CDC25B phosphatase inhibitors. *ChemMedChem* 4 (4), 633-648
- 96 Lavecchia, A. et al. (2006) Modeling of Cdc25B dual specificity protein phosphatase inhibitors: docking of ligands and enzymatic inhibition mechanism. *ChemMedChem* 1 (5), 540-550
- 97 Lazo, J.S. et al. (2002) Identification of a potent and selective pharmacophore for Cdc25 dual specificity phosphatase inhibitors. *Molecular pharmacology* 61 (4), 720-728
- 98 Park, H. et al. (2009) Structure-based virtual screening approach to identify novel classes of Cdc25B phosphatase inhibitors. *Bioorganic & medicinal chemistry letters* 19 (15), 4372-4375
- 99 Brisson, M. et al. (2004) Discovery and characterization of novel small molecule inhibitors of human Cdc25B dual specificity phosphatase. *Molecular pharmacology* 66 (4), 824-833
- 100 Sohn, J. et al. (2003) Inhibition of Cdc25 phosphatases by indolyldihydroxyquinones. *Journal of medicinal chemistry* 46 (13), 2580-2588
- 101 Rosenker, K.M.G. et al. (2015) Synthesis and biological evaluation of 3-aminoisoquinolin-1 (2H)-one based inhibitors of the dual-specificity phosphatase Cdc25B. *Bioorganic & medicinal chemistry* 23 (12), 2810-2818
- 102 Kar, S. et al. (2003) Binding and inhibition of Cdc25 phosphatases by vitamin K analogues. *Biochemistry* 42 (35), 10490-10497
- 103 Pu, L. et al. (2002) Dual G1 and G2 phase inhibition by a novel, selective Cdc25 inhibitor 7-chloro-6-(2-morpholin-4-ylethylamino)-quinoline-5, 8-dione. *Journal of Biological Chemistry* 277 (49), 46877-46885
- 104 Brisson, M. et al. (2005) Redox regulation of Cdc25B by cell-active quinolinediones. *Molecular pharmacology* 68 (6), 1810-1820
- 105 Zhou, Y.-b. et al. (2009) LGH00031, a novel ortho-quinonoid inhibitor of cell division cycle 25B, inhibits human cancer cells via ROS generation. *Acta Pharmacologica Sinica* 30 (9), 1359-1368
- 106 Brezak, M.-C. et al. (2004) A Novel Synthetic Inhibitor of CDC25 Phosphatases BN82002. *Cancer research* 64 (9), 3320-3325
- 107 Brezak, M.-C. et al. (2005) Inhibition of human tumor cell growth in vivo by an orally bioavailable inhibitor of CDC25 phosphatases. *Molecular cancer therapeutics* 4 (9), 1378-1387
- 108 Cazales, M. et al. (2007) Pharmacologic inhibition of CDC25 phosphatases impairs interphase microtubule dynamics and mitotic spindle assembly. *Molecular cancer therapeutics* 6 (1), 318-325
- 109 Lavecchia, A. et al. (2010) Inhibitors of Cdc25 phosphatases as anticancer agents: a patent review. *Expert opinion on therapeutic patents* 20 (3), 405-425
- 110 Hartner, L. et al. (2007) Phase 2 dose multi-center, open-label study of ARQ 501, a checkpoint activator, in adult patients with persistent, recurrent or metastatic leiomyosarcoma (LMS). In *ASCO Annual Meeting Proceedings* (Vol. 25), pp. 20521

- 111 Khong, H. et al. (2007) A phase 2 study of ARQ 501 in combination with gemcitabine in adult patients with treatment naive, unresectable pancreatic adenocarcinoma. In *ASCO Annual Meeting Proceedings* (Vol. 25), pp. 15017
- 112 Lund, G. et al. (2015) Inhibition of CDC25B Phosphatase Through Disruption of Protein-Protein Interaction. *ACS Chemical Biology* 10 (2), 390-394
- 113 Gray-Schopfer, V. et al. (2007) Melanoma biology and new targeted therapy. *Nature* 445 (7130), 851-857
- 114 Schadendorf, D. et al. (2015) Melanoma. *Nature Reviews Disease Primers*, 15003
- 115 Tang, L. et al. (1999) Expression of cell cycle regulators in human cutaneous malignant melanoma. *Melanoma Res* 9 (2), 148-154
- 116 Lau, E. and Ronai, Z.e.A. (2011) Altered Signal Transduction Pathways in Melanoma. In *Melanoma Development: Molecular Biology, Genetics and Clinical Application* (Bossertoff, A., ed.), pp. 137-163, Springer Vienna
- 117 Muñoz-Couselo, E. et al. (2015) Recent advances in the treatment of melanoma with BRAF and MEK inhibitors. *Annals of translational medicine* 3 (15)
- 118 Johnson, D.B. and Sosman, J.A. (2015) Therapeutic advances and treatment options in metastatic melanoma. *JAMA oncology* 1 (3), 380-386
- 119 Lavecchia, A. (2015) Machine-learning approaches in drug discovery: methods and applications. *Drug Discov Today* 20 (3), 318-331
- 120 Lavecchia, A. and Di Giovanni, C. (2013) Virtual screening strategies in drug discovery: a critical review. *Curr Med Chem* 20 (23), 2839-2860
- 121 Durant, J.L. et al. (2002) Reoptimization of MDL keys for use in drug discovery. *Journal of chemical information and computer sciences* 42 (6), 1273-1280
- 122 Rogers, D. and Hahn, M. (2010) Extended-connectivity fingerprints. *Journal of chemical information and modeling* 50 (5), 742-754
- 123 Muchmore, S.W. et al. (2008) Application of belief theory to similarity data fusion for use in analog searching and lead hopping. *Journal of chemical information and modeling* 48 (5), 941-948
- 124 Bales, E.S. et al. (1999) High levels of expression of p27 KIP1 and cyclin E in invasive primary malignant melanomas. *Journal of Investigative Dermatology* 113 (6), 1039-1046
- 125 Monks, T.J. et al. (1992) Quinone chemistry and toxicity. *Toxicology and applied pharmacology* 112 (1), 2-16
- 126 Rudolph, J. (2005) Redox regulation of the Cdc25 phosphatases. *Antioxidants & redox signaling* 7 (5-6), 761-767
- 127 Frenzel, A. et al. (2009) Bcl2 family proteins in carcinogenesis and the treatment of cancer. *Apoptosis* 14 (4), 584-596
- 128 Renault, T.T. and Manon, S. (2011) Bax: Addressed to kill. *Biochimie* 93 (9), 1379-1391
- 129 Bellacosa, A. et al. (2005) Activation of AKT kinases in cancer: implications for therapeutic targeting. *Advances in cancer research* 94, 29-86
- 130 Manning, B.D. and Cantley, L.C. (2007) AKT/PKB signaling: navigating downstream. *Cell* 129 (7), 1261-1274
- 131 Liu, P. et al. (2014) Cell-cycle-regulated activation of Akt kinase by phosphorylation at its carboxyl terminus. *Nature* 508 (7497), 541
- 132 Maddika, S. et al. (2007) Cell survival, cell death and cell cycle pathways are interconnected: implications for cancer therapy. *Drug Resistance Updates* 10 (1), 13-29
- 133 Robertson, G.P. (2005) Functional and therapeutic significance of Akt deregulation in malignant melanoma. *Cancer and metastasis reviews* 24 (2), 273-285
- 134 Lu, M. et al. (2013) Restoring p53 function in human melanoma cells by inhibiting MDM2 and cyclin B1/CDK1-phosphorylated nuclear iASPP. *Cancer cell* 23 (5), 618-633

- 135 Mayo, L.D. et al. (2002) PTEN protects p53 from Mdm2 and sensitizes cancer cells to chemotherapy. *Journal of Biological Chemistry* 277 (7), 5484-5489
- 136 Feng, J. et al. (2004) Stabilization of Mdm2 via decreased ubiquitination is mediated by protein kinase B/Akt-dependent phosphorylation. *Journal of Biological Chemistry* 279 (34), 35510-35517
- 137 Irwin, J.J. et al. (2012) ZINC: a free tool to discover chemistry for biology. *Journal of chemical information and modeling* 52 (7), 1757-1768
- 138 Lipinski, C.A. (2000) Drug-like properties and the causes of poor solubility and poor permeability. *Journal of pharmacological and toxicological methods* 44 (1), 235-249
- 139 Flower, D.R. (1998) On the properties of bit string-based measures of chemical similarity. *Journal of chemical information and computer sciences* 38 (3), 379-386
- 140 Maggiora, G. et al. (2013) Molecular Similarity in Medicinal Chemistry: Miniperspective. *Journal of medicinal chemistry* 57 (8), 3186-3204
- 141 Jorgensen, W.L. et al. (1996) Development and testing of the OPLS all-atom force field on conformational energetics and properties of organic liquids. *Journal of the American Chemical Society* 118 (45), 11225-11236
- 142 Verdonk, M.L. et al. (2003) Improved protein–ligand docking using GOLD. *Proteins: Structure, Function, and Bioinformatics* 52 (4), 609-623
- 143 Romano, S. et al. (2010) Role of FK506-binding protein 51 in the control of apoptosis of irradiated melanoma cells. *Cell Death & Differentiation* 17 (1), 145-157
- 144 Gelzo, M. et al. (2014) Evaluation of cytotoxic effects of 7-dehydrocholesterol on melanoma cells. *Free Radical Biology and Medicine* 70, 129-140
- 145 Albano, F. et al. (2013) Markers of mitochondrial dysfunction during the diclofenac-induced apoptosis in melanoma cell lines. *Biochimie* 95 (4), 934-945
- 146 Bradford, M.M. (1976) A rapid and sensitive method for the quantitation of microgram quantities of protein utilizing the principle of protein-dye binding. *Analytical biochemistry* 72 (1-2), 248-254
- 147 Mirza-Aghayan, M. et al. (2010) Palladium-catalyzed reduction of nitroaromatic compounds to the corresponding anilines. *Applied Organometallic Chemistry* 24 (6), 477-480
- 148 Newman, M.S. et al. (1976) Phenolic and ketonic tautomers in polycyclic aromatic hydrocarbons. *Journal of the American Chemical Society* 98 (11), 3237-3242
- 149 Vilaivan, T. (2006) A rate enhancement of tert-butoxycarbonylation of aromatic amines with Boc 2 O in alcoholic solvents. *Tetrahedron letters* 47 (38), 6739-6742
- 150 Harvey, R.G. and Cortez, C. (1997) Fluorine-substituted derivatives of the carcinogenic dihydrodiol and diol epoxide metabolites of 7-methyl-, 12-methyl- and 7, 12-dimethylbenz [a] anthracene. *Tetrahedron* 53 (21), 7101-7118
- 151 Di Santo, R. et al. (2012) Design, synthesis, and structure–activity relationship of N-arylnaphthylamine derivatives as amyloid aggregation inhibitors. *Journal of medicinal chemistry* 55 (19), 8538-8548
- 152 Akwabi-Ameyaw, A. et al. (2009) FXR agonist activity of conformationally constrained analogs of GW 4064. *Bioorganic & medicinal chemistry letters* 19 (16), 4733-4739